DNA-TR-82-116

STUDY OF THE CAPABILITIES OF SIX ADVANCED SOIL MODELS TO PREDICT RESPONSES TO COMPLEX STRAIN PATHS TYPICAL OF EXPLOSIVELY - INDUCED GROUND MOTION.

H.E. Read
G.Y. Baladi
J.H. Prevost
S.H. Schuster
H.Y. Ko
P.V. Lade
I.S. Sandler
J.G. Trulio
S-CUBED
A Division of Maxwell Laboratories, Inc.
P.O. Box 1620
La Jolla, CA 92038-1620

30 April 1983

Technical Report

CONTRACT No. DNA 001-82-C-0236

APPROVED FOR PUBLIC RELEASE;
DISTRIBUTION UNLIMITED.

THIS WORK WAS SPONSORED BY THE DEFENSE NUCLEAR AGENCY
UNDER RDT&E RMSS CODE B344082466 H11CAXSX00012 H2590D.

Prepared for
Director
DEFENSE NUCLEAR AGENCY
Washington, DC 20305-1000

Destroy this report when it is no longer needed. Do not return to sender.

PLEASE NOTIFY THE DEFENSE NUCLEAR AGENCY, ATTN: STTI, WASHINGTON, DC 20305-1000, IF YOUR ADDRESS IS INCORRECT, IF YOU WISH IT DELETED FROM THE DISTRIBUTION LIST, OR IF THE ADDRESSEE IS NO LONGER EMPLOYED BY YOUR ORGANIZATION.

UNCLASSIFIED
SECURITY CLASSIFICATION OF THIS PAGE

REPORT DOCUMENTATION PAGE

1a. REPORT SECURITY CLASSIFICATION UNCLASSIFIED	1b. RESTRICTIVE MARKINGS
2a. SECURITY CLASSIFICATION AUTHORITY	3. DISTRIBUTION/AVAILABILITY OF REPORT Approved for public release; distribution unlimited.
2b. DECLASSIFICATION/DOWNGRADING SCHEDULE	
4. PERFORMING ORGANIZATION REPORT NUMBER(S) SSS-R-83-6081	5. MONITORING ORGANIZATION REPORT NUMBER(S) DNA-TR-82-116
6a. NAME OF PERFORMING ORGANIZATION S-CUBED, A Division of Maxwell Laboratories, Inc 6b. OFFICE SYMBOL (If applicable)	7a. NAME OF MONITORING ORGANIZATION Director Defense Nuclear Agency
6c. ADDRESS (City, State, and ZIP Code) P.O. Box 1620 La Jolla, CA 92038-1620	7b. ADDRESS (City, State, and ZIP Code) Washington, DC 20305-1000
8a. NAME OF FUNDING/SPONSORING ORGANIZATION 8b OFFICE SYMBOL (If applicable)	9 PROCUREMENT INSTRUMENT IDENTIFICATION NUMBER DNA 001-82-C-0236
8c. ADDRESS (City, State, and ZIP Code)	10. SOURCE OF FUNDING NUMBERS

PROGRAM ELEMENT NO	PROJECT NO	TASK NO	WORK UNIT ACCESSION NO
62715H	H11CAXS	X	DH006217

11. TITLE (Include Security Classification) STUDY OF THE CAPABILITIES OF SIX ADVANCED SOIL MODELS TO PREDICT RESPONSES TO COMPLEX STRAIN PATHS TYPICAL OF EXPLOSIVELY-INDUCED GROUND MOTION

12. PERSONAL AUTHOR(S) H.E. Read, H.-Y. Ko, G.Y. Baladi, P.V. Lade, J.H. Prevost, I.S. Sandler, S.H. Schuster, J.G. Trulio

13a TYPE OF REPORT	13b. TIME COVERED	14 DATE OF REPORT (Year, Month, Day)	15 PAGE COUNT
Technical Report	FROM 82-4-30 TO 82-12-31	1983 April 30	116

16. SUPPLEMENTARY NOTATION
This work was sponsored by the Defense Nuclear Agency under RDT&E RMSS Code B344082466 H11CAXSX00012 H2590D.

17 COSATI CODES			18 SUBJECT TERMS (Continue on reverse if necessary and identify by block number)
FIELD	GROUP	SUB-GROUP	Complex Strain Paths; Measured Stress Histories
8	7		
8	11		

19 ABSTRACT (Continue on reverse if necessary and identify by block number)

The capabilities of six advanced soil models to predict the response of remolded Ralston Valley soil to complex strain paths were investigated in a joint, cooperative effort among several organizations. The complex strain paths were typical of those experienced by soil elements during nearby near-surface explosive ground motion events. The investigation involved both analysis and extensive laboratory testing. Standard laboratory tests were conducted to provide the usual type of data for fitting the models, while non-standard laboratory tests were done to drive the soil around prescribed, fully three-dimensional complex strain paths and simultaneously measure the corresponding stress histories. To avoid possible unknown differences in testing equipment, all laboratory tests were done with a true triaxial device. The models were fit to the data from the standard laboratory tests, and then driven around the prescribed complex strain paths to predict the corresponding stress histories. Comparison between the predicted and measured stress histories formed the basis for evaluating the models. However, because of uncertainties that occurred in the data for the complex strain paths, a meaningful evaluation of the models could not be

20 DISTRIBUTION/AVAILABILITY OF ABSTRACT	21 ABSTRACT SECURITY CLASSIFICATION
☐ UNCLASSIFIED/UNLIMITED ☒ SAME AS RPT ☐ DTIC USERS	UNCLASSIFIED

22a NAME OF RESPONSIBLE INDIVIDUAL	22b TELEPHONE (Include Area Code)	22c OFFICE SYMBOL
Betty L. Fox	202-325-7042	DNA/STTI

DD FORM 1473, 84 MAR — 83 APR edition may be used until exhausted. All other editions are obsolete.

SECURITY CLASSIFICATION OF THIS PAGE
UNCLASSIFIED

19. ABSTRACT (Continued)

conducted. Recommendations are given for improving the testing procedures so that data of the required quality can be obtained in the future.

PREFACE

This technical report describes the results from a joint research program undertaken to determine the extent to which present day advanced soil models are capable of predicting the responses of soils to deformation paths characteristic of near-surface nuclear explosions. The organizations that participated in the effort included, in addition to S-CUBED, the University of Colorado, the University of California, Los Angeles, Princeton University, U.S. Army Engineer Waterways Experiment Station, Applied Theory, Inc., California Research and Technology and Weidlinger Associates. Overall direction and coordination of the program was provided by Dr. H. E. Read (S-CUBED), the Principal Investigator.

The research was originally initiated at the request of Lt. Col. Don Gage, U.S. Air Force BMO, and supported by the BMO under Contract No. F07404-78-C-007 from 1978 to 1980. The final phase of the effort was sponsored by the Defense Nuclear Agency under Contract DNA001-82-C-0236, and monitored by Dr. George Ullrich (SPSS). The authors express their appreciation to Lt. Col. Gage and Dr. Ullrich for support and encouragement throughout the course of this work.

Thanks also go to Dr. Guy Jackson and Dr. John Ehrgott, both of the U.S. Army Engineer Waterways Experiment Station, for providing support for the complex strain path tests.

Further appreciation is extended to Mr. John Thomas, Air Force Weapons Laboratory, who personally took the responsibility for seeing that the University of Colorado was supplied with the necessary soil from the HAVE HOST and Ralston Valley sites to perform the required tests.

Finally, thanks are due to Mr. R. G. Herrmann (S-CUBED) for his expert assistance in processing the various computer predictions supplied by each of the participants, as well as for overall computer support.

TABLE OF CONTENTS

TABLE OF CONTENTS(Concluded)

LIST OF ILLUSTRATIONS

LIST OF ILLUSTRATIONS (Concluded)

LIST OF TABLES

I. INTRODUCTION

1.1 BACKGROUND

The design of strategic land-based missile systems, such as MX, requires a capability to predict, with a prescribed level of accuracy, the explosively-induced ground motions near the system's major structures for a variety of potential nuclear attack scenarios. Such a predictive capability is of crucial importance if one is to develop credible and cost-effective designs for the buried protective structures and other ground support facilities, as well as in the design of guidance and control systems.

During the past decade, there has been an extensive, continuing effort by the defense community to develop techniques for predicting ground motion from explosive sources in various geologies of interest. These efforts have included large-scale field tests, laboratory testing of cored and remolded geologic materials, in situ material properties investigations, constitutive model development, and computer simulation with FD and FE wave propagation codes of explosive ground motion events. Despite this large expenditure of effort, progress toward achieving an acceptable level of predictive capability has been slow, especially for surface explosions over strongly layered media. The main obstacle to a major advancement in predicting explosively-induced ground motion is our present inability to correctly model the response of the in situ materials on a large scale. This inability is probably due to a number of causes, the major ones of which are (1) present limitations in experimental technology that prohibit the acquisition of the needed response data of the in situ materials, (2) possible inability of the constitutive models to describe the response of the geologic materials to the complex deformation histories produced by the explosive loading, and (3) over idealization in modeling the geologies of test sites in computer simulation studies.

The present study is directed toward examining the predictive capabilities of advanced constitutive models for soils. During the

past ten or so years, the ground motion community has relied upon a small number of soil models in its efforts to predict explosively-induced ground motion with large finite difference or finite element wave propagation codes. Questions regarding the extent to which such models are capable of describing responses of soils to complex deformation histories produced by explosive loading have been raised off and on, but never systematically pursued to a final conclusion. The basic forms of the models used in present day ground motion studies have remained largely unchanged since their initial development and introduction a number of years ago.

Generally, data from standard laboratory tests are used to evaluate the parameters in the soil models used in ground motion studies.* In such tests, the soil is subjected to a class of relatively simple deformation paths in which at least two of the principal strains, as well as two of the principal stresses, are equal. Because of the large number of adjustable parameters in most models, they can be fit with reasonably good accuracy to the standard laboratory data. Such good fits do not, however, guarantee that the models can provide comparable accuracy along other considerably different strain paths unless, of course, the models are physically sound. In view of the rather limited success that has been achieved in predicting explosive ground motion during the past ten years, there is some basis for questioning the models' predictive capabilities.

During the past several years, the issue about the adequacy of the soil models has attracted increasing attention, mainly as a result of the polarization of attitudes on the issue. At one extreme are those who claim that, because of the inherent simplicity of the models, one cannot expect them, when they're fit in the usual

*If available, data from dynamic in situ tests, such as CIST, is sometimes used to modify the values of the model parameters determined from the standard laboratory data.

manner to the standard laboratory (and possibly CIST data), to be capable of describing with required accuracy the response of soil to complex deformations which substantially differ from the relatively simple deformations followed to generate the data used in fitting the model. At the other extreme are those who feel that the models may be basically correct and reasonably accurate, but the lack of appropriate data for the dynamic response of the in situ soil prevents the modelers from determining the appropriate values of the parameters in their models. Up to 1978, virtually nothing had been done by the ground motion community to systematically explore these issues.

1.2 PURPOSE OF PRESENT STUDY

From mid-1977 to the end of 1980, S-CUBED was under contract to the U.S. Air Force Ballistic Missile Office (BMO) to provide independent analyses and evaluation of work performed by other organizations as part of the MX Basing Program. One of the major tasks under this contract was to formulate and conduct a systematic study to assess the predictive capabilities of the soil models then being used by the defense community for MX ground motion prediction.[1] This task, which became known as the Soil Models Evaluation (SME) study, increased in scope to include other advanced and promising soil models that were not then in use by the defense community.

The basic goal of the SME study was to provide answers to the following questions:

- How well can the main soil models used by the ground motion community, when fit in the usual manner to standard laboratory data, describe the response of a soil to strain paths which differ significantly from those followed in the standard laboratory tests? In particular, how well can they describe responses to strain paths typical of those which occur in the ground due to a near-surface explosion?

- Are there any other existing advanced soil models which may provide greater modeling capability than those presently used by the defense community?

To address these questions, a joint analytical-experimental research program was formulated,[1] so that the question of the soil models' predictive capabilities could be isolated for detailed study from the other potential sources of error in ground motion prediction, such as, for example, the in situ versus laboratory properties issue. A description of the basic research plan formulated for this purpose is described below.

1.3 BASIC RESEARCH PLAN

The basic plan developed to achieve the research objectives may be summarized as follows: First, select the advanced soil models to be investigated, and a soil of current practical interest. Then, obtain good, reproducible standard laboratory data from carefully remolded samples of the soil, and fit the models in the customary manner to these data. The standard laboratory tests required for this purpose include pure hydrostatic compression, uniaxial strain compression, triaxial compression and triaxial extension at various confining pressures. Next, conduct further laboratory tests on remolded samples of the soil with a true triaxial device by driving the soil around complex strain paths of practical interest; during these tests, measure the corresponding stress histories. Then, drive the soil models (which have been fit to the standard laboratory data) around the same complex strain paths and predict the corresponding stress histories. For each of the complex strain paths, compare the predicted and measured stress histories. On this basis, evaluate the ability of each of the models to predict the stress histories along the complex strain paths to which it was not fit. With this approach, the predictive capabilities of the models can be evaluated independently of the issues of in situ versus laboratory properties, and static versus dynamic properties. An approach for performing such an evaluation is described in Appendix A.

The ultimate success of such a study obviously depends very strongly upon having adequate and reproducible soil data against which the model predictions can be compared. Because of this, considerable care was taken to ensure that the data generated in both phases of testing were reliable and trustworthy. In our efforts to meet this objective, considerable laboratory soil testing was done and, in the course of this testing, some pitfalls in the standard laboratory approaches to soil testing were uncovered and remedied.[2] All of the laboratory testing was done by Professor Hon-Yim Ko and his staff at the University of Colorado.

Although several different soils were examined during the course of this study,* the soil that eventually was chosen for use in evaluating the models was a near-surface sandy alluvial soil from Ralston Valley near Tonopah, Nevada. At the time this selection was made, Ralston Valley was an area of considerable interest to the Air Force in regard to possible MX deployment. To reduce the large scatter that is typical of laboratory data from so-called "undisturbed" soil samples, the Ralston Valley soil was carefully remolded for use in the laboratory tests.

All of the standard laboratory tests were axisymmetric, with two principal stresses and two principal strains equal, and could have been performed with a conventional triaxial device. The complex strain path tests were fully three-dimensional, and require a test device which is capable of independently controlling the three principal stresses and strains. To avoid any unknown differences between testing devices, all phases of the soil testing were performed in the same multi-axial cubical test device developed by Professor Ko and his colleagues at the University of Colorado. Each test was repeated at least once to provide insight into the degree of reproducibility of the data. Details of the laboratory tests conducted on Ralston Valley soil can be found in References 3 and 4. A description of the multi-axial cubical test device used in this study is given later on in Section 2.2.

*See Section 2.1 for a summary of the soil testing program.

1.4 SOIL MODELS

Six advanced soil models were selected for detailed consideration in the study. These included the following models, which have been used extensively by the defense community in ground motion studies:

- AFWL Engineering Model[5]
- Weidlinger Cap Model[6]
- WES Cap Model[7],

as well as three other advanced soil models that have recently appeared in the literature:

- Lade's Elasto-Plastic Model[8]
- Prevost's Nested Surfaces Model[9]
- S-CUBED Endochronic Model[10]

The models chosen for the latter group were selected because they appeared to offer improvements in modeling capability over those in the first group, and also because they represent considerably different approaches to modeling soil behavior. All of the above models are fully three-dimensional and computer programs exist for each of them.

1.5 COMPLEX STRAIN PATHS

For the present study, three complex strain paths were specified by Applied Theory, Inc.,[12] and, in the sequel, they are referred to as complex strain paths Nos. 1, 2 and 3. These paths were determined by Applied Theory from the results of a series of axisymmetric numerical studies of explosively-driven ground motion events in both dry and wet sandy alluvial soils, and they represent the best estimate of the characteristic deformation paths that soil elements at three different locations will experience, as a result of a nearby, near-surface nuclear explosion. The histories of the strain components were monitored at various locations during these numerical calculations and later processed to provide the

specification of the three principal strains along the strain paths. From the numerical studies, it was found that, regardless of whether the soil was dry or saturated, the basic shapes of the strain paths at a given (yield-scaled) location were essentially the same. Path No. 1 is representative of deformations that occur near the ground surface, but at some range from the explosive source. Path No. 2 is typical of deformations that take place at some range from the source but at a greater depth than Path No. 1. Finally, Path No. 3 describes the type of deformation which arises at moderately deep locations near the axis of symmetry.

The three complex strain paths are depicted graphically in Figures 1 to 3, where the variations of the three principal strains, ϵ_1, ϵ_2 and ϵ_3, along each of the paths are shown. A numerical description of each path is provided in Appendix D.

It is important to note that the principal strains shown in these figures, and listed in the tables of Appendix D, are measured from the ends of the initial hydrostatic compression states. The initial hydrostatic states, which may be viewed as overburden, were not specified by Applied Theory, but were selected by Professor Ko so that, when a laboratory soil specimen was driven around any of the complex strain paths, none of the principal stresses became tensile. This restriction was necessary since the cubical triaxial device used for the testing was not capable of applying tensile stress to the soil.

1.6 EVALUATION OF MODELS

It seems appropriate and natural to base the evaluation of the models upon their relative abilities to predict, for each of the three complex strain paths, the corresponding stress histories measured by the cubical triaxial device. Adopting this approach, one must then define a measure of discrepancy between the predicted and measured stress histories, and there appears to be no unique way to do this.

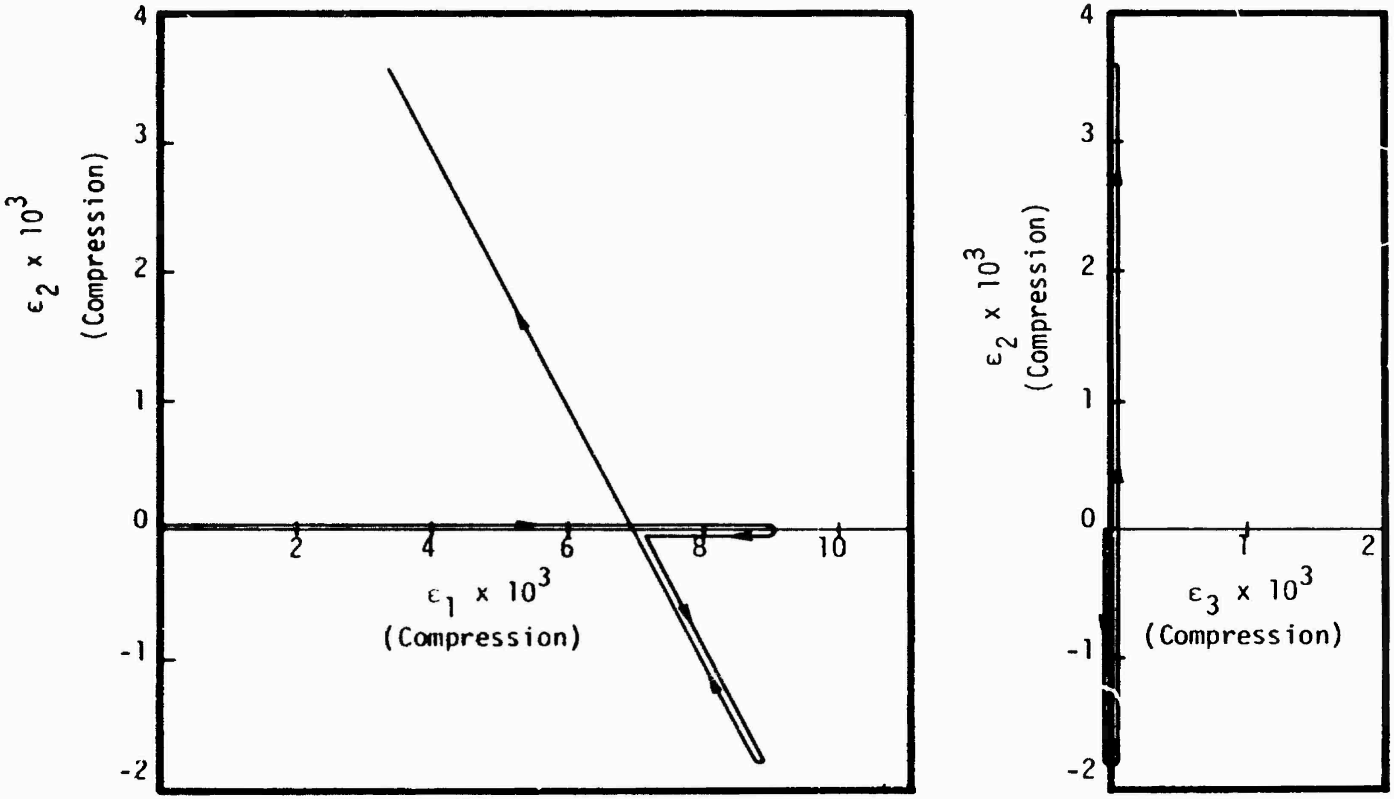

Figure 1. Complex strain path No. 1. For this path, the hydrostatic prestress is 300 psi.

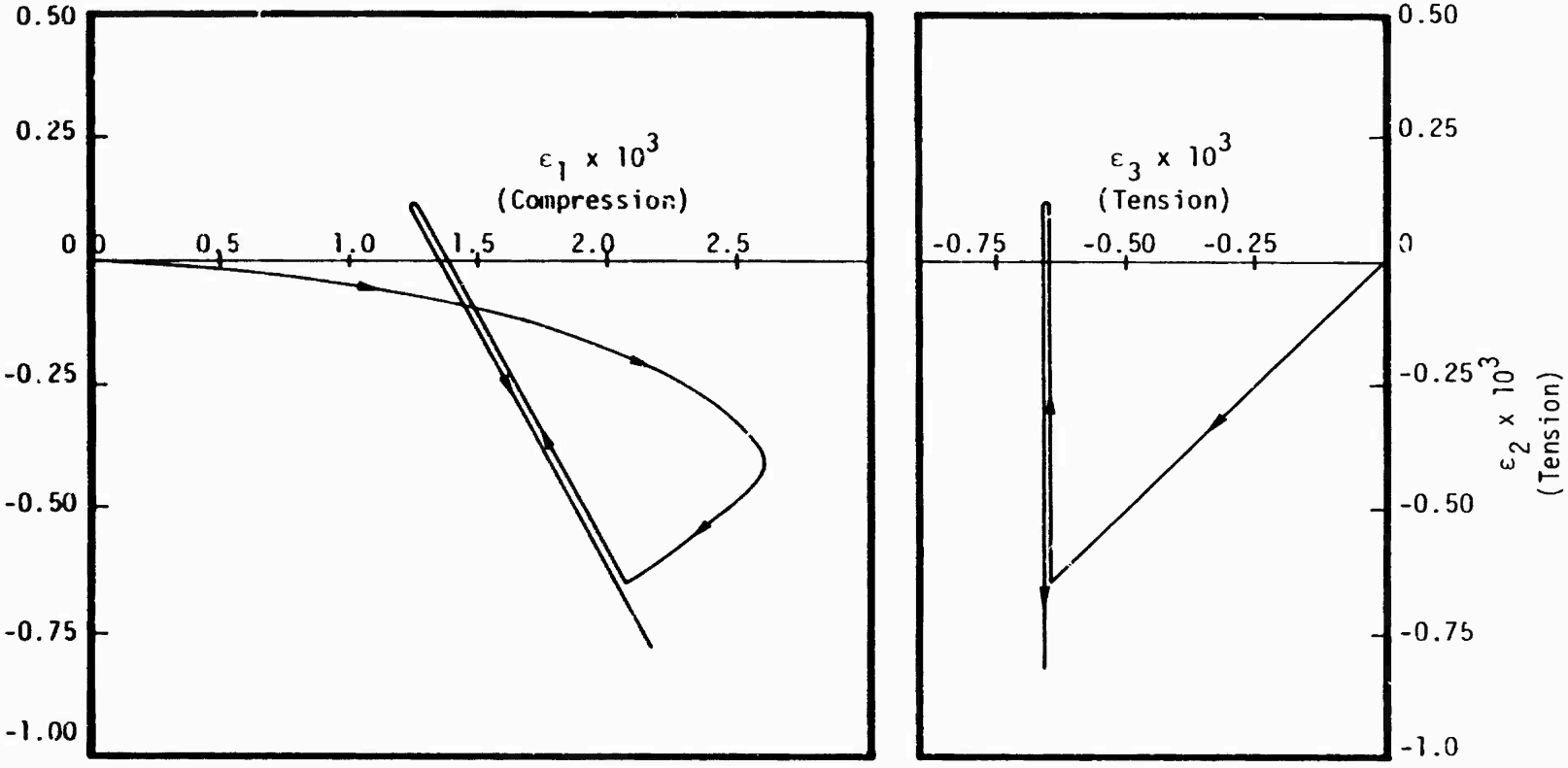

Figure 2. Complex strain path No. 2. For this path, the hydrostatic prestress is 550 psi.

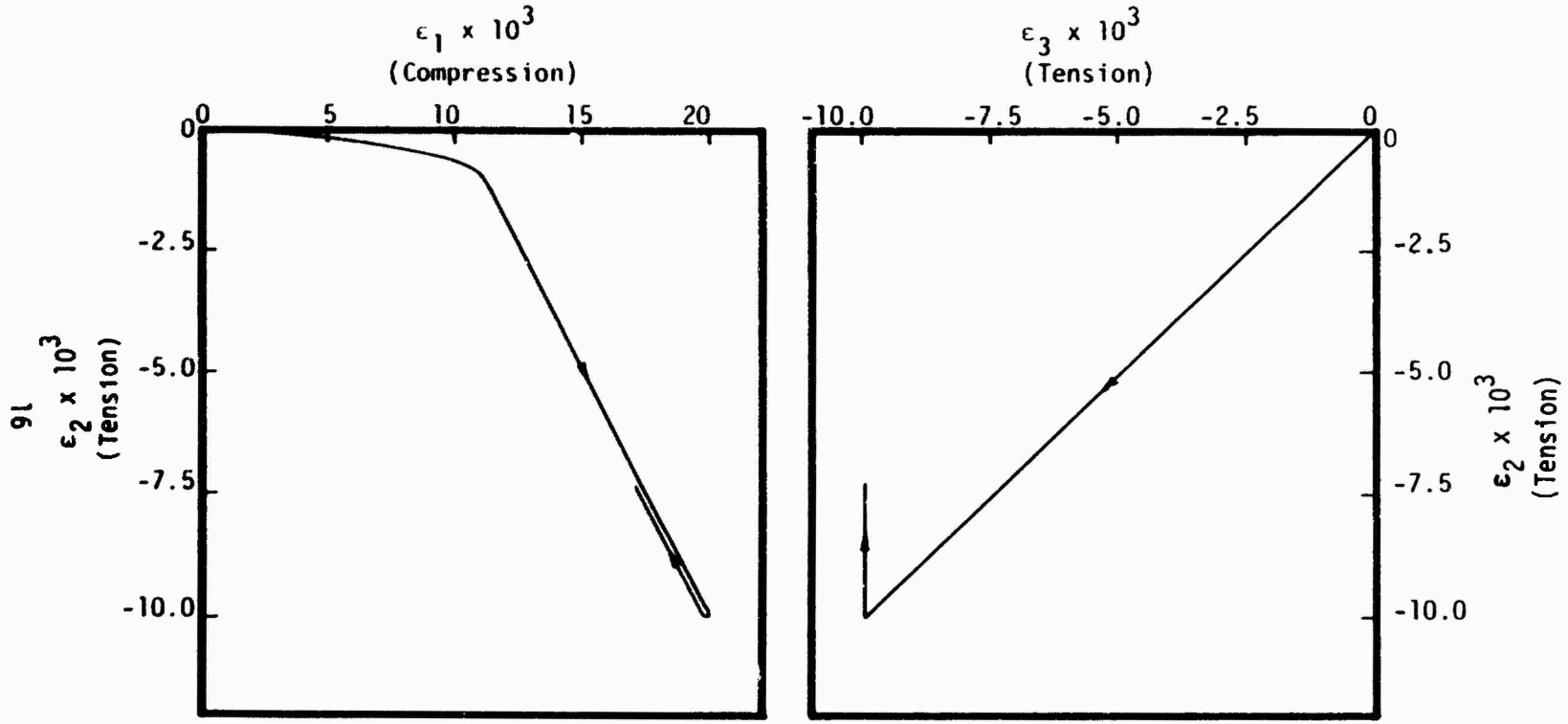

Figure 3. Complex strain path No. 3. For this path, the hydrostatic prestress is 900 psi.

An approach developed in the present study, and described in detail in Appendix A, utilizes an evaluation criterion based on the integrated mean square deviation between the predicted and measured stress histories over the entire path. The success of this approach depends upon having precision data from the complex strain path tests in which the prescribed strain paths have been followed with acceptable accuracy.

2. SOIL TESTING

The success of this study depends very strongly upon having an adequate and accurate suite of soil response data for use in evaluating the predictive capabilities of the models. Accordingly, considerable effort was made during the course of the study to ensure that the data obtained for this purpose were accurate and reproducible. Considerable laboratory soil testing was done and, in the process, a great deal was learned about the subtleties involved in generating accurate laboratory test data from remolded soil samples. All of the soil testing for this study was done by Professor Hon-Yim Ko and his staff at the University of Colorado at Boulder, Colorado.

In the following sections, the various phases of soil testing conducted as part of the present study are summarized, and details of the multi-axial cubical triaxial device used in the soil tests are provided. The results from the complex strain path tests conducted on remolded Ralston Valley soil are described, and finally some general comments on the testing program and the results obtained thereform are given.

2.1 SUMMARY OF SOIL TESTING -- SOME LESSONS LEARNED

At the time this investigation was begun, there was considerable interest within the defense community, in general, and the Air Force, in particular, in the constitutive properties of the sandy alluvial soils from potential MX basing sites in the western part of the United States. The Air Force BMO accordingly directed us to evaluate the selected soil models in terms of their capabilities to predict response to complex strain paths in such soils. In the course of this investigation, laboratory testing was done on three different soils, including Ottawa sand, remolded soil from the HAVE HOST test site in Yuma, Arizona, and remolded soil from Ralston Valley near Tonopah, Nevada. The tests conducted on these soils are discussed below.

2.1.1 Ottawa Sand

At the beginning of the investigation, we focussed attention on a readily available sandy soil for which there was considerable constitutive data already available in the literature, namely, Ottawa sand. The Ottawa sand was obtained, and a series of standard laboratory tests was conducted on this material with a conventional triaxial device at the University of Colorado. Upon reviewing the results from these tests, which were reported in Reference 13, it became apparent that this rather idealized soil behaved quite differently from the near-surface soils at the potential MX sites, which contained some clayey components. The test specimens of Ottawa sand exhibited highly nonlinear unloading behavior, which led to large recoverable strains on unloading, while the soils from the potential MX basing sites unloaded in a much more linear manner with only smaller recoverable strains. The Ottawa sand also exhibited substantial anisotropy (transverse isotropy), probably as a result of the pluviation process used to prepare the specimens. On the other hand, the near-surface soils from candidate basing sites appear to be reasonably isotropic. Because of these essential differences in constitutive behavior, it was decided that Ottawa sand should be dropped from further consideration, and that we would turn attention to a real soil from one of the candidate sites.

2.1.2 HAVE HOST SOIL

At the direction of the Air Force BMO, we next focussed attention on near-surface soil from the HAVE HOST test site near Yuma, Arizona, a site where considerable field testing was being done at the time as part of the MX program. In December 1979, the Air Force Weapons Laboratory shipped a supply of near-surface soil from the HAVE HOST site to the University of Colorado for testing in the present investigation. Standard laboratory tests on remolded samples of the soil were done in a conventional triaxial device, including pure hydrostatic, uniaxial strain, triaxial compression

and triaxial extension at several confining pressures, and the results were reported in Reference 14. Subsequent tests were done to determine if the soil characteristics measured with the conventional triaxial device represented the true soil response, or if they also reflected some particular features of the particular triaxial device employed. To investigate this, the uniaxial strain (UX) tests were redone with a standard oedometer, and the hydrostatic compression (HC) tests were repeated using a true triaxial device.

The outcome of these tests revealed some interesting, as well as disturbing, facts. First, the results from the UX tests conducted with the standard oedometer were in substantial disagreement with data from the UX tests performed with the conventional triaxial device. Figure 4 depicts the systematic discrepancy between the two sets of data. On the other hand, the HC results from the true triaxcial device were in reasonably good agreement with those from the HC tests conducted with the conventional triaxial device. This raised an interesting question: Why did the HC tests performed with two different devices show reasonably consistent results, while the UX tests, also done in two different devices, show a large, systematic disagreement. This appeared to be an important question to the geotechnical testing community, inasmuch as it is standard practice in many soil testing laboratories to use more than one device in the process of generating standard laboratory data. Thus, there appears to be a likely potential for producing inconsistent data.

Secondly, the HC tests revealed that the remolded specimens of HAVE HOST soil, which were essentially isotropic in their initial state, developed substantial stress-induced anisotropy as the deformation proceeded. Moreover, the form of anisotropy developed by the remolded specimens appeared to be quite different from that observed in undisturbed samples of similar soil.

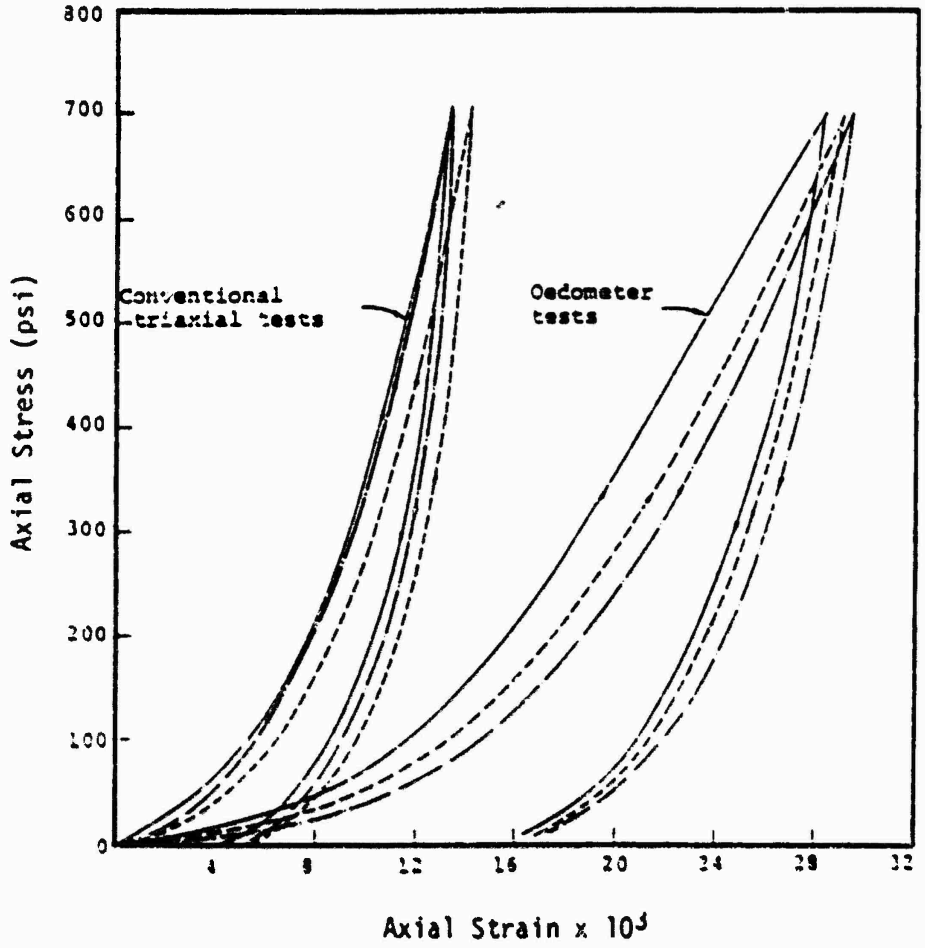

Figure 4. Uniaxial strain response of remolded HAVE HOST soil up to 700 psi. Comparison between results obtained from conventional triaxial device and from standard oedometer (from Reference 2).

In an effort to establish why the UX test results were inconsistent, the normal procedure for remolding specimens was reexamined. From this, we found that the discrepancy in the UX results, as well as the consistency of the HC results, could be explained in terms of the differences in the heterogeneity and stiffness of the specimens used in the various test devices. Specifically, the normal remolding procedure was found to produce inhomogeneous specimens, the degree of inhomogeneity increasing with the number of lifts used in forming the specimen. Tests performed on individual lifts, which were carefully removed from normally remolded specimens revealed that the stiffness of a lift increased as subsequent lifts were added to the specimen. Thus, the remolded specimens used in the conventional triaxial tests, which were formed from five (5) lifts, were found to be more inhomogeneous and stiff than the specimens used in the oedometer tests, which were formed from only two (2) lifts; this explained the discrepancy between the two sets of UX data. The HC tests were done on remolded specimens that had nearly the same number of lifts; those done with the true triaxial device had four (4) lifts, while those done with the conventional triaxial device had five (5) lifts. Thus, the inhomogeneities in both sets of remolded specimens were nearly the same, as were the overall stiffnesses.

In an effort to revise the standard remolding procedure so that the specimens would be more homogeneous, we explored the use of undercompaction[15] in remolding the specimens, and found it to be beneficial and feasible. Accordingly, undercompaction was employed to form the specimens used in the subsequent testing. A critical review of the results from all of the testing performed on the soil from the HAVE HOST test site has been given in Reference 2.

As noted above, the additional tests performed on the HAVE HOST soil revealed some inconsistencies in the original standard laboratory data reported in Reference 14, and needed to be redone, using specimens remolded with undercompaction. Moreover, the

additional tests consumed virtually all of the HAVE HOST soil that had been supplied to the University of Colorado by the AFWL. Thus, a decision had to be made whether to obtain additional HAVE HOST soil for this purpose or to obtain some other soil.

2.1.3 Ralston Valley Soil

In June 1980, a decision was made jointly by the Air Force BMO and S-CUBED to shift the focus of the SME study to near-surface soil from Ralston Valley near Tonopah, Nevada. This decision stemmed from the fact that the Ralston Valley area was, at the time, fast becoming a center of considerable focus in regard to MX basing, while the HAVE HOST test site was being phased out. Again, the AFWL volunterred to assist the SME study by supplying the University of Colorado with near-surface Ralston Valley soil, and the soil arrived at the University of Colorado in July, 1980. Standard laboratory tests were performed on specimens of this soil remolded with undercompaction. All tests were done with a cubical triaxial device to eliminate any possible unknown effects that might arise if the standard laboratory tests were done with one device and the complex strain path tests with another. The standard laboratory tests on Ralston Valley soil were completed in December 1980, and the results were reported in Reference 3.

In November 1980, the Air Force BMO terminated all research efforts which were not directly related to the full-scale engineering development of the MX system. As a result, the support for the SME study from the Air Force was terminated in January, 1981.

There were no further activities in the SME study for about a year. The U.S. Army Engineer Waterways Experiment Station became interested in seeing the work completed and, in September 1981, provided support to the University of Colorado to conduct the complex strain path tests on the Ralston Valley soil. These tests were completed in late 1981, and are reported in Reference 4. At

this point, all of the testing of Ralston Valley soil needed to perform the evaluation of the models had been completed. Then, in May 1982, The Defense Nuclear Agency undertook support of the final phase of the SME study.

Parenthetically, it may be of interest to note that, although not part of the present study, another quite comprehensive laboratory study of the response of remolded Ralston Valley soil to complex strain paths similar to those considered herein has recently been reported by Ko and Meier.[16] This study focussed upon clayey sand from Ralston Valley which had been graded to resemble soil from Nellis Air Force Base.

2.2 THE TRUE TRIAXIAL DEVICE

A series of true, cubical triaxial devices has been developed at the University of Colorado for testing the behavior of materials under general, three-dimensional, compressive loading conditions. The capacities of these devices range from 100 psi to 20,000 psi, with the specimen sizes ranging from 2 to 8 inches. For the purpose of the present investigation, the test device described by Ko and Sture[17] was selected primarily because of its stiffness, loading capacity, and available graphics output equipment. Details of this device, as well as evidence in support of its accuracy, are provided in the sections which follow.

2.2.1 Description

The true triaxial device used in the present study is shown schematically in Figures 5 and 6. A four-inch cubical test specimen is loaded by hydraulic pressures through fluid cushions mounted on the walls of the test cell. Because of the flexibility of the cushions, a known, purely compressive state of stress is applied to the specimen while the deformations of the specimen are monitored by proximity transducers mounted on the walls. These transducers,

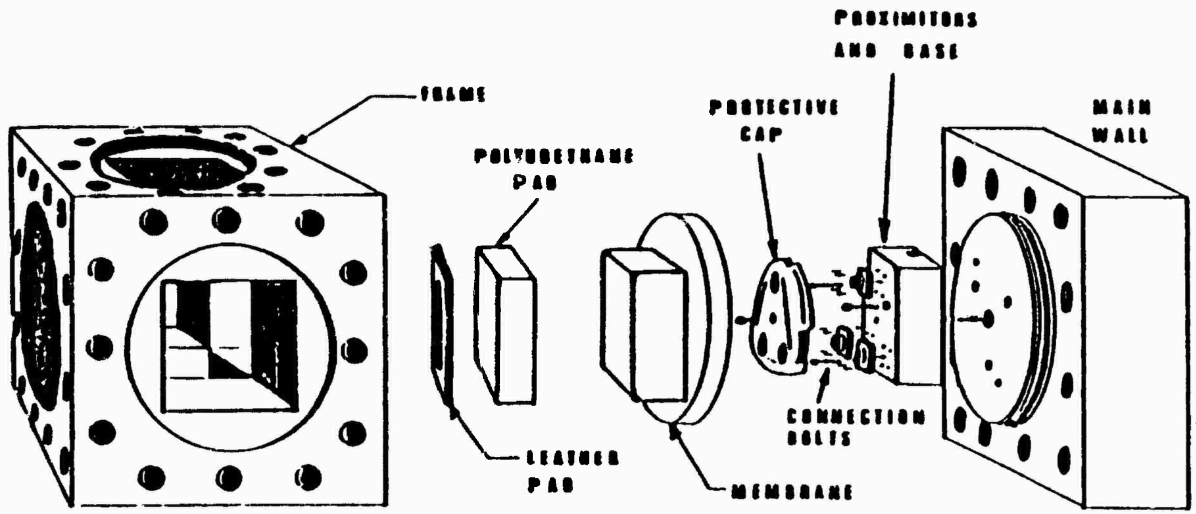

Figure 5. Exploded view of the true triaxial device.

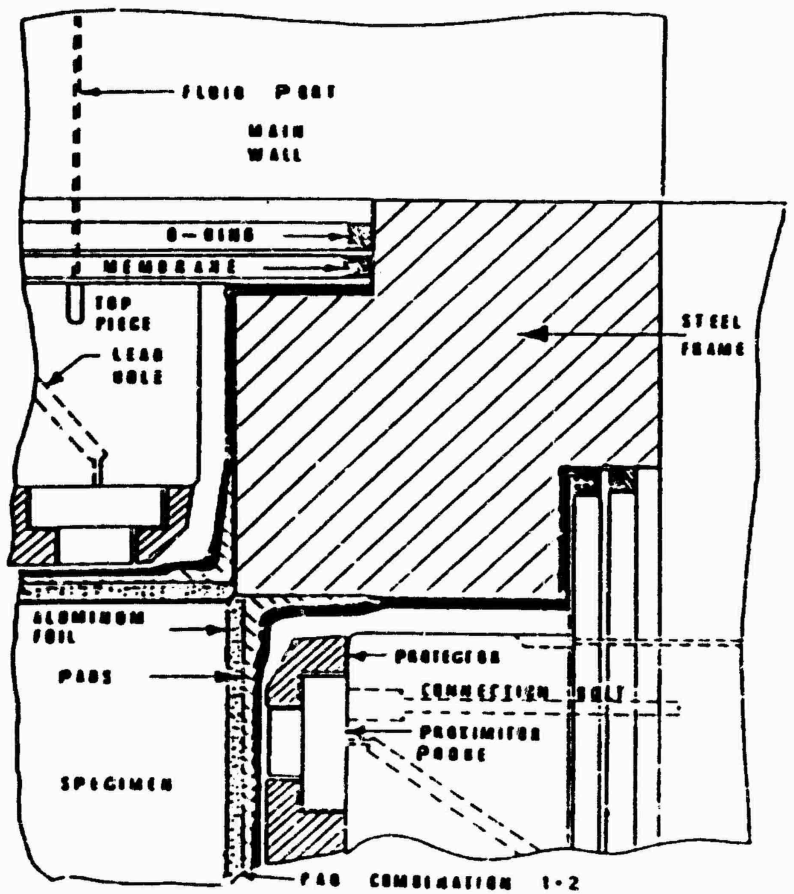

Figure 6. Details of assembled true triaxial device (from Reference 18).

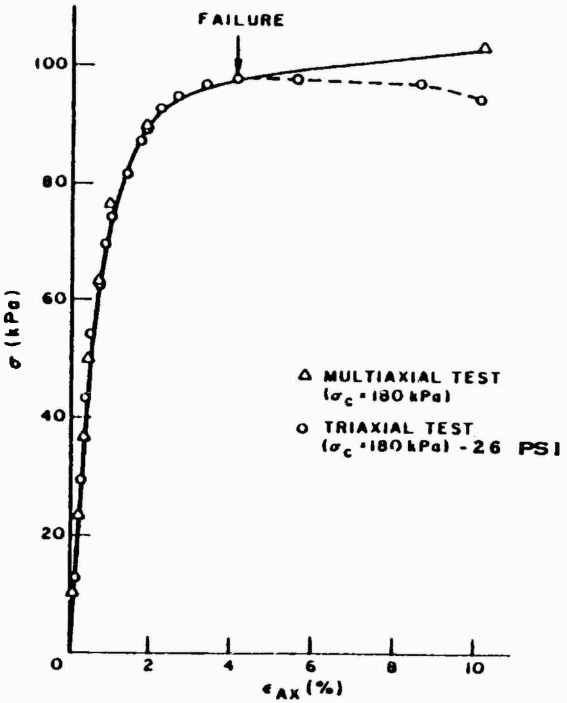

Figure 7. Stress-strain curves for triaxial and multiaxial tests (from Reference 18).

operating on the inductive principle, sense the movement of an aluminum foil target placed on the surface of the specimen, and have sensitivity on the order of 1×10^{-5} inches. Three such transducers are used on each side of the cell. The sum of the mean readings of opposite groups of transducers gives the normal strain in that direction, while the three transducer readings on each side define the plane of the deformed specimen on that side. The scalar product of the outward normal vectors on adjacent planes will then define the shear strain between those planes. Thus, the complete strain state is defined from the readings of the 18 proximity probes. The ability to measure the shear strains makes this device particularly suitable for testing anisotropic materials.

This device was originally designed and used for testing rocks, concrete and composites to 20,000 psi, materials which are much stiffer than soil. It was, therefore, ideally suited for the present program since the system flexibility would be negligible compared to specimen deformation. The pressures applied to the specimen through the fluid cushions were generated by hand pumps. A data acquisition system fed the proximity transducer readings to an HP 9830 calculator which analyzed the data and drove a plotter to produce stress-strain curves. This on-line data reduction enables decisions to be made during the test for changes in the load path.

Although the true triaxial device is stress-controlled, it can be made to follow a prescribed strain path through intricate manual operation. This approach was used in the present study, and was accomplished by, first, examining the stress-strain behavior of a test specimen after each load increment and then, on the basis of the previous response, predicting the next load increment so that the prescribed strain path would be followed. The success of this procedure clearly depends upon the operator's ability to predict the next load increment, which requires considerable knowledge of the general constitutive behavior of the soil being tested. The results from standard laboratory tests conducted earlier were of particular value in this regard.

With the true triaxial device, one seeks to apply an ideal set of boundary conditions to a cubical test specimen that are known, uniform and controlled. To the extent that such conditions are not achieved, the measured behavior will reflect the effects of the nonuniformity and the unknown effects. Only when conditions of uniform stress and uniform strain can be shown to exist within a test specimen, or when the deviations from these ideal conditions are considered to be acceptable, can one have confidence that the true material properties are being measured. The success of the present study clearly depends upon having high quality soil data. Since all of the data in this study were obtained with the cubical triaxial device described in Reference 17, some comments about the ability of this device to apply homogeneous states of stress and strain to a specimen are given below.

2.2.2 Validation

The cubical test device used in the present study has evolved from earlier designs developed by Ko and his coworkers, and represents the latest advancement in such devices. In recent years, considerable effort has been made to investigate the ability of these fluid cushion true triaxial devices to generate homogeneous states of stress and strain within a specimen. Most of this work has utilized photoelastic techniques to measure the deviation of shear stress within a specimen from the ideal homogeneous state. In other work, direct comparison between cubical triaxial data and conventional triaxial data have been made.

For the cubical triaxial device used in the present study, Berends and Ko[18] have reported the results of an investigation to validate its ability to apply homogeneous states of stress and strain. For this purpose, a photoelastic study of the response of a polyurethane cube to bi-axial loading was conducted, and the results from the cubical test were compared with those from a conventional triaxial device. The photoelastic study showed that the deformation

was most homogeneous when the ratio of the biaxial normal stresses was large (uniaxial loading), and became less homogeneous as that ratio approached unity (equal biaxial loading). Furthermore, the inhomogeneity increased with the magnitude of deformation. Based upon the test results, it was concluded that the use of this device should be limited to normal strains of 10 percent or less and to normal strain ratios of 0.75 or less. At 10 percent normal strain, the maximum shear strain deviation from homogeneity was found to be 4 percent and concentrated at the corners. Below the above operational limits, Nymoen found,[19] through photoelastic techniques, that the homogeneity of stress and strain is at least twice as good as that found in a conventional triaxial device.

Laboratory tests were also conducted on a remolded clay using both the cubical triaxial device and a conventional triaxial device. In both cases, the clay was subjected to triaxial compression at a confining pressure of 180 kPa (26 psi). The results from these tests are depicted in Figure 7, where it can be seen that the stress-strain responses measured by both devices are in excellent agreement up to the point of failure.

On the basis of the results from the studies described above, it is believed that the fluid cushion true triaxial device used in this study generates states of stress and strain within a test specimen that are very nearly homogeneous, and is therefore capable of providing measurements of the true constitutive properties of the soil tested, provided that the soil is homogeneous.

2.3 LABORATORY TESTS ON RALSTON VALLEY SOIL

The results from the laboratory tests performed on Ralston Valley soil have been described in detail in References 3 and 4. The purpose of this section is to identify and discuss any special aspects of the testing and data which should be taken into consideration when using the data for the purpose of evaluating models.

2.3.1 Standard Laboratory Tests

The standard laboratory tests reported in Reference 3 were performed with skill and care, as is evidenced by the reasonably good reproducibility of the data. There are, however, several aspects of the tests and data that should be noted.

First of all, there's the issue of precompression. In each of the soil tests, the remolded test specimen was first compressed hydrostatically up to some small pressure to ensure that it was fully seated in the device. The test data reported in Reference 3 actually start from this initial precompressed state. Unfortunately, the initial precompression imposed on the specimens was not the same in all the tests; it varied from 25 psi (for the hydrostatic compression tests up to 150 psi) to 75 psi (for two of the hydrostatic compression tests up to 700 psi). Inasmuch as the soil was quite compactive, the differences in initial precompression would have a significant effect upon the resulting response data, particularly the hydrostatic data.

Because of the differences in initial prestrain, it was necessary for the modelers to take these differences into account in fitting their models to the hydrostatic data. If some provision is made for the initial prestrains, however, the hydrostatic data appear to be quite consistent, as illustrated in Figure 8. To construct this figure, the data from the two hydrostatic tests up to 150 psi, i.e., tests 6-HC-160-1 and 9-HC-150-2, were plotted without modification. Then, the curve for test 5-HC-700-2, which had an initial precompression of 50 psi, was translated to the right along the strain axis by an amount $\Delta\epsilon_v = 0.007$ until the initial point on the curve at 50 psi fell midway between the two existing curves at the 50 psi level. Similarly, the curves for tests 3-HC-700-1 and HC-700-3 were translated to the right by an amount $\Delta\epsilon_v = 0.011$ until the initial points of the curves at 75 psi fell midway between the existing curves at the 75 psi level. In future testing, it is

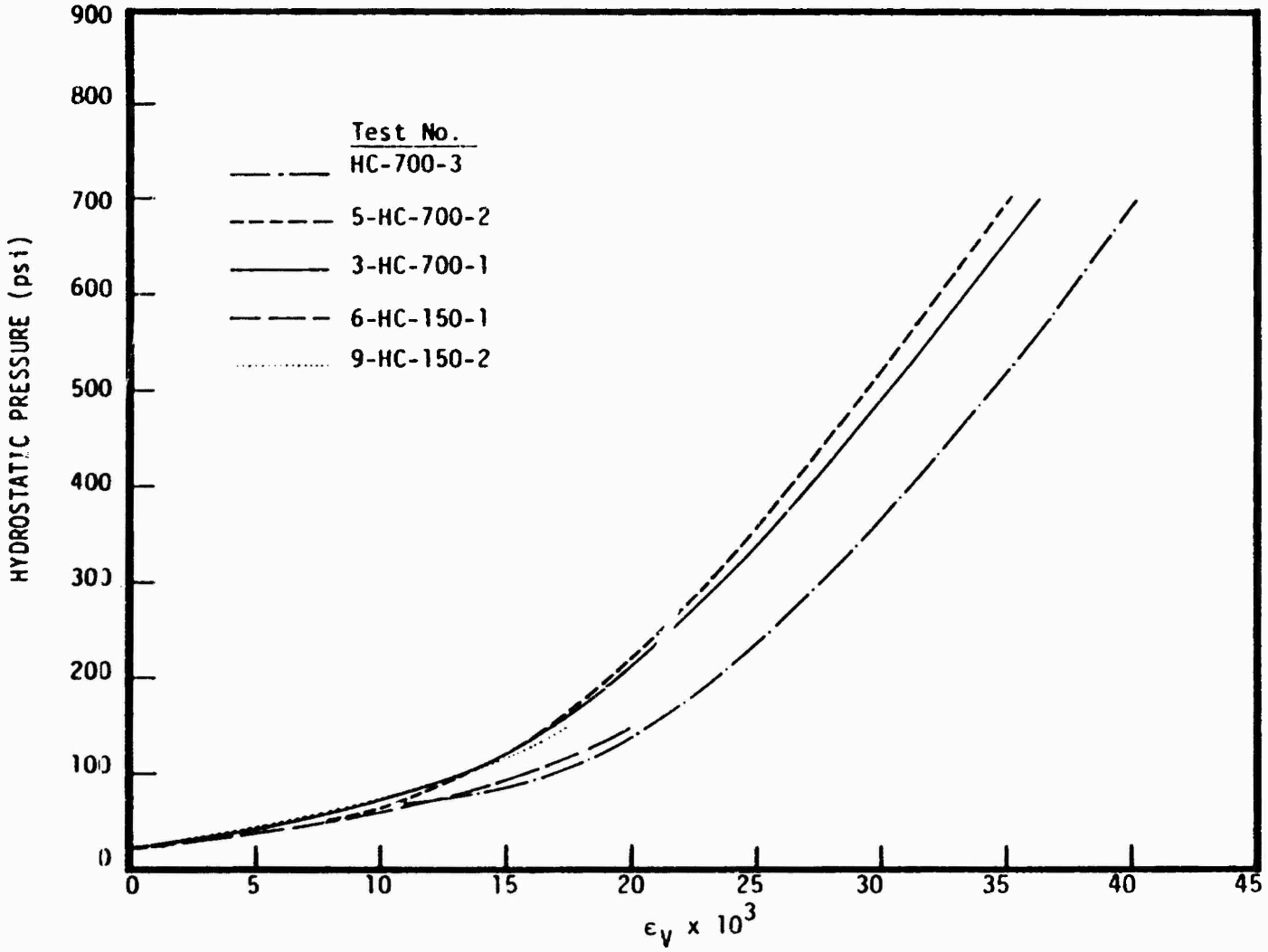

Figure 8 . Summary of measured loading paths for hydrostatic compression of Ralston Valley soil. Paths have been suitably shifted to allow for differences in initial pre-compression states. (Data are from Reference 3.)

recommended that a single initial precompression state be used on all test specimens, to eliminate the difficulties mentioned above in using the data for fitting models.

The results from the hydrostatic compression tests can also yield valuable information about the possible anisotropy of the remolded test specimens. If a specimen is initially isotropic and remains so during straining, pure hydrostatic compression will result in isotropic straining in which all three principal strains are equal. However, if the specimen is initially anisotropic, or if it develops anisotropy through straining, pure hydrostatic compression will result in unequal principal strains. In view of the fact that the specimens used in this study were remolded through a process of anisotropic consolidation under uniaxial strain conditions, there was a possibility that the specimens might exhibit some initial anisotropy. Such anisotropy, if it exists, would probably be of a form called transverse isotropy, in which there is a plane of isotropy perpendicular to the direction of compaction. If this exists in the specimens, one would expect the hydrostatic data to systematically show that $\epsilon_1 < \epsilon_2 = \epsilon_3$, where ϵ_1 is the strain in the direction of the initial consolidation and ϵ_2, ϵ_3 are the two lateral strains.

A review of the hydrostatic data presented in Appendix A of Reference 3 does not reveal any systematic trend in the three principal strains that would provide evidence of anisotropy in the specimens. It is possible that some small amount of anisotropy was initially present in the specimens, but was masked by the overall scatter in the data. In any event, the available data do not contradict the assumption implicit in all of the models considered herein that the soil is initially isotropic.

2.3.2 Complex Strain Path Tests

As noted earlier, the complex strain path tests on Ralston Valley soil were conducted about a year after the standard

laboratory tests reported in Reference 3. Both series of tests were performed by the same personnel and with the same equipment. Nevertheless, it was felt necessary to repeat some of the earlier tests reported in Reference 3 to ensure that the soil, the specimen preparation and the test procedure had not changed in the meantime. For this purpose, four verification tests were done, and the results from these tests were reported in Reference 4. It was found that the new data fell within the scatter of the previous data, but with a slight bias toward a stiffer response. On this basis, it was concluded that no significant changes had taken place in the soil or the test procedures, and that the earlier data reported in Reference 3 were still valid for use in fitting the models.

The results from the complex strain path tests are depicted in Figures 9 to 11. The strain paths, as shown, are measured from the ends of the initial hydrostatic compressions, while the entire stress paths are shown from the initial unstressed state. A small black circle with the letter s denotes the start of a complex stress path. In the figures, the σ_i and ϵ_i are the principal stresses and principal strains, respectively. The subscript 1 corresponds to the direction in which the soil was compacted during the remolding process, while the subscripts 2 and 3 denote directions perpendicular to the compaction axis. Keeping in mind that the magnitudes of the strains in path No. 2 are considerably smaller than those in either paths No. 1 and 3, it can be seen from the figures that paths 1 and 2 were followed in the laboratory tests with about the same relative error. As far as path 3 is concerned, one of the laboratory tests followed the prescribed path quite accurately, except for the final leg of the path, while the other test involved considerable discrepancy. Unfortunately, one cannot predict the extent to which errors in tracing these paths translate into errors in the stress response, since this would require an exact constitutive model of the soil.

It is unfortunate that the standard laboratory tests did not cover the stress range encompassed by complex strain path No. 3.

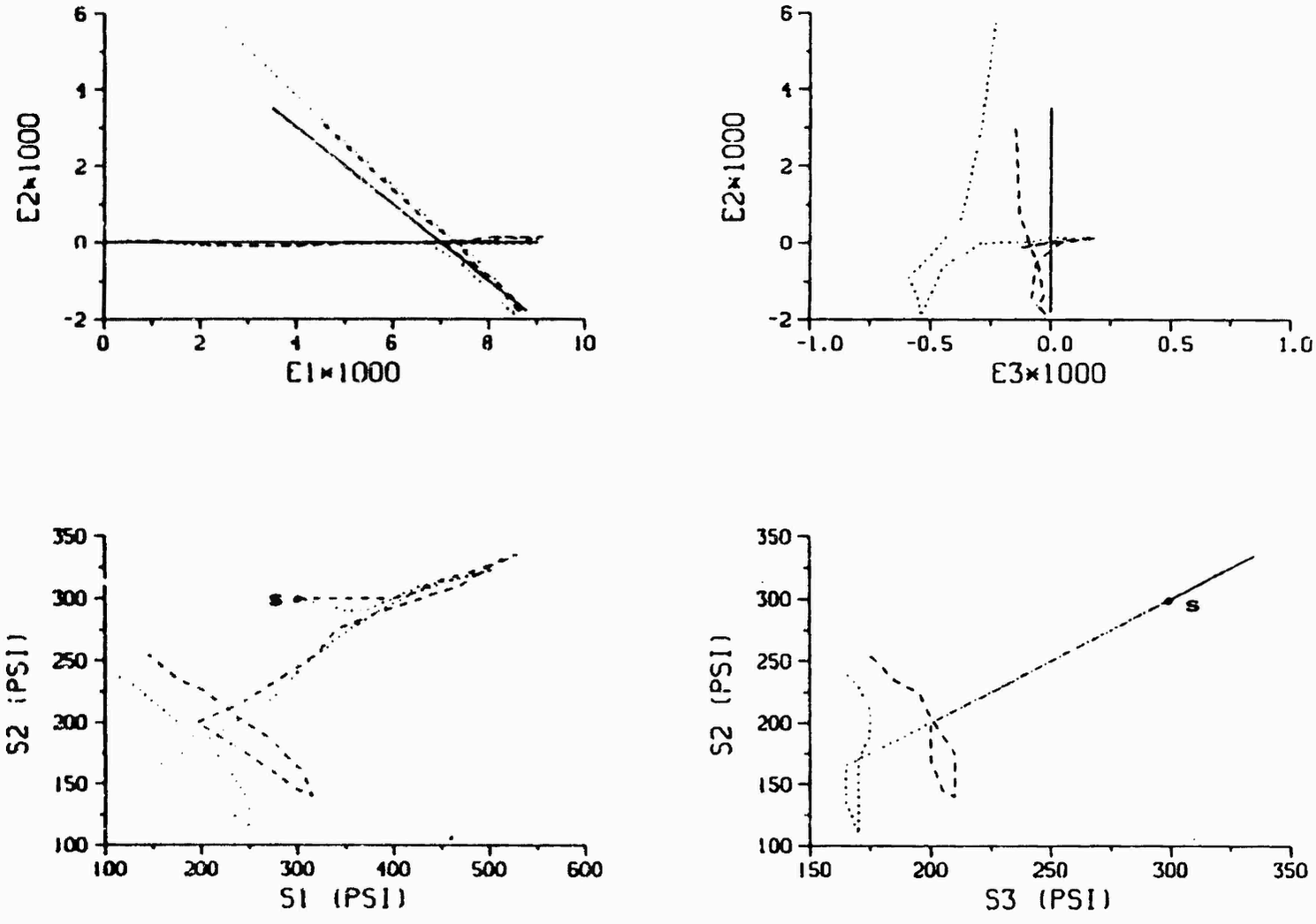

Figure 9. Results from laboratory tests on Ralston Valley soil for complex strain path No. 1.

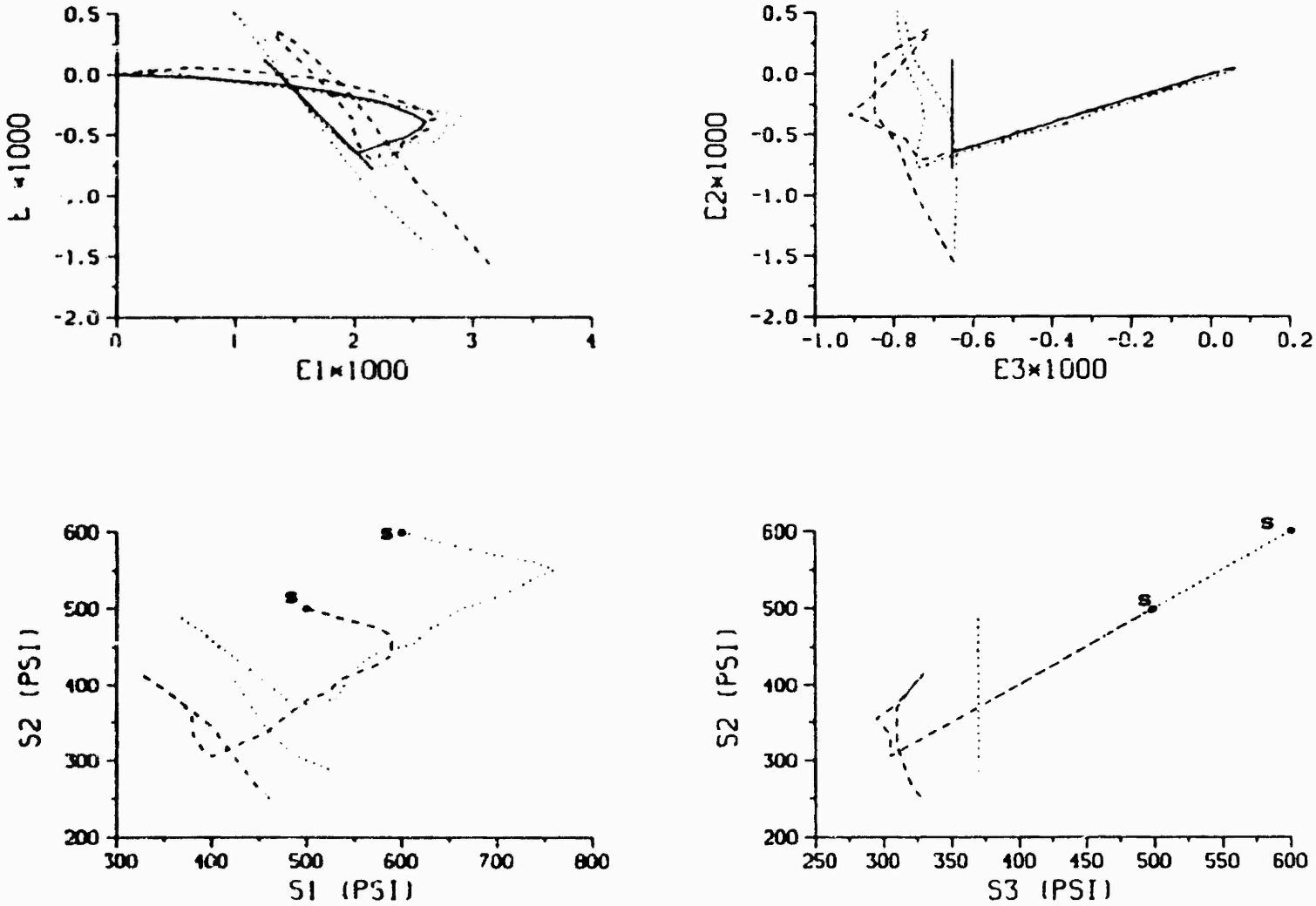

Figure 10. Results from laboratory tests on Ralston Valley soil for complex strain path no. 2.

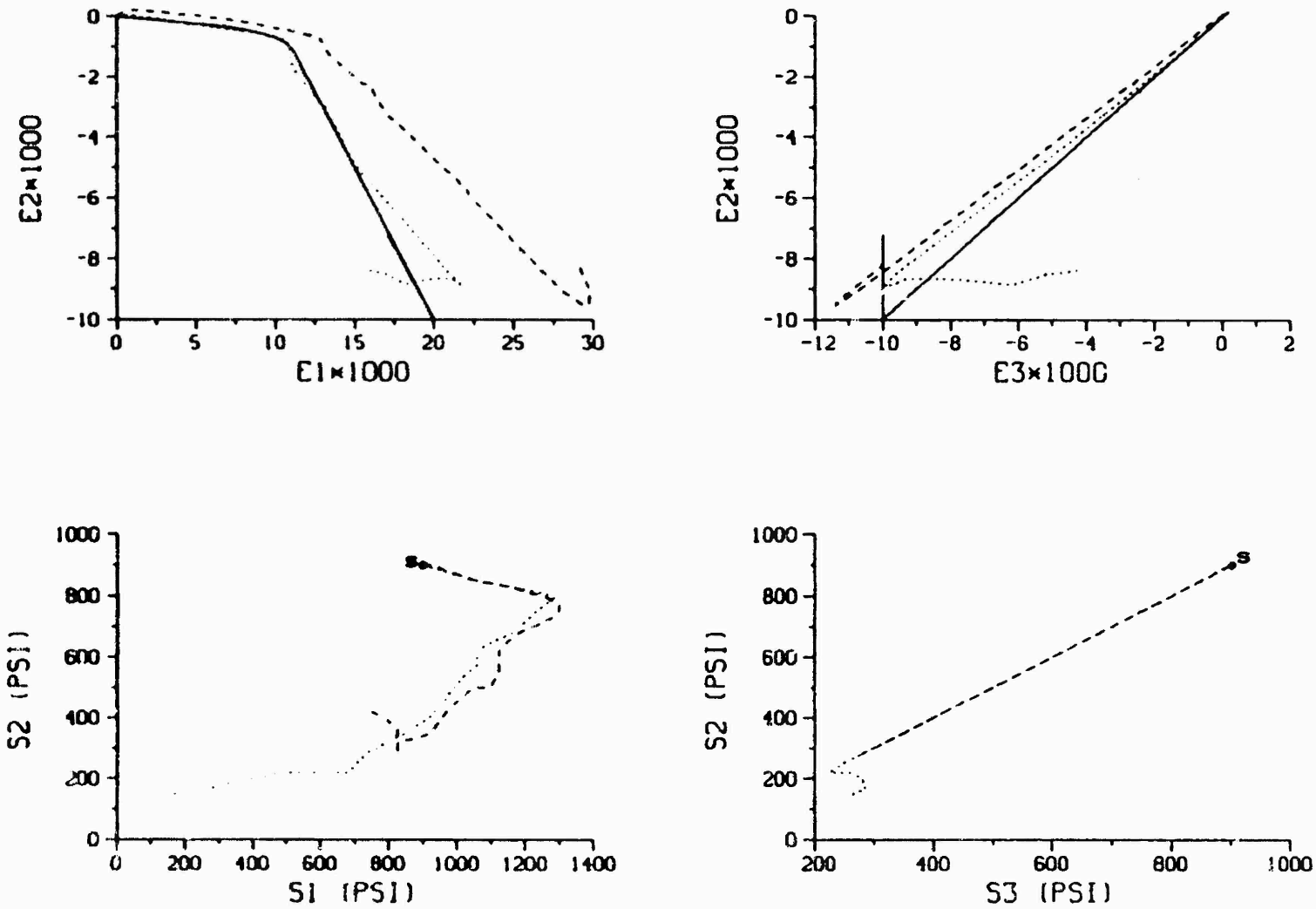

Figure 11. Results from laboratory tests on Ralston Valley soil for complex strain path No. 3.

This was due to the fact that these tests were designed and conducted well before the complex strain path tests were performed. As noted earlier, the initial hydrostatic states from which the complex strain path tests were initiated, were selected by Professor Ko, after some experimentation, so that none of the principal stresses ever became tensile during a strain path excursion. For complex strain path No. 3, the initial hydrostatic compression that was found necessary to satisfy this requirement was 900 psi, which was well outside the pressure range covered by the standard laboratory tests reported in Reference 3. In view of this, the laboratory data reported in Reference 4 for complex strain path No. 3 are not considered to be a valid standard for use in the present study to evaluate the models' predictive capabilities.

3. THE SOIL MODELS

The purpose of this section is to briefly describe each of the six advanced soil models considered in the present study, and to indicate what, if any, revisions were made in each model for special application to the present study. Since detailed mathematical descriptions of the models can be found in the literature, we refer the reader to the appropriate references cited herein for further details. Specific values of the material parameters used with each of the models in the present study can be found in Appendix C.

3.1 THE AFWL ENGINEERING MODEL

The AFWL Engineering Model, also known as the "stick" model, has been used by the AFWL and its associate contractors in ground motion studies for a number of years. Basically, it is an elastic-plastic model, but not in the classical sense, since it employs a non-associated plastic flow rule and allows for strain softening. It contains a failure surface and, in effect, a capped yield surface. The failure surface is of the Drucker-Prager form at low pressures, and becomes a von Mises surface at higher pressures. The capped yield surface, which is not explicitly treated, is nevertheless, a plane perpendicular to the hydrostatic axis. As material undergoes volumetric compaction, the cap moves irreversibly outward along the hydrostatic axis. At any instant, the cap intersects the hydrostatic axis at a point corresponding to the maximum hydrostatic pressure attained up to that time. The deviatoric and volumetric components of plastic strain are governed by separate and uncoupled flow rules. Deviatoric plastic strain follows a non-associated flow rule in which the plastic potential is of the von Mises type. The volumetric plastic strains are, in effect, governed by an associated flow rule, where the association is which the planar capped yield surface. As a result, the model cannot describe either dilatancy or densification due to shearing.

The predictions reported in this study for the AFWL Engineering Model were made by Dr. Sheldon Schuster (California Research and Technology). Except for one modification, the basic version of the model described in Reference 5 was used for this purpose. The modification consisted of revising the hydrostatic unloading behavior to account for nonlinearity. Details of this modification, as well as a listing of the values of the model's parameters used in this study, are given in Appendix C. The model requires 32 material parameters.

3.2 LADE'S ELASTO-PLASTIC MODEL

This model was developed by Professor P. V. Lade (UCLA) and is described in detail in Reference 8. Basically, it is an elastic-plastic model which contains a spherical cap and a failure surface. The spherical cap expands outward due to work hardening, while the failure surface work hardens up to a point and then work softens. The trace of the failure surface in the deviatoric plane is essentially triangular, and is in excellent agreement with failure data for a variety of soils. Elastic behavior is governed by an incremental form of Hooke's law in which the moduli are taken to depend in a nonlinear manner on stress. The plastic flow rules embodied in the model were developed from data on sands. If the deformation is such that the behavior is controlled solely by the spherical cap, an associated plastic flow rule is employed. Conversely, a non-associated flow rule is used when plastic flow is governed by the failure surface. For the cases in which the cap and failure surface jointly control the behavior, such as when a stress state lies near the intersection of the cap and failure surface, a combination of associated and non-associated flow rules is used, so that Koiter's rule for plastic flow at the corner of a yield surface is satisfied. Additionally, the model accounts for coupling between volumetric and deviatoric components of deformation, and therefore can describe both dilatancy and densification.

The predictions reported in the present study for this model were made by Professor Lade, using the version of the model described in Reference 8. No special modifications were made to the model for this study. A list of the values of the 14 material parameters of the model used in the present study is given in Appendix C.

3.3 PREVOST'S NESTED SURFACES MODEL

This model is an elasto-plastic model that exploys a system of nested yield surfaces which translate and expand (or contract) with the deformation. It was developed by Professor J.-H. Prevost (Princeton University) and is described in detail in Reference 9. It is built upon the combined notions of kinematic and isotropic hardening plasticity, and incorporates concepts from critical state theory. The nested yield surfaces are taken to have the shapes of ellipsoids in principal stress space. A small purely elastic region exists in the interior of the smallest ellipsoidal surface. The allowable states of stress are bounded by a plane perpendicular to the hydrostatic axis and cutting it at zero pressure, and an outer yield surface; the model, therefore, does not allow hydrostatic tension.

A non-associated plastic flow rule is used in conjunction with all of the interior yield surfaces, while an associated flow rule is employed with the outer yield surface. The non-associated flow rule is chosen so that the projection of the plastic strain increment vector is always normal to the trace of the corresponding inner yield surfaces in an octahedral plane. The yield surfaces cut the octahedral plane in circles which, in general, are not concentric with each other nor with the origin of the octahedral plane.

The model accounts for the effect of pressure on plastic yield, and for coupling between the deviatoric and volumetric modes of deformation; therefore, it can describe both dilatancy and

densification. Additionally, it can describe strain softening. The nested yield surfaces provide the model with the capability to describe hysteretic response, including cyclic creep (ratcheting).

The predictions for the present study were made by Professor Prevost, using the version of the model described in Reference 9. No modifications to this model were made for the present study. A total of eight (8) nested yield surfaces were used. A listing of the values of the 79 material parameters used in this model can be found in Appendix C.

3.4 S-CUBED ENDOCHRONIC MODEL

This model, which is described in detail in Reference 10, was recently developed by Dr. H. E. Read (S-CUBED), Dr. J. A. Trangenstein (S-CUBED) and Professor K. C. Valanis (University of Cincinnati). It is an outgrowth from a new and improved endochronic plasticity theory for soils described in Reference 11. The model represents a radical departure from the other soil models considered in this study in that it does not require the notion of yield surface nor the introduction of loading or unloading criteria. It predicts that plastic deformation will accumulate in a gradual continuous manner from the onset of loading, a feature which allows it to describe hysteretic behavior during unload-reload cycles, including cyclic creep (ratcheting).

In essence, the model is based upon the hypothesis that the current state of stress is a linear functional of the entire history of deformation, where the history is defined with respect to a "time" scale, called intrinsic time, which is itself a property of the material at hand. The intrinsic time is defined as the path length in plastic strain space. Although the model does not have a yield surface, it does exhibit a failure surface, which intersects an octahedral plane in the form of a circle concentric with the origin. Due to the absence of a yield surface, the plastic flow behavior predicted by the model cannot be classified as either associated or non-associated. However, it can be shown that the

plastic strain increment predicted by the model is coaxial with the immediately preceding stress increment. In summary, the model consists of a linear functional relating the stress to the history of plastic strain, an incremental form of Hooke's law in which the moduli depend on the pressure, and an expression relating the intrinsic time to the length of the plastic strain path.

The predictions for this model reported in the present study were made by Dr. Read and Mr. R. G. Herrmann (S-CUBED). For this purpose, the model described in Reference 10 was used with several modifications. A complete description of the basic equations of the model used herein is given in Appendix C. together with a listing of the values of the material parameters. The model has 27 parameters.

3.5 THE WEIDLINGER CAP MODEL

The Weidlinger Cap model was developed by Professor F. L. DiMaggio (Columbia University) and Dr. I. S. Sandler (Weidlinger Associates), and has been in use for about a decade in the defense community. Complete details of the model, as well as a corresponding computer program, can be found in Reference 6. In essence, the model consists of an ultimate failure surface, a capped yield surface, and an associated plastic flow rule. The cap expands or contracts depending upon whether the plastic volumetric strain increases or decreases, respectively. Additionally, the failure surface cuts the octahedral planes in circles concentric with the origin. Elastic behavior is governed by an incremental form of Hooke's law with constant moduli. The model allows for shear-volumetric coupling and, consequently, it is capable of describing both dilatancy and densification. However, since the model is governed by the principles of classical plasticity, it is not capable of describing strain softening. Finally, the effect of air-filled porosity in soils is accounted for through an irreversible hydrostat, which is controlled by the cap.

Dr. Sandler made the predictions with this model for the present study. The basic version of the model described in Reference 6 was used for this purpose, with one exception, namely, the bulk modulus was taken to be pressure dependent. Details of this revision are given in Appendix C, together with a list of the values of the 9 material parameters used in the study.

3.6 THE WES CAP MODEL

The WES Cap model is an outgrowth of joint work by Dr. George Baladi (WES), Dr. Ivan Sandler (Weidlinger Assocs.) and Professor Frank DiMaggio (Columbia University), and has been in use by the defense community for about a decade. Details of the model are given in Reference 7. It has many features in common with the original cap model described in Reference 6, but it also differs in significant ways. Basically, the model consists of an ellipsoidal, capped yield surface joined to a Drucker-Prager type failure envelope, and an associated plastic flow rule. Elastic behavior is governed by an incremental form of Hooke's law in which the moduli depend, in general, upon the pressure and the plastic work associated with the failure surface. The slope of the Drucker-Prager failure surface is not fixed, but depends upon the plastic work, thereby allowing the surface to expand (harden) or contract (soften) isotropically. The capped yield surface exhibits strain hardening which depends upon the history of the plastic volumetric strain.

The predictions reported in this study for the WES Cap model were made by Dr. Baladi, using a modified version of the basic model described in Reference 7. The modifications were as follows: The expressions for the elastic moduli, which normally depend upon the pressure and plastic work, were generalized to also include dependence upon the deviatoric stress state and the plastic volumetric strain. Moreover, the cap hardening parameter, κ, was redefined in terms of the variable X. Finally, the expression for the dependence

of the slope of the Prager-Drucker surface on the plastic work was revised. Details of these revisions to the model can be found in Appendix C. A complete list of the values of the model's 28 parameters used in the present study is also given in this appendix.

3.7 CLOSURE

In Table I, some of the salient features of the advanced soil models described in the preceding sections are summarized. Here, the wide diversity between the models becomes apparent, as well as the large differences between the number of material parameters required by the models. The models were selected for consideration in this study because they represent the present state of the art in modeling soil behavior, and also because they represent a variety of different approaches to modeling. In the following section, the ability of these models to describe the measured responses to the three basic complex strain paths will be considered.

TABLE 1

Some Properties of the Advanced Soil Models Considered in the Present Study

Model Name	Model Type	Plastic Flow Rule	Isotropic Behavior	Shear-Volumetric Coupling	No. of Matl. Parameters
AFWL Engineering	Elastic-Plastic	Non-Associated	Yes	No	32
Lade Elasto-Plastic	Elastic-Plastic	Non-Associated	Yes	Yes	14
Prevost Nested Surfaces	Elastic-Plastic	Non-Associated	No	Yes	79
S-CUBED Endochronic	Endochronic	Endochronic	Yes	Yes	27
Weidlinger Cap	Elastic-Plastic	Associated	Yes	Yes	9
WES Cap	Elastic-Plastic	Associated	Yes	Yes	28

4. COMPARISONS BETWEEN PREDICTED AND MEASURED STRESS HISTORIES

This section contains the major results from the present investigation. The stress histories obtained by driving the six selected soil models around the three complex strain paths are presented, and compared with the corresponding stress histories measured in the laboratory with the true triaxial device. The precision with which each of the prescribed complex strain paths was actually followed in the laboratory tests was discussed and illustrated earlier in Section 2.3. Accordingly, in that which follows, we shall present only the predicted and measured stress histories.

The predicted and measured stress histories for the three complex strain paths are shown in Figures 12 to 29. In each case, the stress history shown in a figure begins at the point where the principal stresses σ_1, σ_2 and σ_3 are all equal to the corresponding initial hydrostatic prestress. For complex strain paths Nos. 1, 2 and 3, the initial prestresses were 300 psi, 550 psi and 900 psi, respectively. As before, σ_1 is the principal stress in the direction in which the test specimens were compacted during the remolding procedure, and σ_2, σ_3 are the principal stresses in directions normal to σ_1.

In each figure, the model predictions are shown by the solid line, while the dashed and dotted lines denote the measured stress histories. The symbols Δ and o are used in the figures to identify the measured stress histories which correspond to strain histories shown in Figures 9 to 11.

In comparing the various figures, one must keep in mind that the horizontal and vertical scales differ, in general, from figure to figure. As a result, one cannot simply overlay figures to compare the predictions from different models.

4.1 COMPLEX STRAIN PATH NO. 1

As noted earlier, complex strain path No. 1 is representative of the deformations that soil elements located near the surface and at some range from the source, experience as a result of a nearby near-surface explosion. It consists of uniaxial strain compression, followed by uniaxial strain unloading, and then pure shear. The stress histories predicted by each of the models for this complex strain path are shown, together with the corresponding stress histories measured in the laboratory tests, in Figures 12 to 17. The strain histories begin at the point $\sigma_1 = \sigma_2 = \sigma_3 = 300$ psi, which is the initial hydrostatic prestress state for this path.

If we return to Figure 9, it is seen that the actual strain paths followed in the laboratory tests replicated the prescribed strain path with considerable precision. In view of this, and the close agreement between the two corresponding measured stress histories, it might be concluded that the measured stress histories shown in the figures for complex strain path No. 1 provide a valid test of the models' predictive capabilities. However, there is an additional factor that must be considered.

Two series of tests were actually conducted for this strain path, with an interval of about a year between them. The first series, which was reported in Reference 4, was unsatisfactory for the purposes of the present study because the strain paths differed too greatly from the prescribed path. Consequently, at the request of S-CUBED, a second series of tests was conducted for this strain path about a year later, and considerable precision was achieved in following the prescribed path; the data from these tests are depicted in Figures 12 to 17. Unfortunately, the second series of tests was done by a different operator than the first series and no standard laboratory tests were done at the time to verify that the soil, its preparation and the testing technique were still essentially the same as in the standard laboratory tests reported in

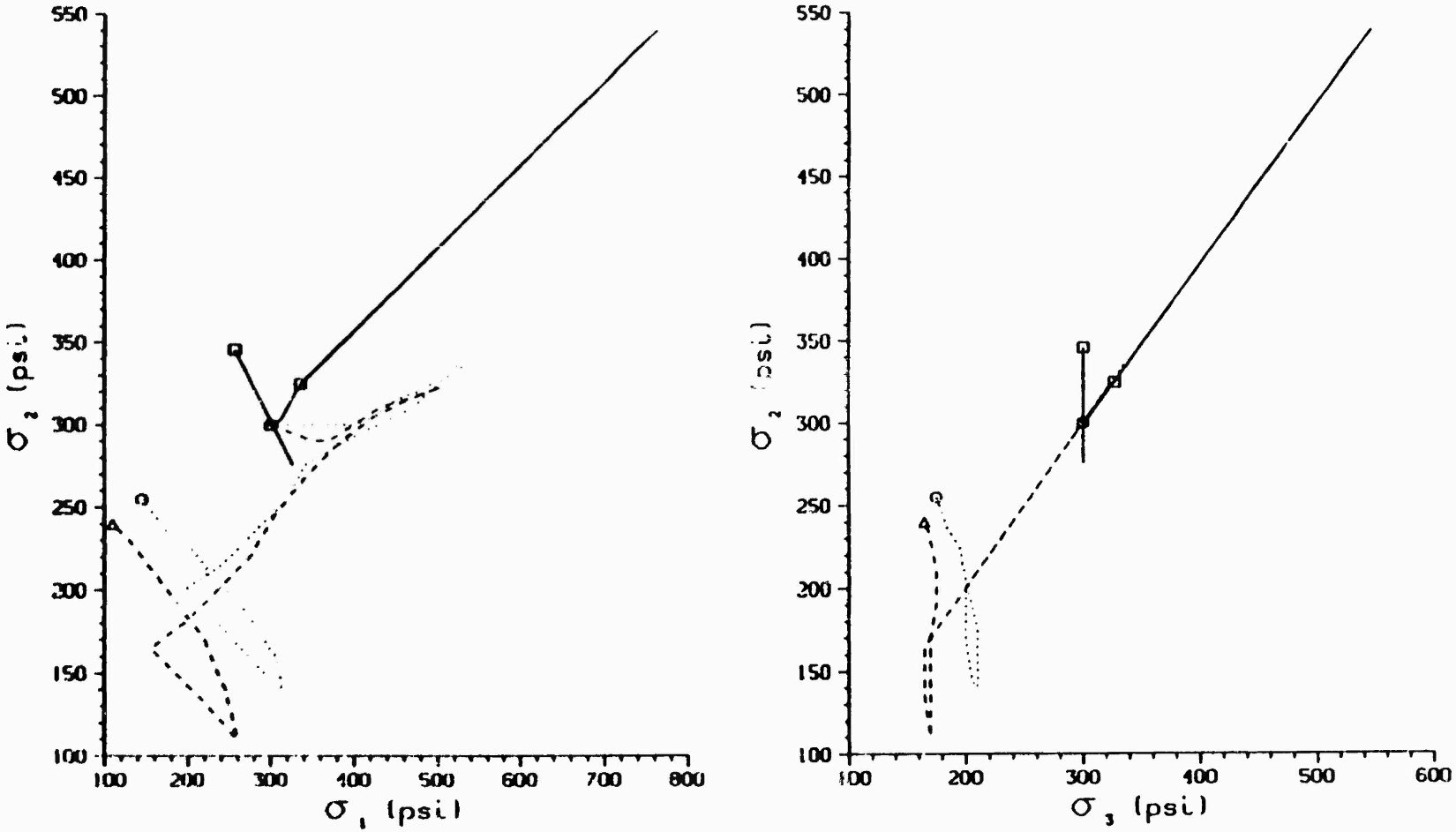

Figure 12. Stress history predicted by AFWL model for complex strain path No. 1. Measured stress histories are shown by dashed and dotted lines.

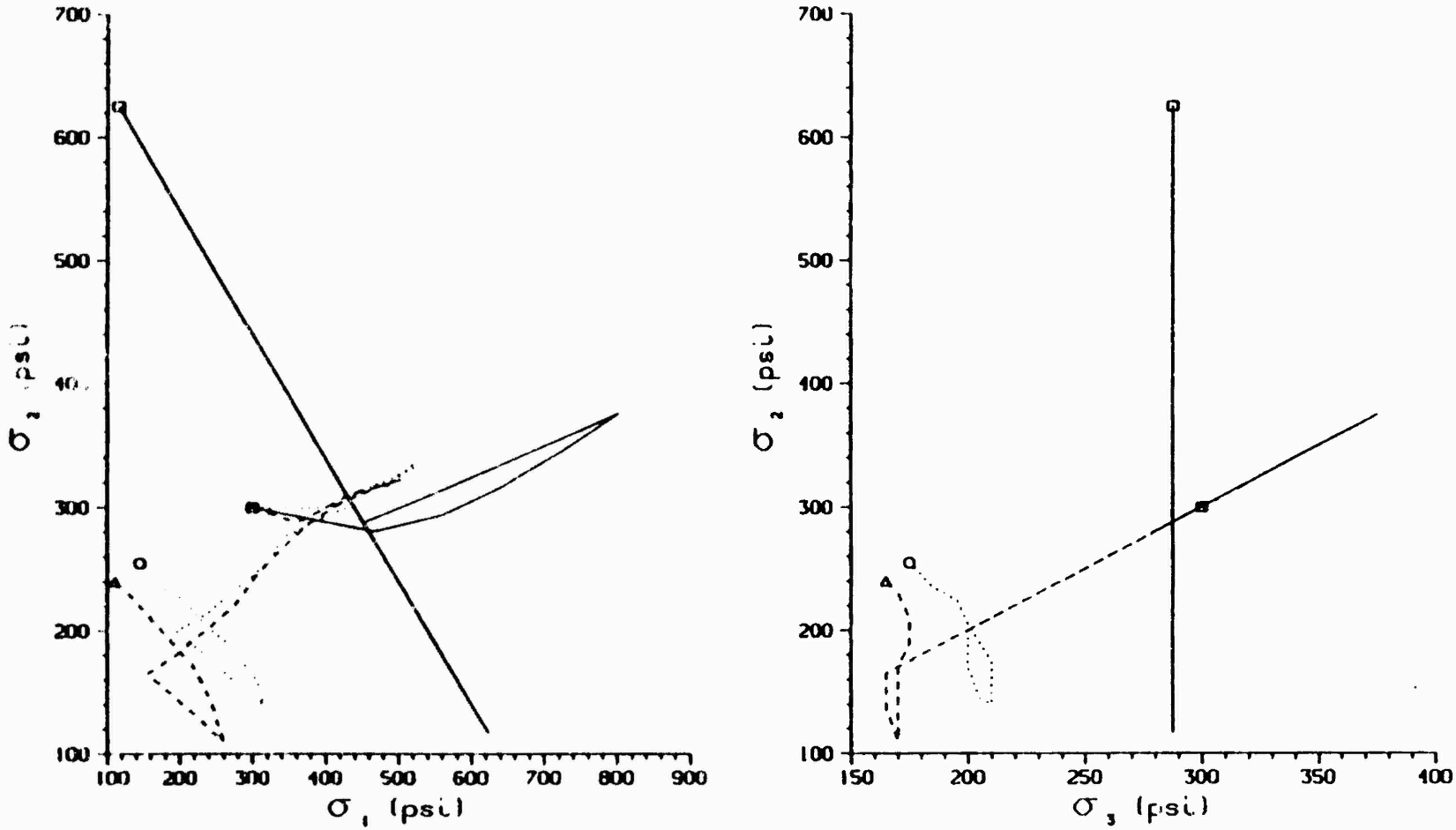

Figure 13. Stress history predicted by Lade's model for complex strain path No. 1
Measured stress histories are shown by dashed and dotted lines.

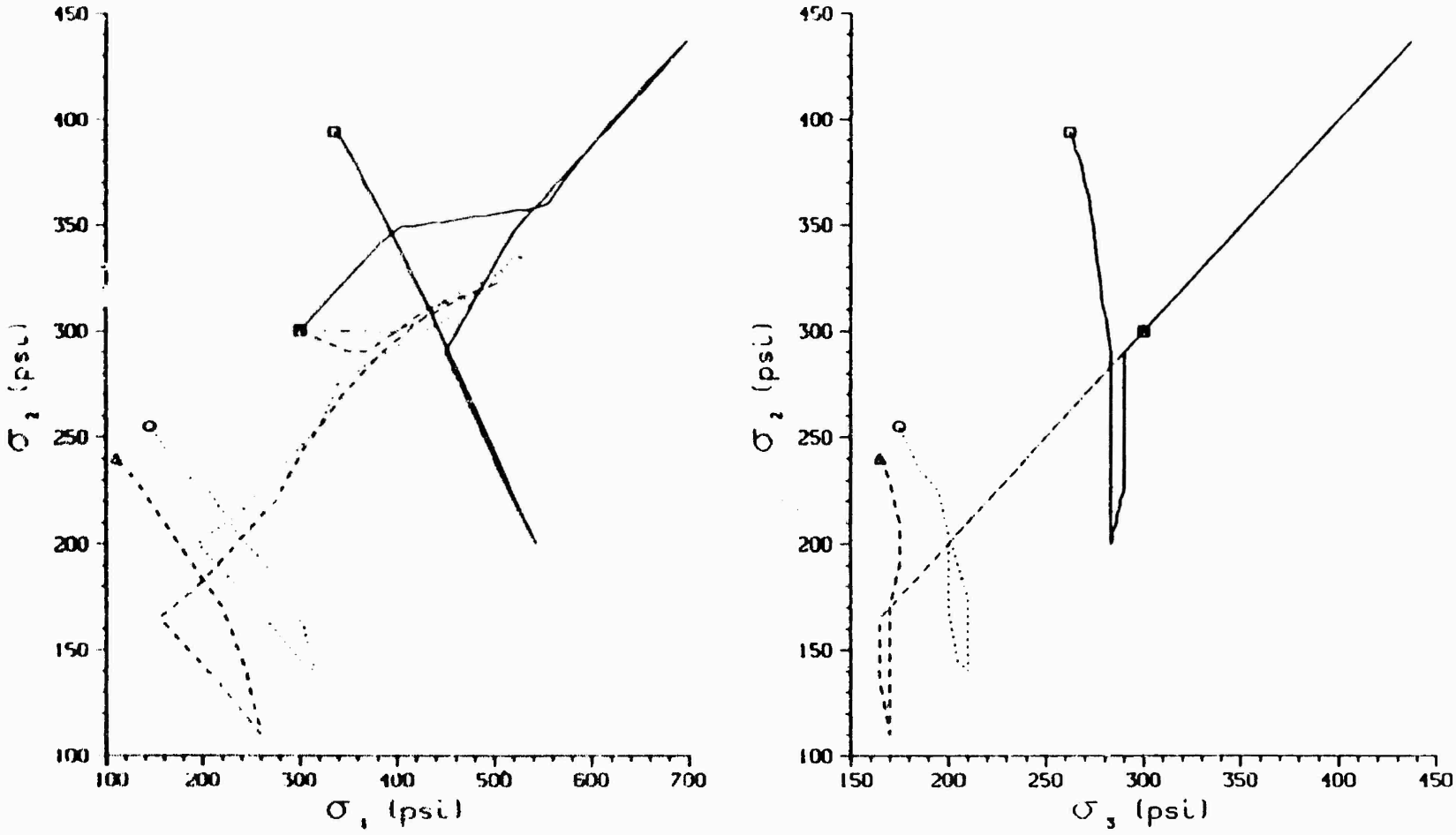

Figure 14. Stress history predicted by Prevost's model for complex strain path No. 1
Measured stress histories are shown by dashed and dotted lines.

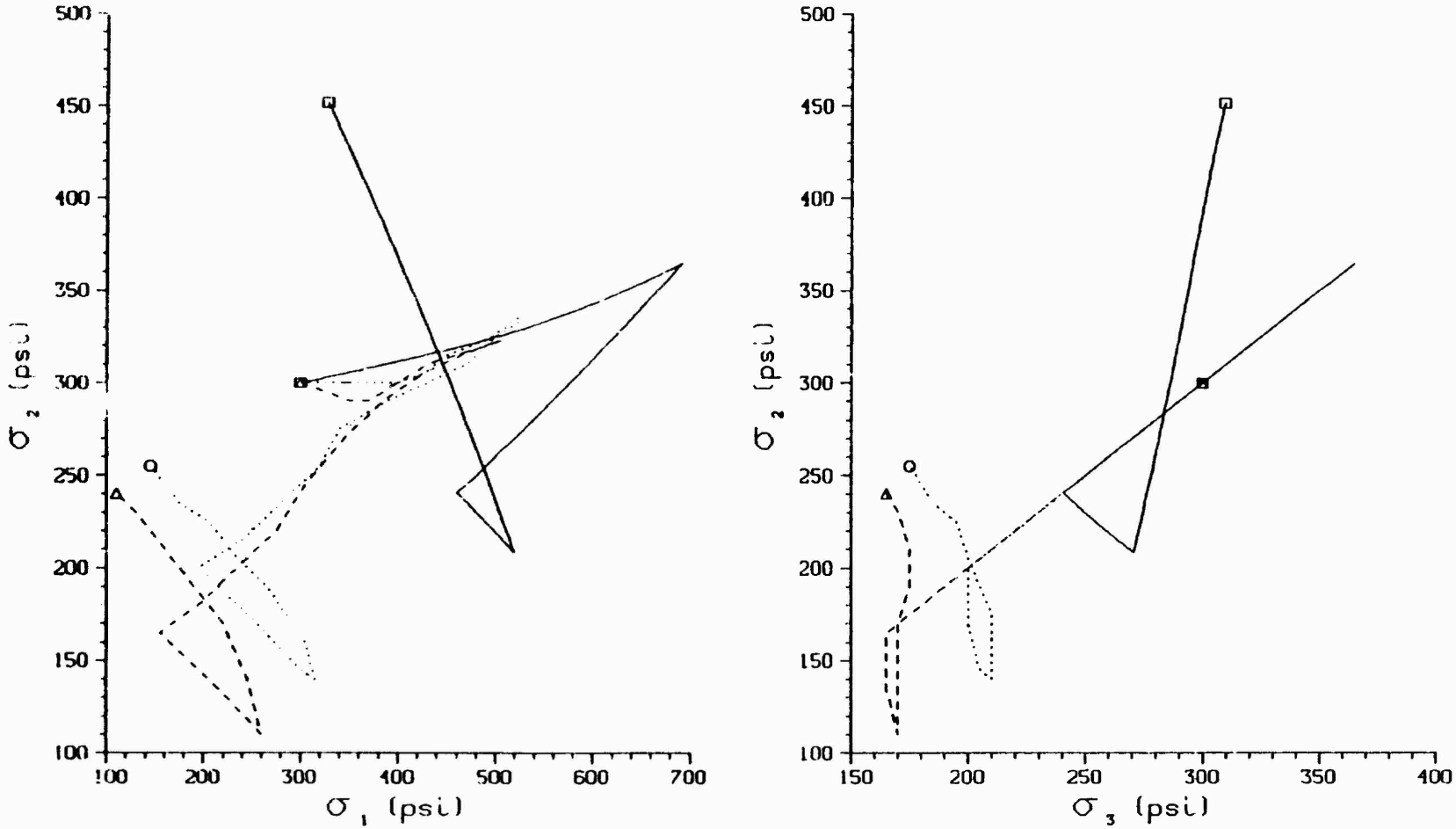

Figure 15. Stress history predicted by S-CUBED Endochronic model for complex strain path No. 1. Measured stress histories are shown by the dashed and dotted lines.

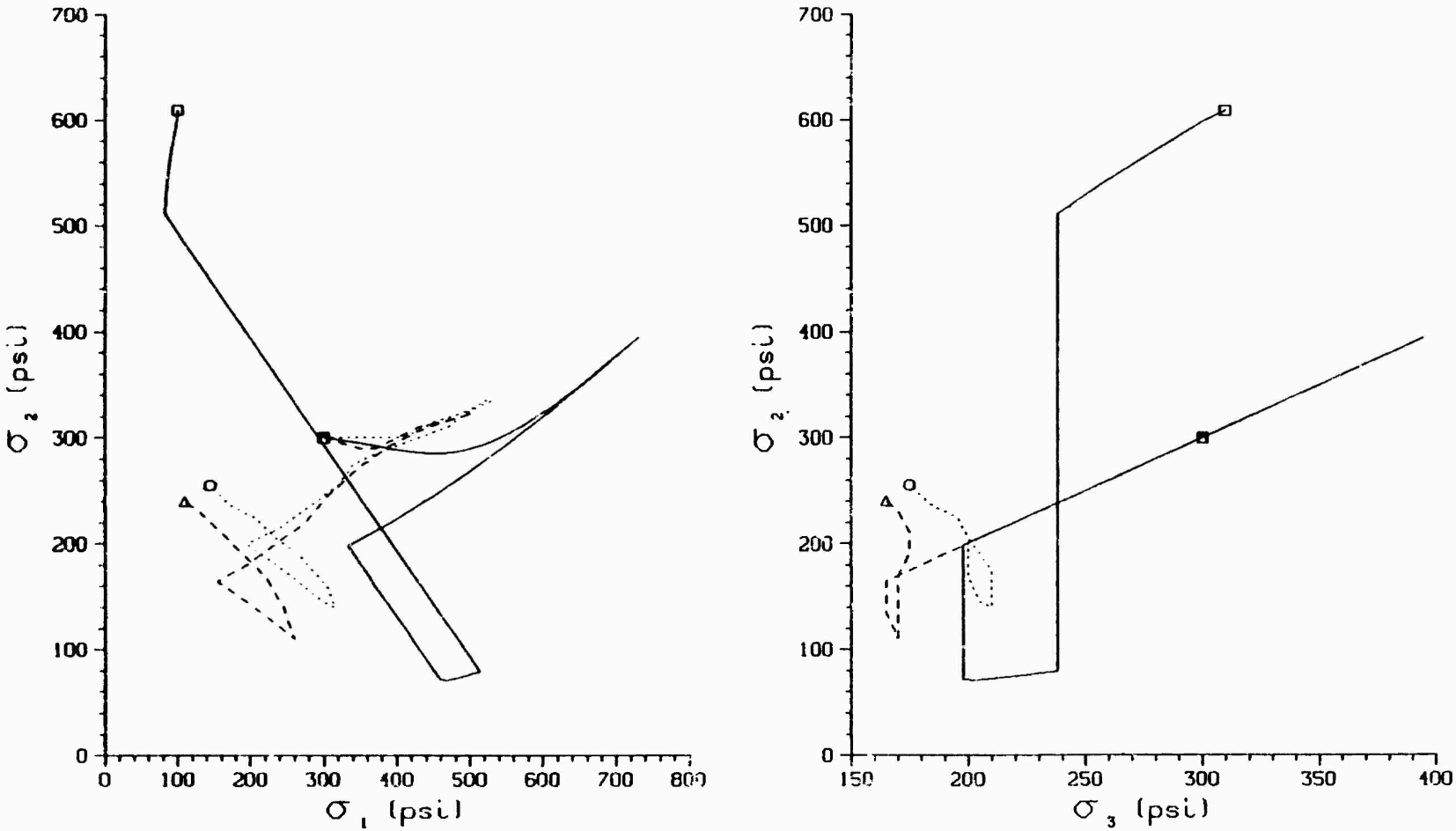

Figure 16. Stress history predicted by the Weidlinger Cap model for complex strain path No. 1. Measured stress histories are shown by the dashed and dotted lines.

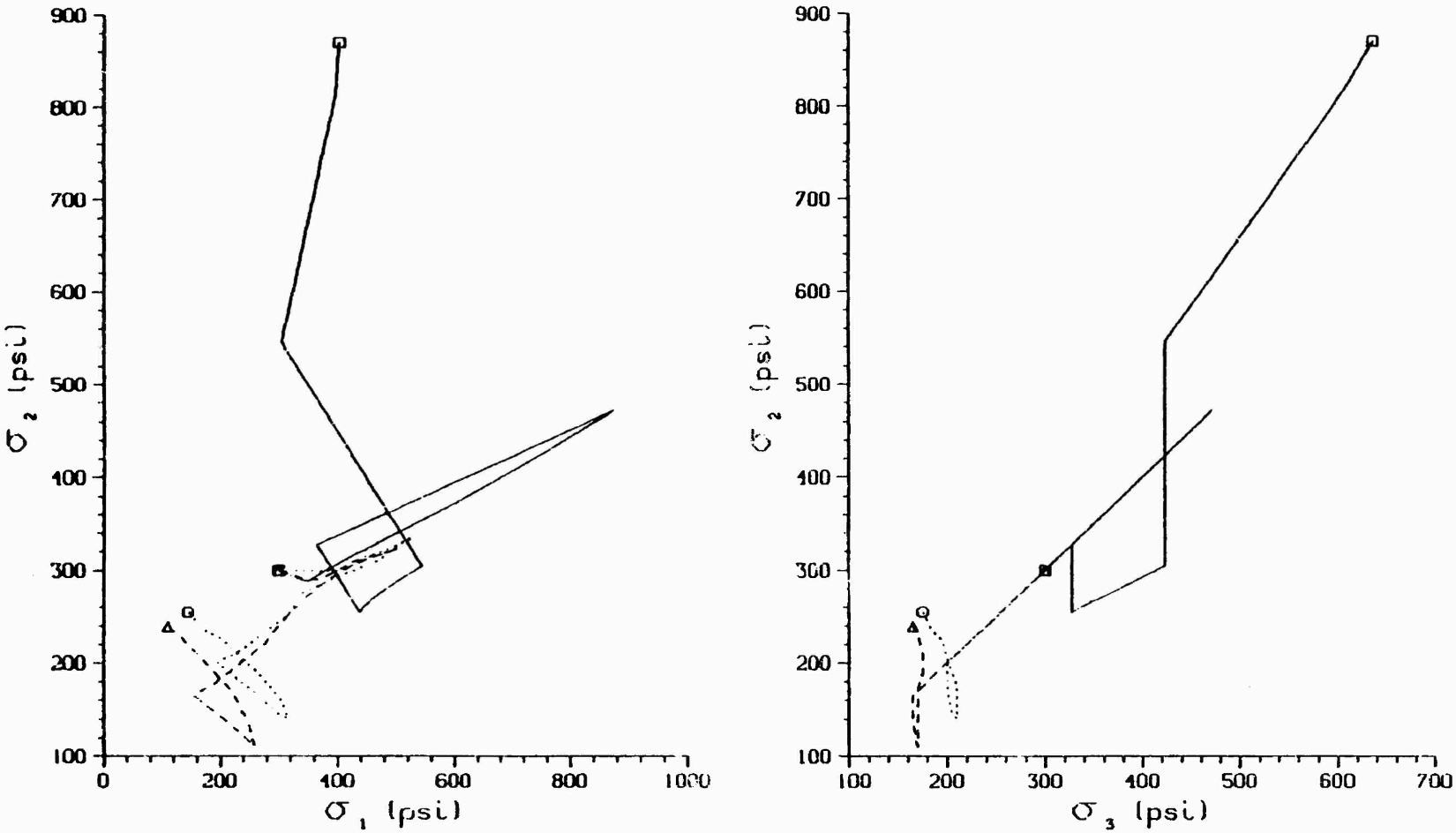

Figure 17. Stress history predicted by the WES Cap model for complex strain path No. 1. Measured stress histories are shown by the dashed and dotted lines.

Reference 3. As a consequence, we cannot say with certainty that the data from the second series of tests are consistent with those reported earlier in Reference 3, which were used in fitting the models. Therefore, despite the excellent reproducibility of the measured stress histories shown in the figures for this case, there may be some question about the validity of using these measured stress histories to judge the models' predictive capabilities against. As an inspection of Figures 12 to 17 will reveal, none of the models does a good job of predicting the measured stress histories.

4.2 COMPLEX STRAIN PATH NO. 2.

Complex strain path No. 2 is associated with soil elements located at some range from the explosive source and at a significant depth. The strain path consists of an initial load-unload process that is very near to being uniaxial strain, followed by pure shear. As reference to Figures 1 and 2 will reveal, the amplitudes of the principal strains for this case are substantially smaller than in complex strain path No. 1. Additionally, the relative error in following the prescribed strain path in the two laboratory tests appears to be somewhat greater in path No. 2.

The stress histories predicted by each of the models for this path are shown, together with the corresponding measured stress histories, in Figures 18 to 23. Note that the predicted stress histories begin at a hydrostatic prestress of 550 psi, while the measured stress histories begin at 500 psi and 600 psi. The reason for this is as follows. It was originally planned that the tests for this strain path would begin from an initial hydrostatic prestress of 500 psi. While one of the two tests was done from this pressure state, the other one was inadvertently started from 600 psi. Unfortunately, no additional tests were done from either of these initial hydrostatic states to establish the reproducibility of the data. Despite this, however, the data from these two tests

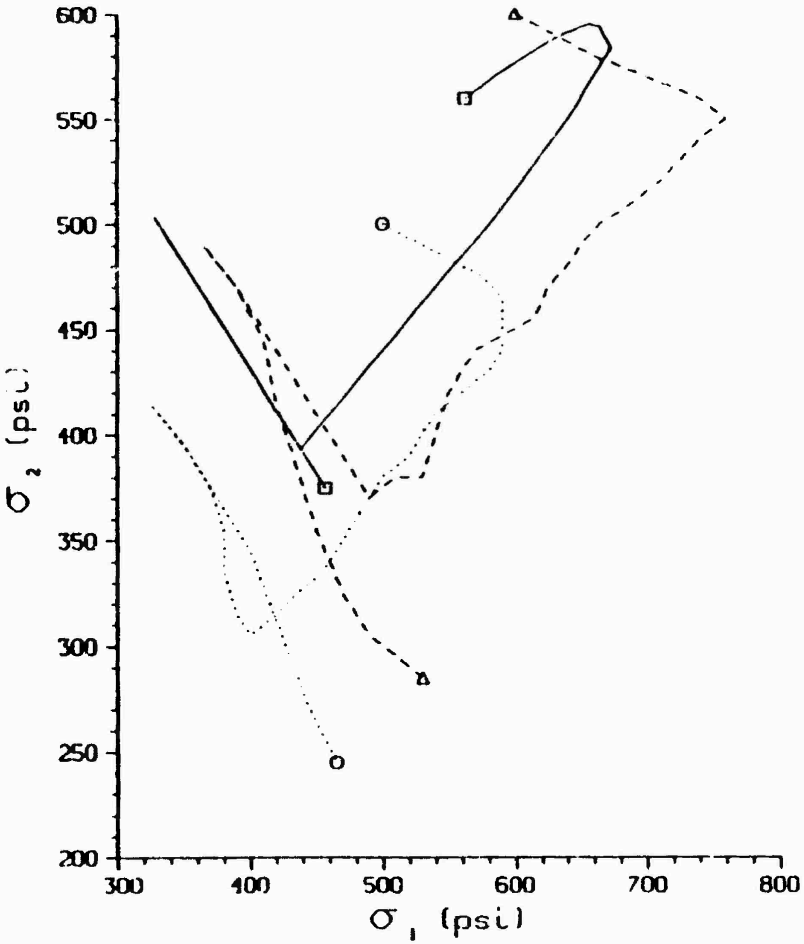

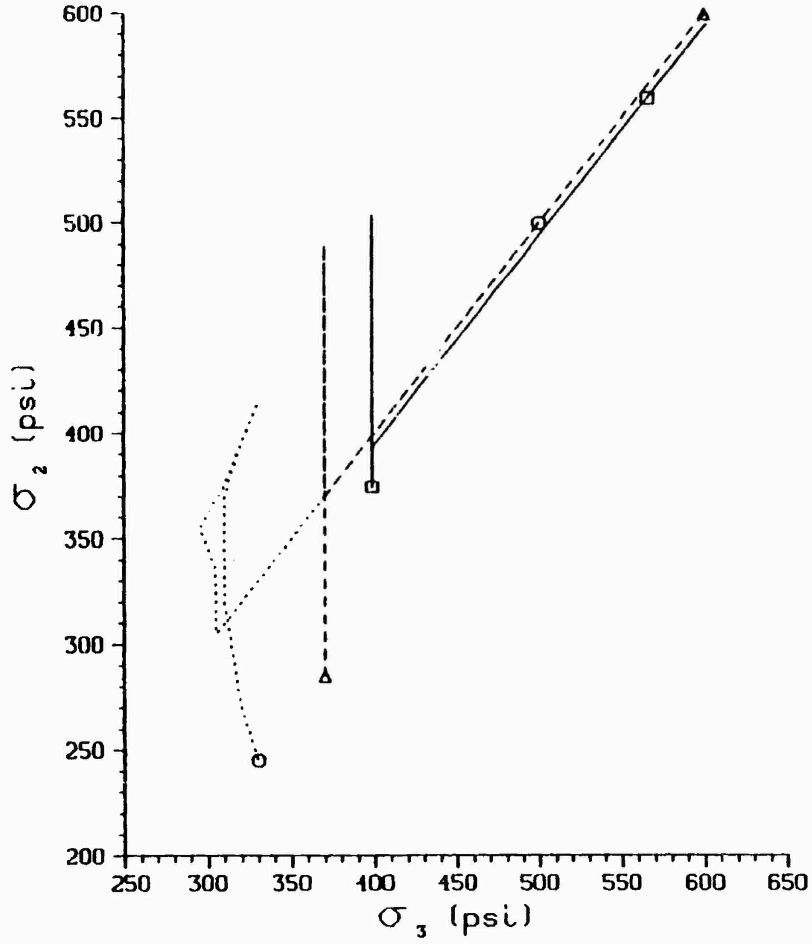

Figure 18. Stress history predicted by the AFWL model for complex strain path No. 2. Measured stress histories are shown by the dashed and dotted lines.

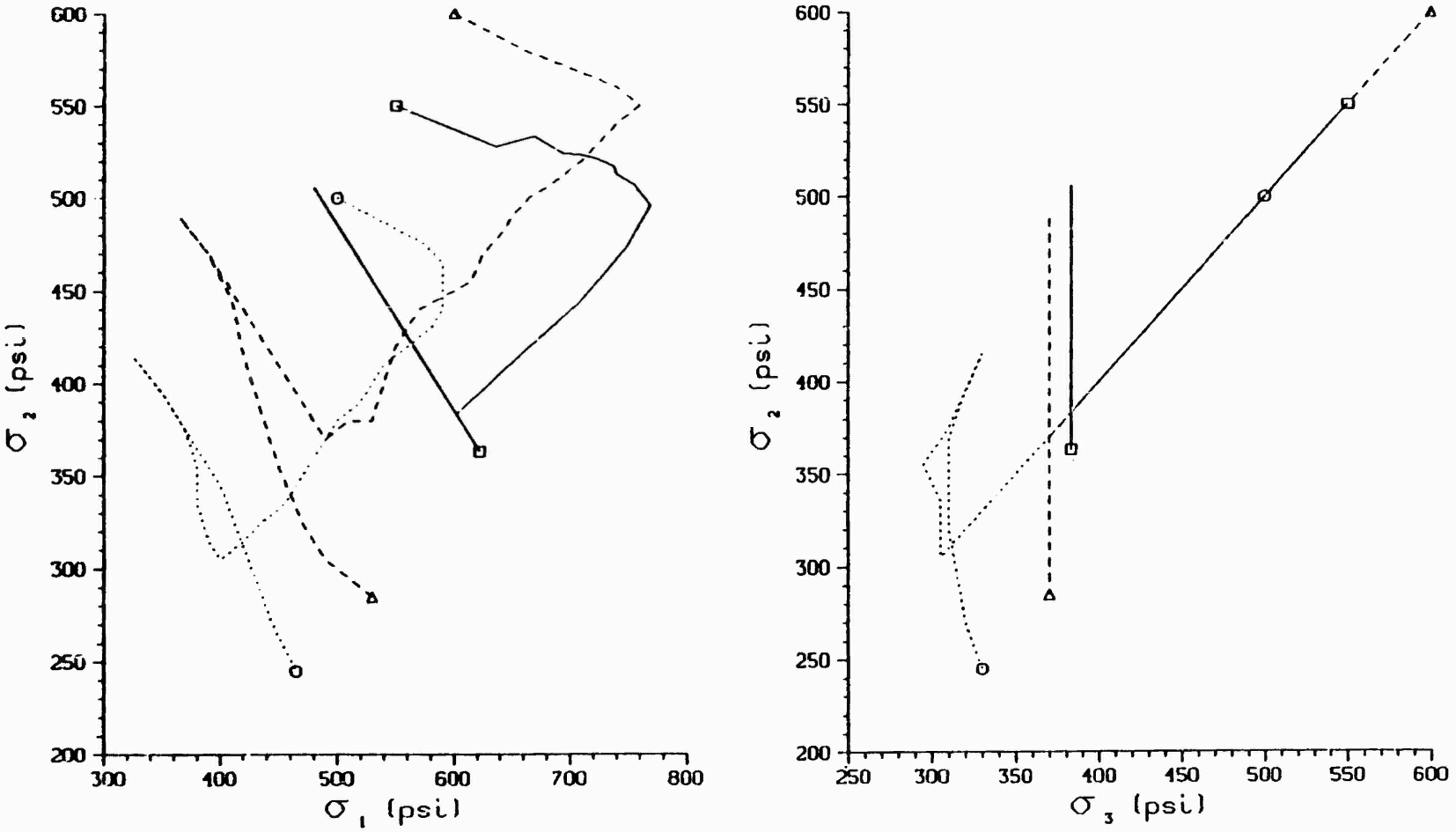

Figure 19. Stress history predicted by Lade's model for complex strain path No. 2. Measured stress histories are shown by the dashed and dotted lines.

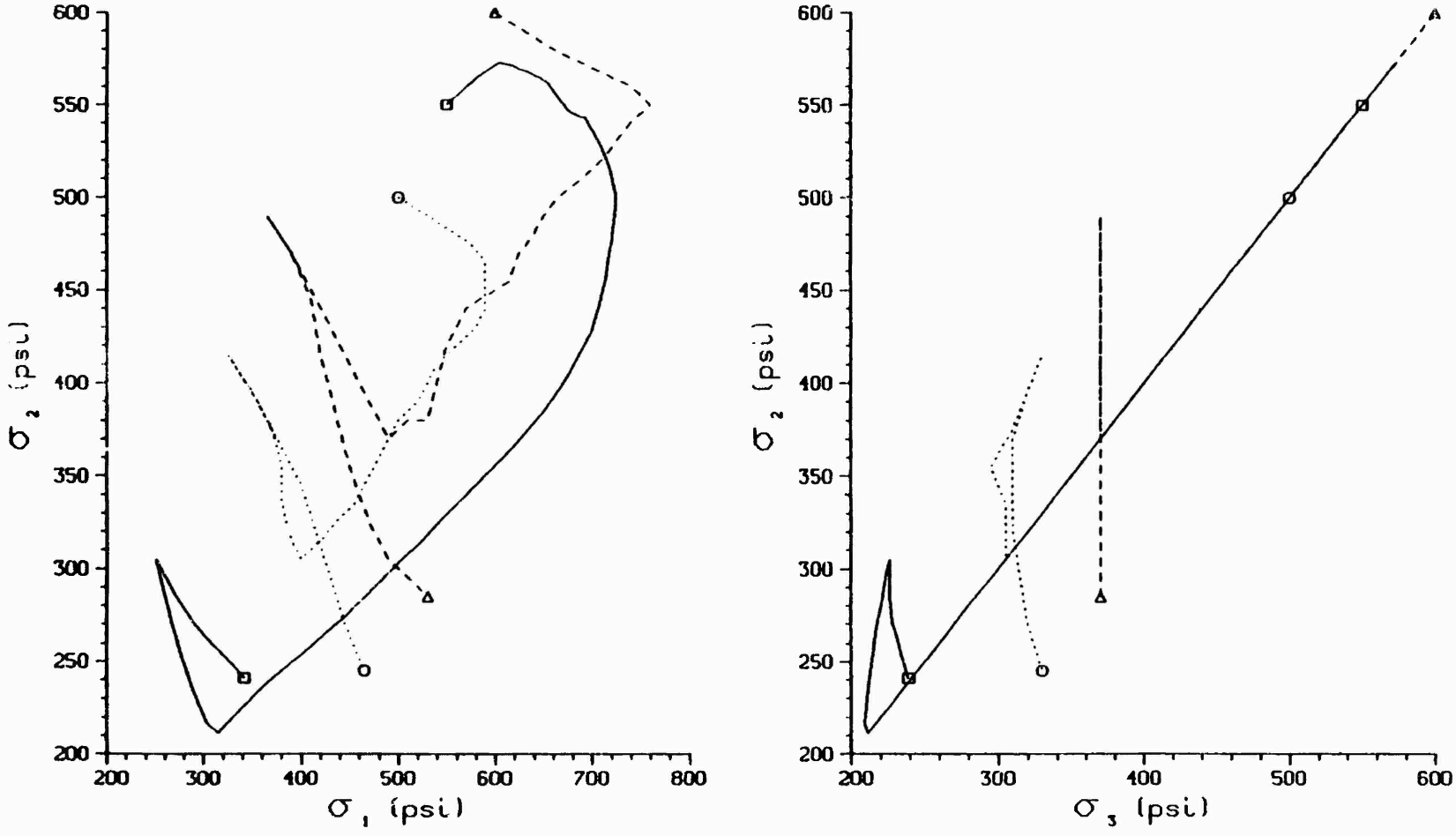

Figure 20. Stress history predicted by Prevost's model for complex strain path No. 2. Measured stress histories are shown by the dashed and dotted lines.

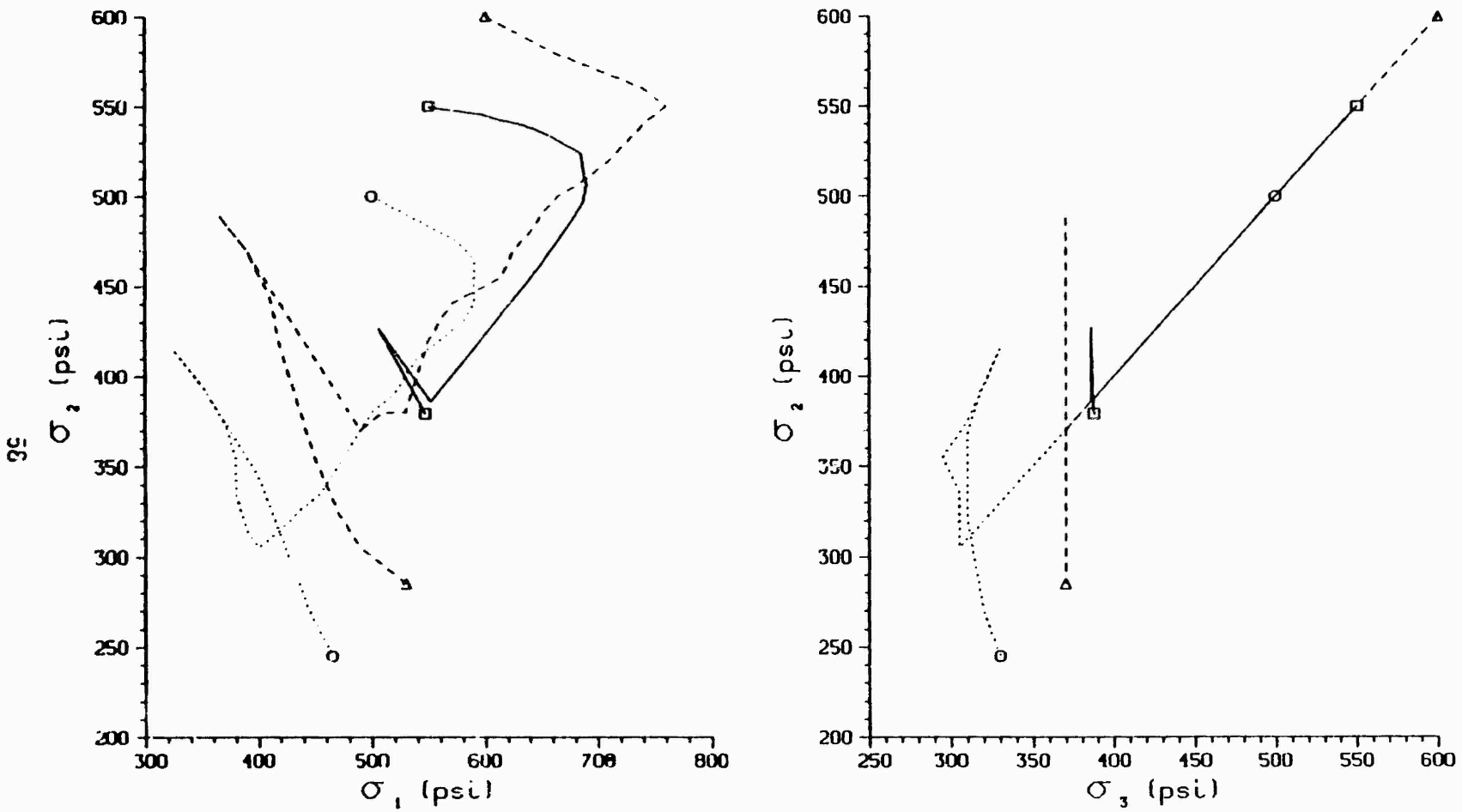

Figure 21. Stress history predicted by the S-CUBED Endochronic model for complex strain path No. 2. Measured stress histories are shown by the dashed and dotted lines.

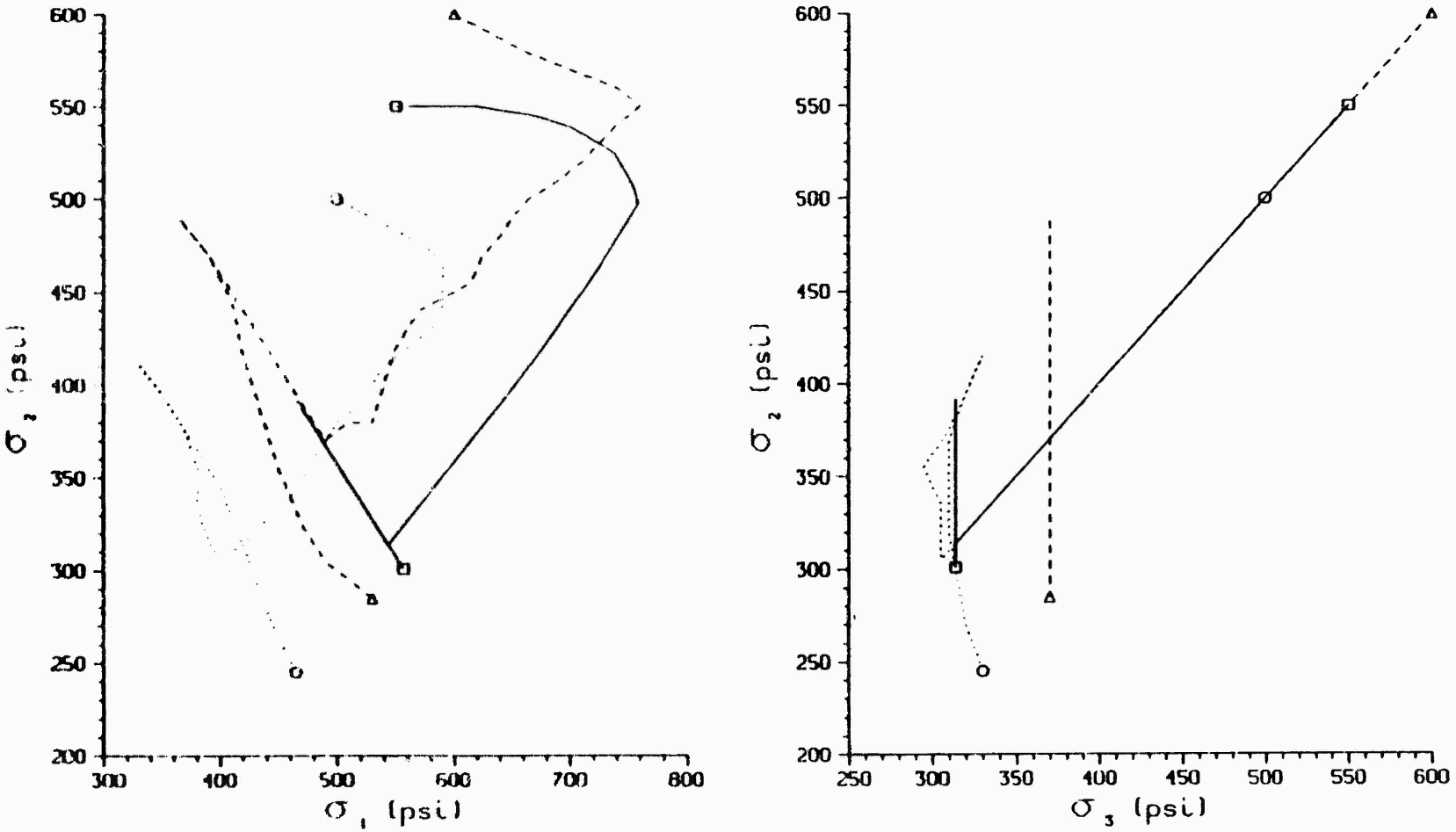

Figure 22. Stress history predicted by the Weidlinger Cap model for complex strain path No. 2. Measured stress histories are shown by the dashed and dotted lines.

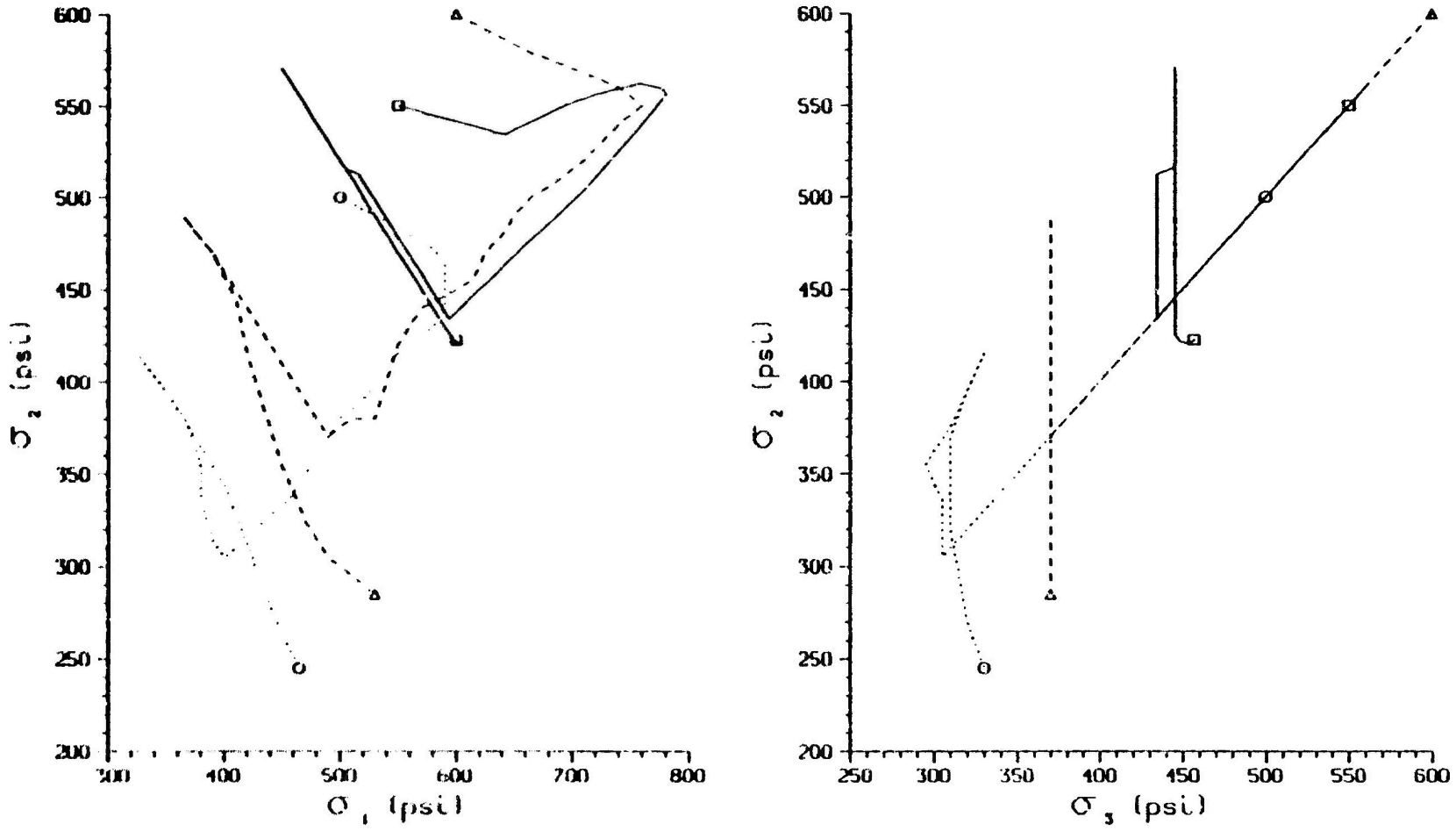

Figure 23. Stress history predicted by the WES Cap model for complex strain path No. 2. Measured stress histories are shown by the dashed and dotted lines.

appear to be qualititatively similar and quite consistent, if allowance is made for the difference in the initial hydrostatic states. The two measured stress histories should be expected to bound the stress history for an initial prestress of 550 psi. If this is true, the predicted stress histories should fall between the two measured stress histories, provided the models are correct. As the figures reveal, most of the predicted stress histories are qualitatively similar to those that were measured, and several of them are, in fact, in reasonably good agreement with the measurements.

4.3 COMPLEX STRAIN PATH NO. 3.

This strain path is characteristic of soil elements located almost directly below an explosive source and at a significant depth. As comparison of Figures 1, 2 and 3 reveals, the strains developed along complex path No. 3 are considerably larger than in either of the other complex strain paths. Also, the discrepancies between the actual and prescribed paths are evidently larger for this path than for the other two; this is especially true for the test represented by the dotted line.

As noted earlier, the starting condition for complex strain path No. 3 unfortunately fell outside of the range investigated in the standard laboratory tests reported in Reference 3. In those tests, the hydrostatic and uniaxial strain behavior were measured for stress levels up to 700 psi, while the standard triaxial tests were done at maximum confining pressures of 500 psi. The initial hydrostatic prestress for complex strain path No. 3, however, was 900 psi. Because of this, it was felt that the stress histories for complex strain path No. 3 would not be valid standards to use in evaluating the models' predictive capabilities. To do so would require, first, extrapolation of the models into a region of response not covered in the standard laboratory tests and, secondly, driving them around a complex strain path in a region unexplored in

the standard laboratory tests. Nevertheless, all of the modelers, with the exception of Prevost, submitted predictions for this strain path, and the results are shown in Figures 24 to 29. One of the striking features of these figures is the notably large differences between the slopes of the measured and predicted stress paths at the beginning of the paths.

4.4 SUMMARY

In the preceding sections, the stress histories predicted by each of the models for the three complex strain paths have been presented and discussed, together with the corresponding stress histories measured in the laboratory. The various uncertainties in each of the complex strain path tests were noted and, for convenience, are summarized in the table below.

TABLE 2

UNCERTAINTIES IN THE COMPLEX STRAIN PATH TESTS

Complex Strain Path	Major Uncertainties
No. 1	• The tests for this path were conducted almost two years after the standard laboratory tests reported in Reference 3 and by a different operator. • No check tests were done to verify that the soil preparation and testing techniques had not changed in the meantime.
No. 2	• One of the tests conducted for this path was done from the prescribed initial hydrostatic state of 500 psi, while the other test was inadvertently done from 600 psi. • No further tests were done to establish the reproducibility of the data from either of these initial hydrostatic states.

TABLE 2 (Cont'd)
UNCERTAINTIES IN THE COMPLEX STRAIN PATH TESTS

Complex Strain Path	Major Uncertainties
No. 3	• The tests for this path started from an initial hydrostatic state of 900 psi, which was outside of the range covered by the standard laboratory tests reported in Reference 3. • Actual strain paths followed in the tests differed significantly from the prescribed path.

For the measured stress histories to provide meaningful standards against which the predicted stress histories can be compared, the stress history data must be accurate, reproducible and free of doubt. As the above table indicates, there were significant uncertainties in the data from each of the three complex strain path tests, which were felt to be too large to justify a detailed evaluation of the models according to the procedure described in Appendix A. Therefore, no formal evaluation of the models was done.

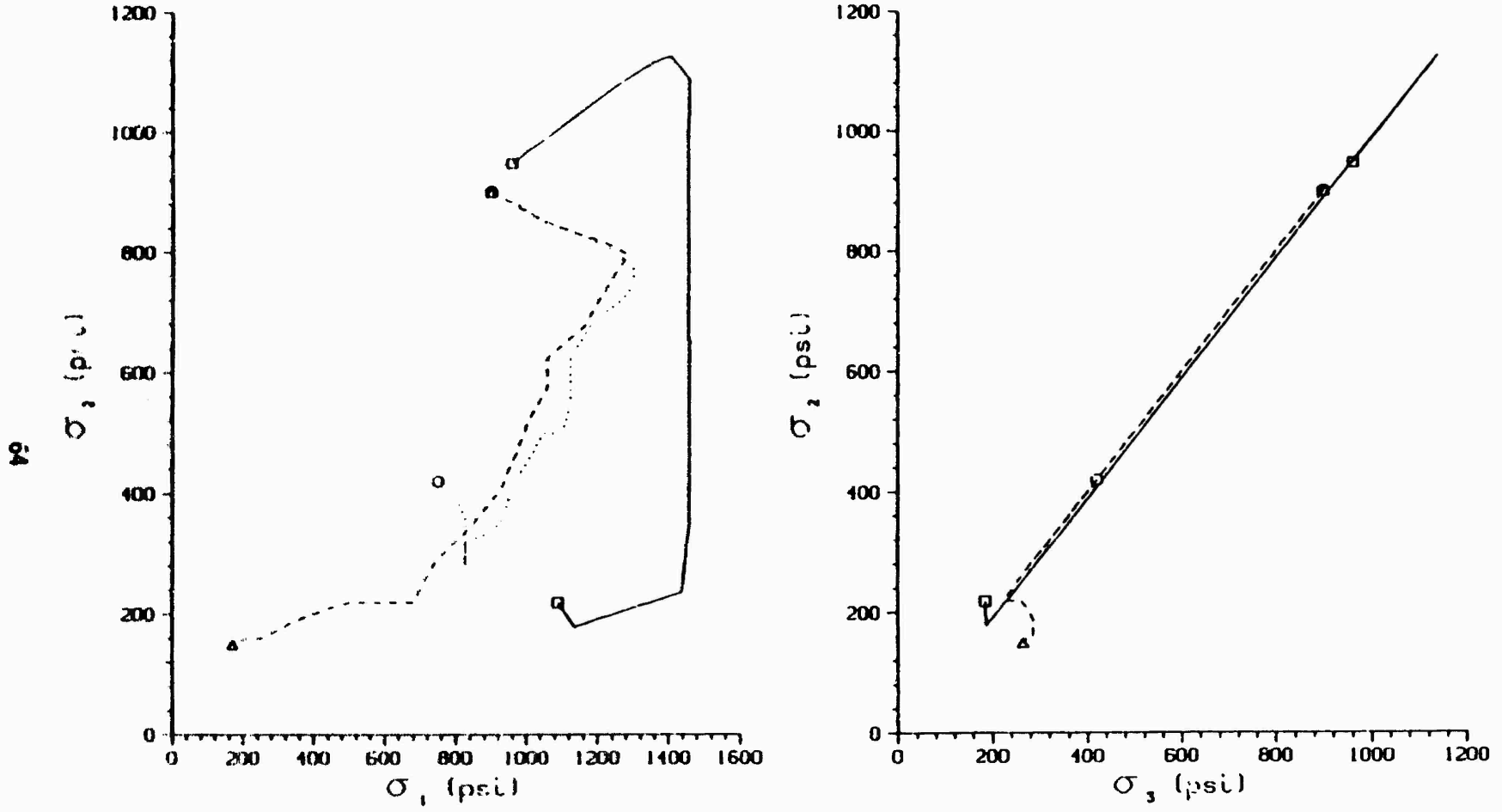

Figure 24. Stress history predicted by the AFWL model for complex strain path No. 3. Measured stress histories are shown by the dashed and dotted lines.

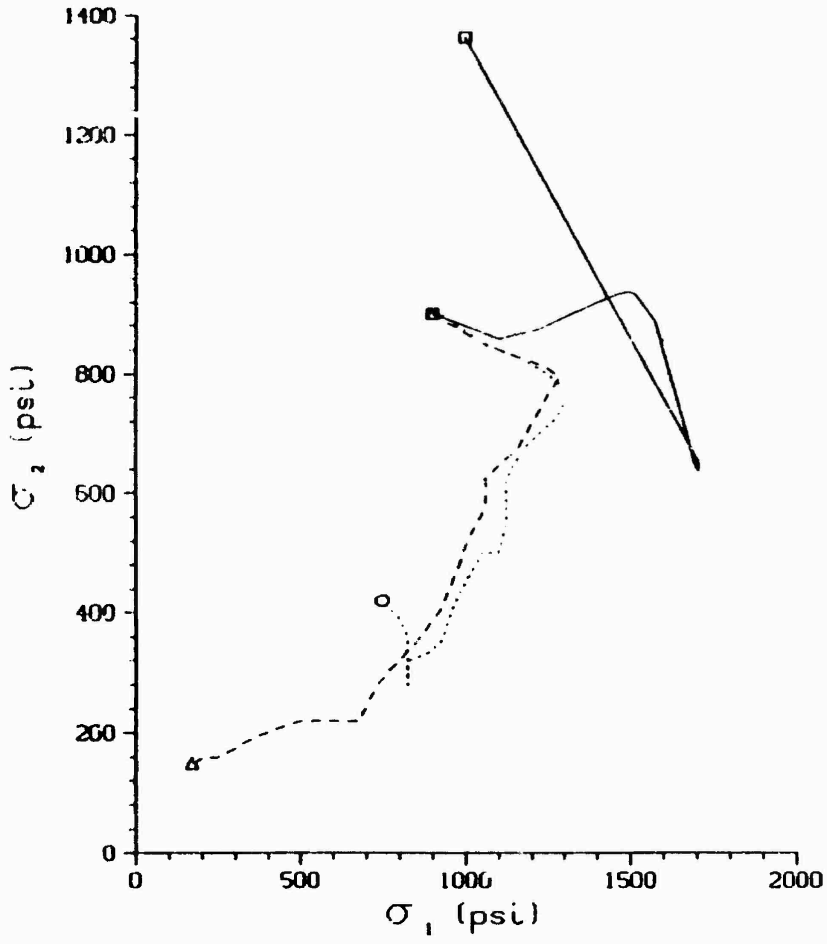

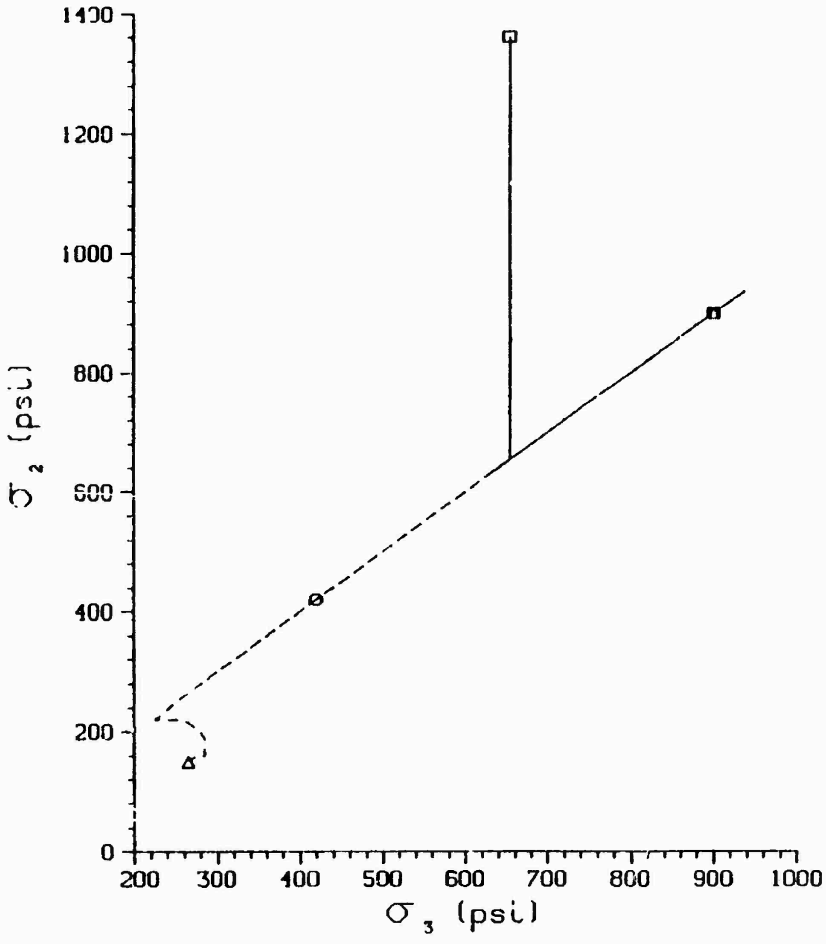

Figure 25. Stress history predicted by Lade's model for complex strain path No. 3. Measured stress histories are shown by the dashed and dotted lines.

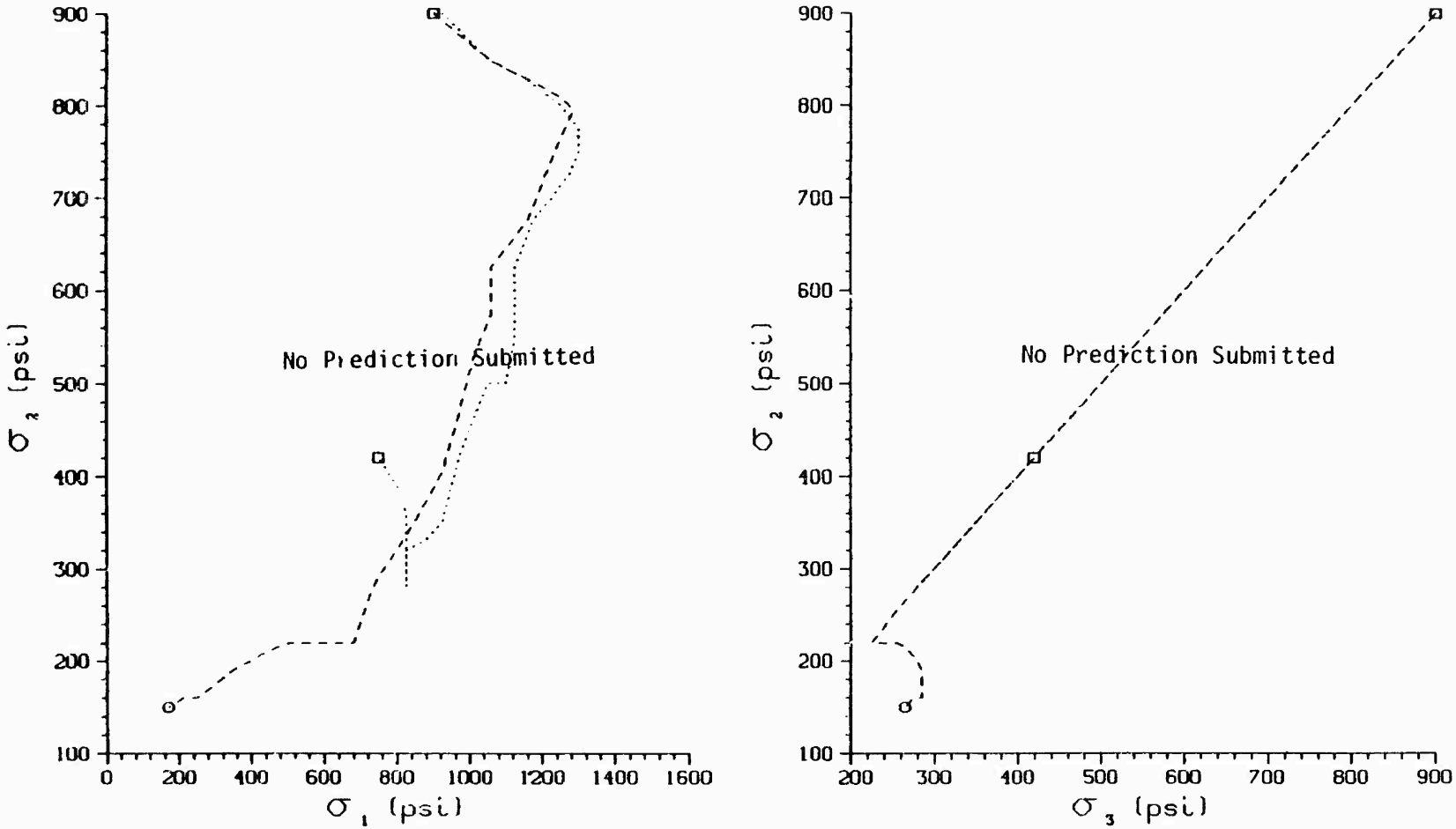

Figure 26. Stress history predicted by Prevost's model for complex strain path No. 3. Measured stress histories are shown by dashed and dotted lines.

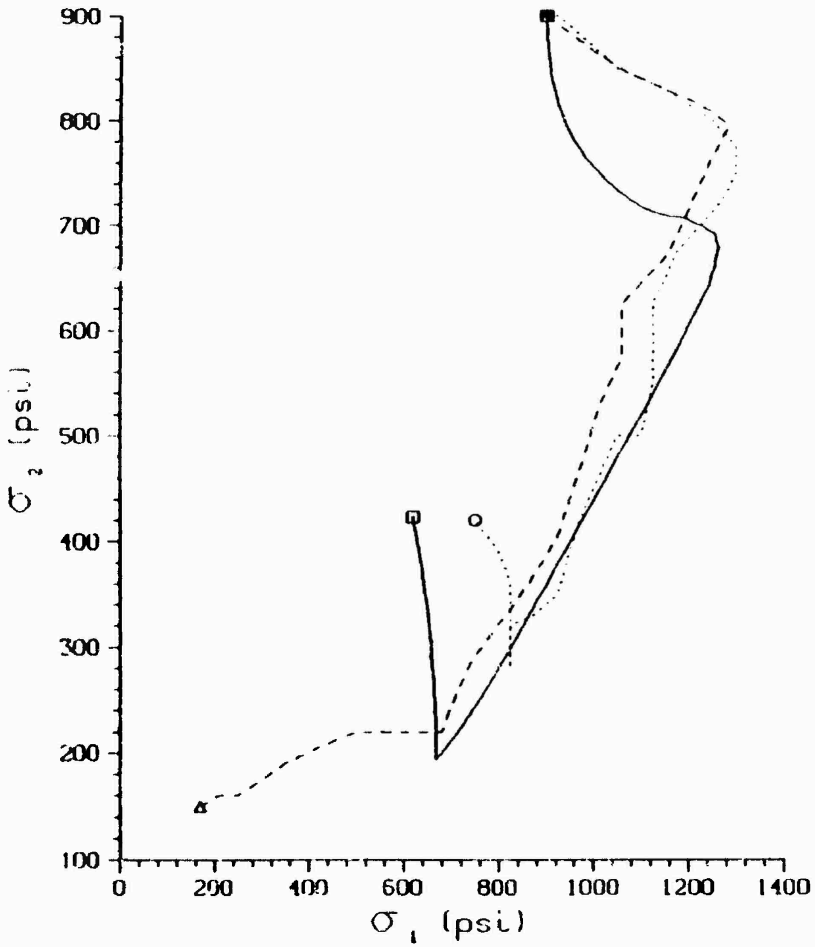

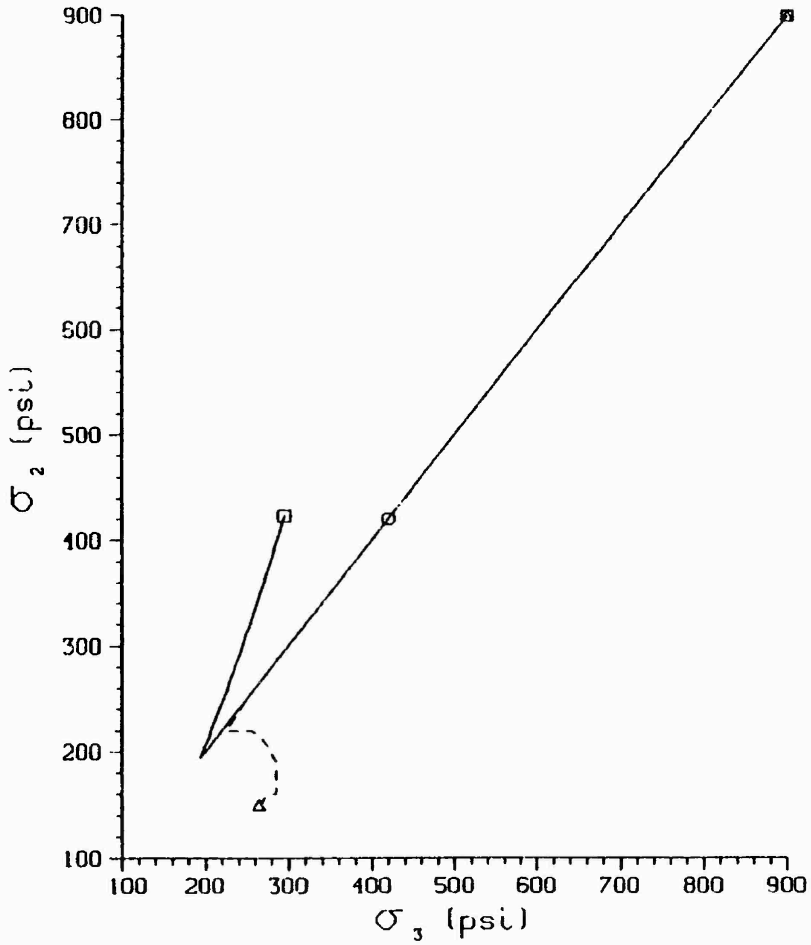

Figure 27. Stress history predicted by the S-CUBED Endochronic model for complex strain path No. 3. Measured stress histories are shown by the dashed and dotted lines.

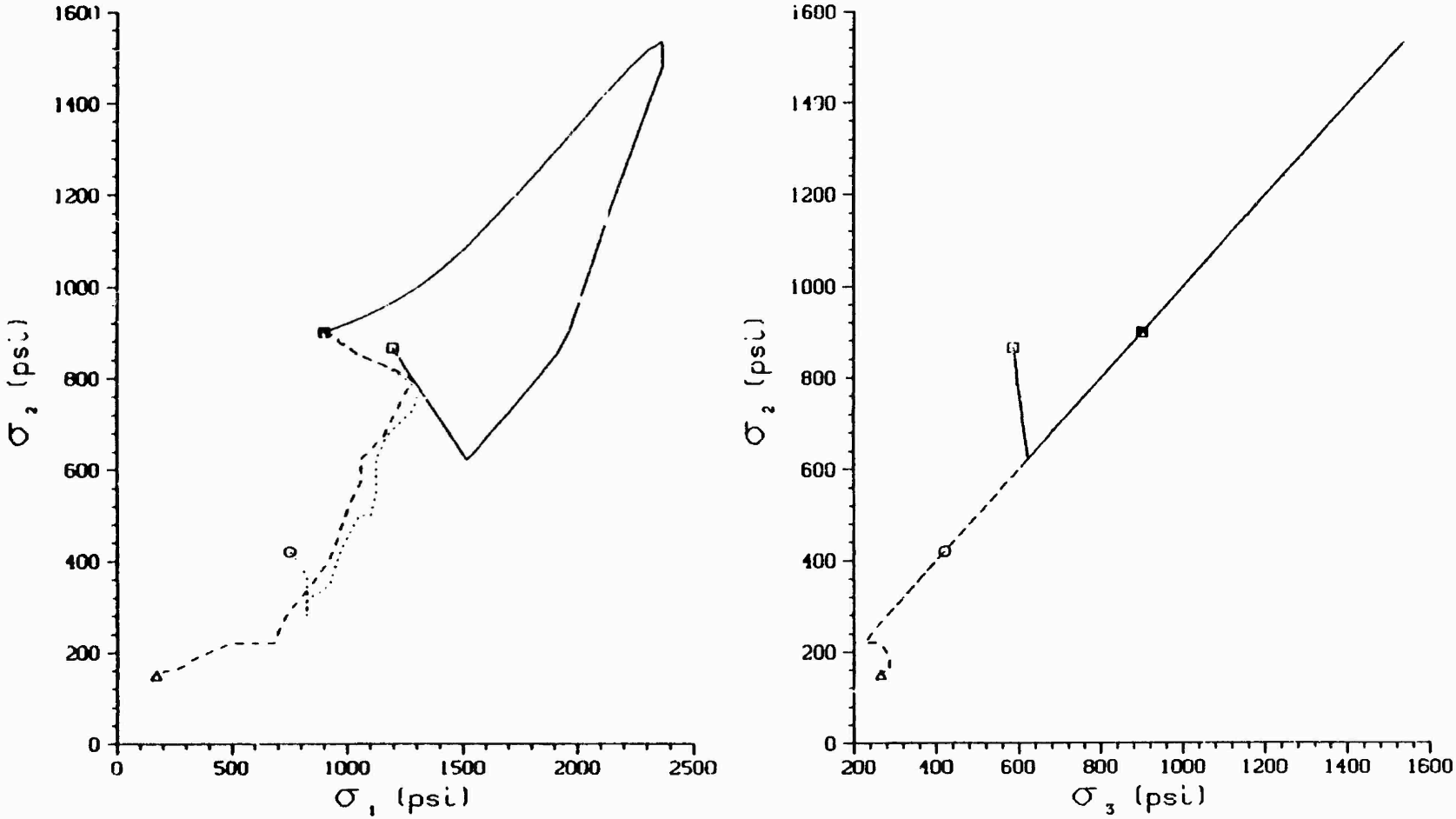

Figure 28. Stress history predicted by the Weidlinger Cap model for complex strain path No. 3. Measured stress histories are shown by the dashed and dotted lines.

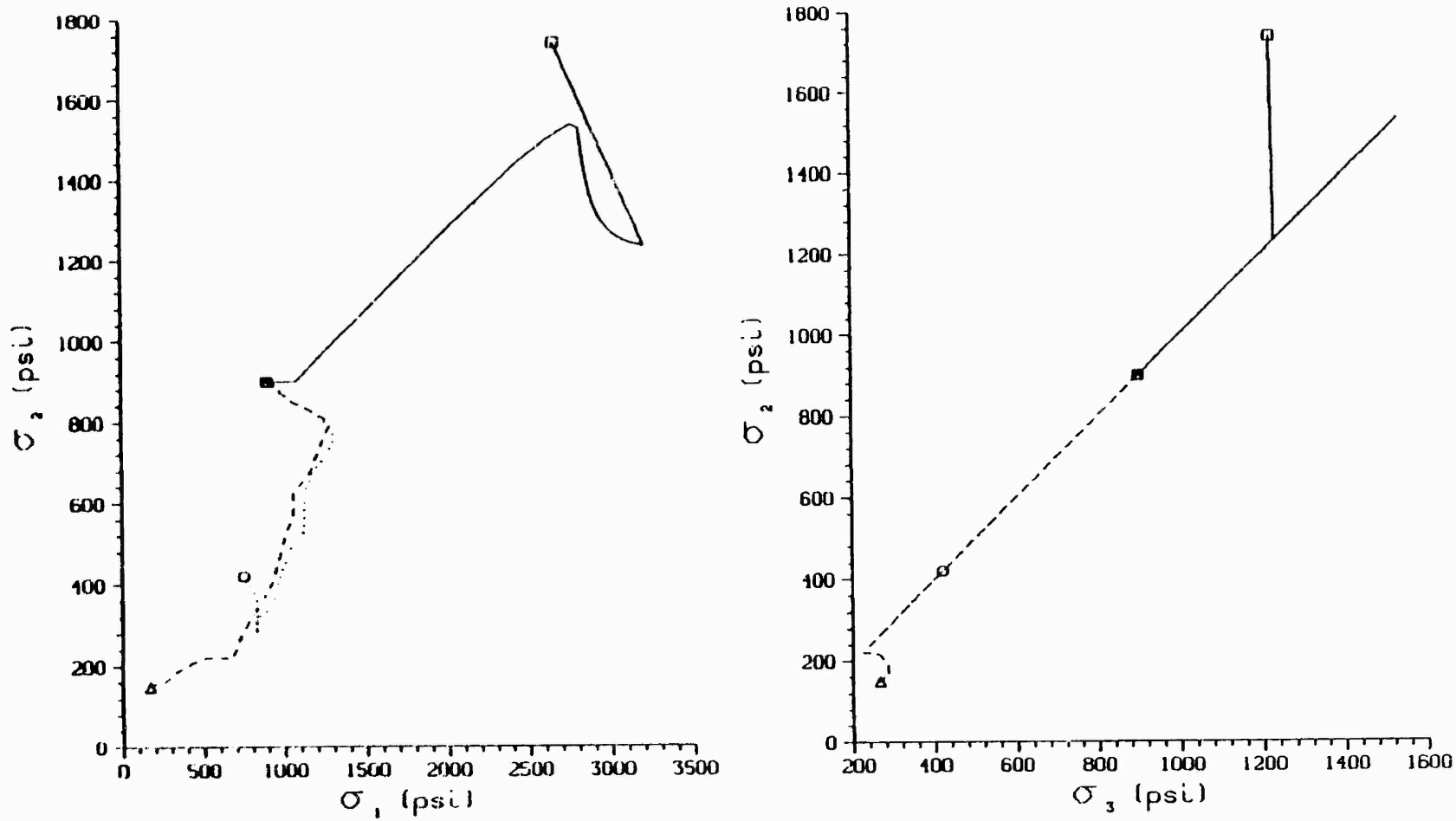

Figure 29. Stress history predicted by the WES Cap model for complex strain path No. 3. Measured stress histories are shown by the dashed and dotted lines.

5. CONCLUSIONS AND RECOMMENDATIONS FOR FUTURE STUDIES

This is the first study which has attempted to systematically explore the capabilities of advanced soil models to predict responses to complex strain paths typical of explosively-induced ground motion. The focus of the study has been on a soil from Ralston Valley, a region which has recently received considerable attention lately in regard to the MX program. The success of such a study obviously depends very strongly upon having accurate and reproducible data against which the model predictions can be compared. As planned, the measured stress histories from the complex strain path tests were to provide the standards against which the predicted stress histories would be compared and, on the basis of these comparisons, the models would be evaluated, according to the procedure described in Appendix A. Clearly, for such an evaluation to be meaningful, the measured stress histories must be accurate, reproducible and free of doubt. Due to difficulties related to the experimental portion of the study, there were sufficient uncertainties in the data that it did not appear justifiable to use the data to perform a detailed evaluation. Consequently, no formal evaluation of the models was done in the present study.

As one reviews the predictions from the various models for each of the three complex strain paths, there is a feature worthy of note. Despite the fact that each of the models was fit to the same set of standard laboratory data, there are nevertheless large differences between the various model predictions for each of the strain paths. This implies that there are substantial differences between the predictive capabilities of the models and, additionally, that the three complex strain paths exercise the models in such a way as to bring out these differences.

The basic approach followed in this study appears to be both sound and feasible and with improvements in the quality of the

laboratory data should lead to a true evaluation of the predictive capabilities of the models. In the course of the study, a great deal was learned, mainly from the laboratory testing portion of the effort, which should help us in the future to avoid the pitfalls encountered in the present work. Some of these difficulties undoubtedly resulted from the two gaps in funding which the program experienced. With the following revisions in the experimental part of the effort, we are confident that high quality data, of the type required to allow a meaningful evalution of the models to be made, can be generated:

1. Conduct all laboratory tests with the same operator and without a major gap in time between tests, to ensure that the soil, its preparation and the testing methods do not significantly change during the course of testing.

2. Perform the complex strain path tests before the standard laboratory tests. This will permit the standard laboratory tests to be properly designed so that they cover the range of stresses encountered in the complex strain path tests.

3. In the standard laboratory tests, use the same magnitude of hydrostatic pressure to seat the soil specimens in the testing device. This will make the data more consistent and easier for the predictors to work with.

4. Prepare a critique of the standard laboratory data and the complex strain path data before the modelers make their predictions to ensure that the data are of sufficient quality to meet the requirements of the study. Such a critique might take the form of a report similar to Reference 2.

5. Drive the soil specimens around the complex strain paths with greater accuracy. That such an improvement in accuracy is possible with the manually operated true triaxial device is evident from the excellent test results recently reported in Reference 16. It appears therefore that the true triaxial device used both in the present study and to generate the data reported in Reference 16 can, with sufficient care and experience on the part of the operator, generate data of the required quality.

It is therefore recommended that the present investigation, with the changes noted above, be repeated.

REFERENCES

1. Read, H. E., "Evaluation of Material Models for MX Siting. Volume I: Soil Models," S-CUBED, La Jolla, California, Report No. SSS-R-80-4155 to the U.S. Air Force BMO, November 1979.

2. Read, H. E., and H.-Y. Ko, "Laboratory Tests on Remolded Soil from the HAVE HOST Site: An Evaluation of Data Consistency, Remolding Procedures and Anisotropy," S-CUBED, La Jolla, California. Report SSS-R-81-4673 to the U.S. Air Force BMO, October 1980.

3. Ko, H.-Y., and R. Scavuzzo, "Cubical Test Data on Ralston Valley Soil. Part I: Standard Loading Paths," University of Colorado, Boulder, S-CUBED Report No. SSS-R-82-5607, June 1982.

4. Ko, H.-Y., and R. Scavuzzo, "Cubical Test Data on Ralston Valley Soil. Part II: Complex Strain Path Tests," University of Colorado, Boulder, Report to U. S. Army Engineer Waterways Experiment Station, Vicksburg, Mississippi, January 1982.

5. Amend, J., G. W. Ullrich and J. H. Thomas, "HAVE HOST Cylindrical In-Situ Test (CIST) Data Analysis and Material Model Report," Air Force Weapons Laboratory, Albuquerque, New Mexico, Report No. AFWL, TR-77-81, February 1977.

6. Sandler, I. S., and D. Rubin, "An Algorithm and a Modular Subroutine for the Cap Model," Intl. J. Num. Methods in Geomechanics, Vol. 3, No. 2 (1979), 173.

7. Baladi, G. Y., "An Elastic-Plastic Isotropic Conscitutive Model for Sand (Material C)," in Limit Equilibrium, Plasticity and Generalized Stress-Strain in Geotechnical Engineering, Proceedings of Workshop at McGill University, Montreal, May 28-30, 1980. Published by American Soc. of Civil Engineers, New York, NY.

8. Lade, P. V., "Elasto-Plastic Stress-Strain Theory for Cohesionless Soil with Curved Yield Surfaces," Intl. J. Solids and Structures, Vol. 13 (1977), 1019.

9. Prevost, J.-H., "Plasticity Theory for Soil Stress-Strain Behavior," J. Engr. Mechs. Div., ASCE, Vol. 104, No. EM5 (1978), 1177.

10. Read, H. E., J. A. Trangenstein and K. C. Valanis, "A New Endochronic Constitutive Model for Soils," S-CUBED, La Jolla, California, Report No. SSS-R-81-4926 to the EPRI, November 1981.

11. Valanis, K. C., and H. E. Read, "A New Endochronic Plasticity Model for Soils," in Soil Mechanics -- Transient and Cyclic Loads: Constitutive Relations and Numerical Treatment, Ed. by G. N. Pande and O. C. Zienkiewicz, John Wiley and Sons, Ltd., 1982.

12. Trulio, J. G., Applied Theory, Inc., Los Angeles, Informal Letter to S-CUBED, dated August 18, 1980.

13. Ko, H.-Y., and K. W. Cargill, "Axisymmetric Tests of Loose Ottawa Sand," University of Colorado, Boulder, Colorado, Report No. SSS-R-80-4525 to S-CUBED, September 1979.

14. Ko, H.-Y., M. M. Kim and K. W. Cargill, "Axisymmetric Tests of HAVE HOST Soil from Luke Bombing and Gunnery Range," University of Colorado, Boulder, Colorado, Report No. SSS-R-80-4391 to S-CUBED, February 1980.

15. Ladd, R. S., "Preparing Test Specimens Using Undercompaction," Geotechnical Testing Journal, Vol. 1 (1978), 16.

16. Ko, H.-Y., and R. W. Meier, "Cubical Test Data and Strain Path Testing on Nellis Baseline Sand," University of Colorado, Boulder, Colorado, Report to U. S. Army Engineer Waterways Experiment Station, January 1983.

17. Ko, H.-Y., and S. Sture, "Three-Dimensional Mechanical Characterization of Anisotropic Composites," J. Composite Maths., Vol. 8 (1974), 178.

18. Berends, B. E., and H.-Y. Ko, "Cubical Multiaxial Cell for Testing Cohesive Soils," J. Geot. Engr. Div., ASCE, Vol. 106 (1980), 106.

19. Nymoen, L., "The Effects of Boundary Conditions on Test Response in a Granular Material," Ph.D. Thesis, University of Colorado, Boulder, Colorado (1970).

APPENDIX A
A PLAN FOR EVALUATING SOIL MODELS

In this study, the evaluation of the soil models is based upon their abilities to predict the measured stress histories for the complex strain paths. This requires that a measure of discrepancy between predicted and measured stress histories be defined. To this end, we have developed an approach for evaluating the models which is based upon the integrated mean square deviation between the predicted and measured stress histories over the entire stress path. Details of this approach are given below.

Figure A-1(a) schematically shows a prescribed complex strain path in principal strain space. Figure A-1(b) shows several stress paths in principal stress space which correspond to the prescribed strain path. A measured stress path is represented in the figure by a dashed line and is the average from several tests. The stress paths labeled "Model A" and "Model B" denote predictions from two different soil models. To each point P on the prescribed strain path there are corresponding points Q, Q_A and Q_B on the stress paths, as shown.

There will generally be a difference between a predicted stress state, such as Q_A, for example, and the measured stress state, Q. In order to quantitatively define such a discrepancy e in the stress state, we adopt the mean square deviation for this purpose, where:

$$e = \sqrt{\sum_{i=1}^{3} (\bar{\sigma}_i - \sigma_i)^2} \qquad \text{(A-1)}$$

Here, the $\bar{\sigma}_i$ represent the (average) measured principal stresses, and the σ_i denote the principal stresses predicted by the models. If we now introduce the length, x, of the strain path, defined as:

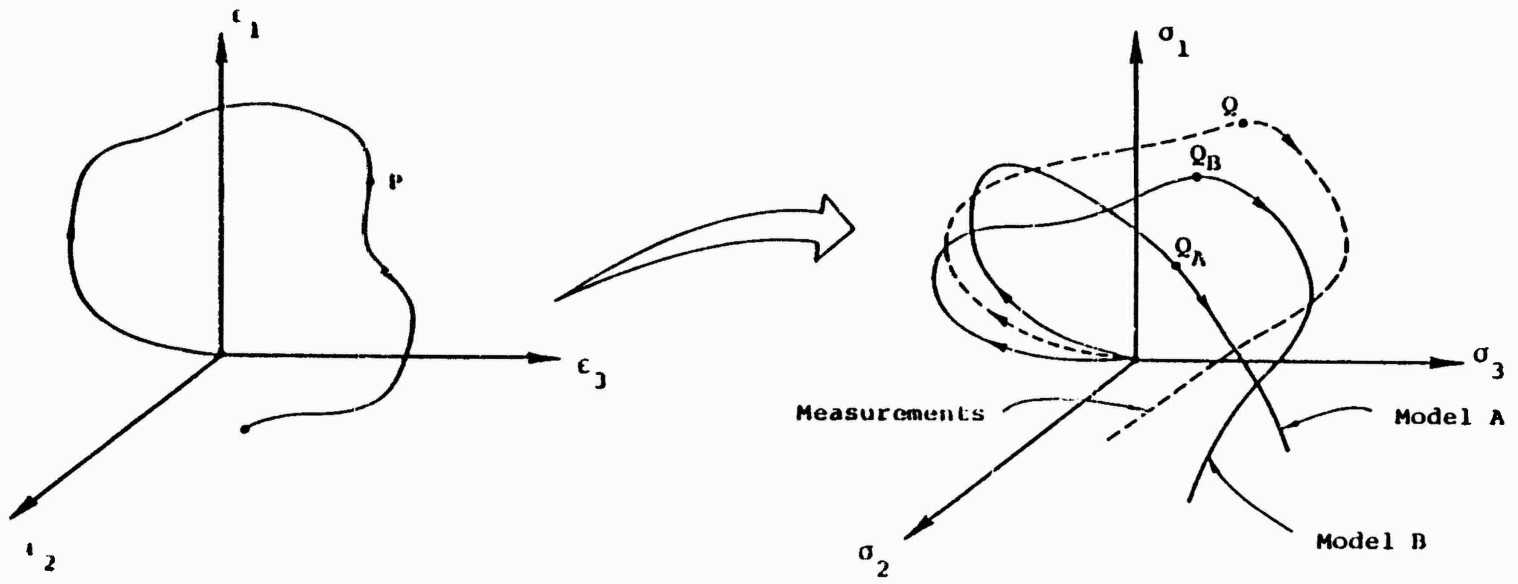

(a) Prescribed strain path in principal strain space

(b) Corresponding stress paths in principal stress space

Figure A-1. Stress Paths Corresponding to Prescribed Strain Path.

$$x = \int_{path} \sqrt{\sum_{i=1}^{3} (d\varepsilon_i)^2} \qquad \text{(A-2)}$$

then, a relationship of the form $e = e(x)$ can be constructed for each of the models under consideration. This relationship describes the discrepancy between the predicted and measured stress histories at each point of the strain path.

To illustrate these ideas graphically, consider Figure A-2, which shows the manner in which e might vary with x for two models. Also shown on this figure is a curve labeled "measurements," which describes the maximum scatter between the measured stress histories and their average value. The stress measurement error curve can prove useful in identifying possible situations where the error of the various predictions may be on the order of the scatter in the stress history data. From an inspection of the results depicted in Figure A-2, one would conclude, for example, that (a) the errors in stress measurement are considerably smaller than the differences between the predictions, and (b) Model B has greater overall predictive capability than Model A.

For the purpose of ranking various models, a composite of the e-versus-x curves for all of the models would be constructed for each of the three prescribed strain paths. If the e-versus-x curves are sufficiently separated, the ranking would be done through inspection, as was possible for the curve shown in Figure A-2. If the e-versus-x curves are not well separated, then the error history, E, defined as:

$$E = \int_{path} e(x)dx \qquad \text{(A-3)}$$

should be calculated for each model, and the ranking done on the basis of this integrated error measure. Clearly, the success of this approach depends strongly upon having precision data from the complex strain path tests in which the prescribed paths have been followed with acceptable accuracy.

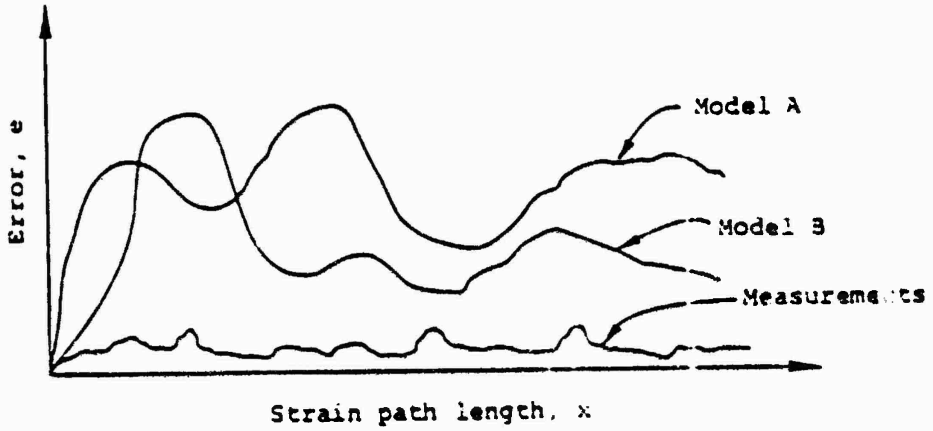

Figure A-2. Error Measure Versus Strain Path Length.

APPENDIX B
LABORATORY DATA FROM THE COMPLEX STRAIN PATH TESTS

This appendix contains a complete listing of the laboratory data for the three complex strain paths considered herein. The data were generated by Professor H.-Y. Ko and his staff at the University of Colorado. The data are presented here for completeness, since Reference 4 has had only very limited distribution and, moreover, because the data considered herein for complex strain path No. 1 have not been previously published.

In the tables which follow, S_1, S_2, S_3 and E_1, E_2, E_3 denote the principal stresses and principal strains, respectively. The subscript 1 refers to the direction in which the soil specimens were compacted during the remolding process, and the subscripts 2 and 3 refer to directions perpendicular to the 1-direction. The stresses are given in units of psi. Note that the tables provide a description of the total behavior of each specimen, including a description of the hydrostatic compression up to the specified initial prestress from which the complex strain path was initiated. The solid horizontal line in each table denotes the end of the initial hydrostatic compression phase of the test.

TABLE B-1

COMPLEX STRAIN PATH NO. 1

TEST NO. 1

PT	E1*1000	E2*1000	E3*1000	S1	S2	S3
1	.000	.000	.000	0	0	0
2	2.760	1.510	1.360	100	100	100
3	5.160	3.990	3.460	175	175	175
4	6.060	5.350	4.980	225	225	225
5	6.800	7.110	6.760	275	275	275
6	7.170	8.320	7.790	299	299	299
7	7.210	8.490	7.990	300	300	300
8	7.280	8.540	8.030	325	295	295
9	8.690	8.450	7.920	350	290	290
10	9.450	8.380	7.870	370	290	290
11	10.630	8.390	7.880	400	300	300
12	11.850	8.460	7.930	430	310	310
13	13.180	8.460	7.940	460	315	315
14	14.800	8.450	7.910	490	320	320
15	15.980	8.440	7.920	505	323	323
16	16.270	8.490	7.950	505	323	323
17	16.250	8.560	8.010	465	315	315
18	16.090	8.590	8.040	425	305	305
19	15.880	8.620	8.060	385	290	290
20	15.640	8.630	8.050	345	270	270
21	15.410	8.640	8.010	305	245	245
22	15.180	8.510	7.890	275	220	220
23	14.870	8.510	7.800	235	200	200
24	14.510	8.470	7.690	195	180	180
25	13.860	8.520	7.710	155	165	165
26	14.700	7.830	7.540	215	135	165
27	15.770	6.560	7.450	260	110	170
28	15.590	7.000	7.440	245	140	170
29	15.290	7.600	7.400	220	170	170
30	14.870	8.140	7.490	190	190	175
31	13.910	9.160	7.620	160	210	175
32	11.890	11.470	7.700	130	230	170
33	9.800	14.260	7.760	110	240	165

TABLE B-2

COMPLEX STRAIN PATH NO. 1

TEST NO. 2

PT	E1*1000	E2*1000	E3*1000	S1	S2	S3
1	-.010	-.010	-.010	30	30	30
2	.140	.320	.460	50	50	50
3	3.420	2.190	2.040	100	100	100
4	5.340	3.490	3.320	150	150	150
5	6.790	5.150	5.010	200	200	200
6	7.690	6.910	6.820	250	250	250
7	8.420	8.560	8.870	295	295	295
8	8.490	9.080	9.110	300	300	300
9	9.530	9.120	9.130	350	300	300
10	11.450	8.970	9.000	400	300	300
11	12.410	8.980	9.000	425	305	305
12	13.330	9.040	9.060	450	315	315
13	14.230	9.060	9.090	475	320	320
14	15.260	9.090	9.120	495	325	325
15	16.020	9.130	9.170	510	330	330
16	16.560	9.220	9.220	520	335	335
17	17.210	9.220	9.240	530	335	335
18	17.600	9.230	9.260	530	335	335
19	17.590	9.240	9.270	500	325	325
20	17.450	9.160	9.240	470	310	310
21	17.210	9.160	9.240	430	300	300
22	17.050	9.180	9.240	390	290	290
23	16.680	9.220	9.300	340	275	275
24	16.620	9.130	9.200	320	255	255
25	16.320	9.110	9.180	280	235	235
26	15.950	9.090	9.150	240	215	215
27	15.670	9.090	9.150	210	205	205
28	15.490	9.090	9.150	195	200	200
29	16.070	8.560	9.050	255	170	200
30	16.560	7.700	9.030	300	145	205
31	16.920	7.610	9.030	300	145	205
32	17.160	7.200	9.090	315	140	210
33	17.120	7.470	9.060	305	160	210
34	16.930	7.700	9.050	285	175	210
35	16.690	8.010	9.070	265	190	205
36	16.240	8.450	9.060	235	205	200
37	15.800	9.070	9.020	205	225	195
38	15.030	9.310	8.980	175	235	185
39	12.970	12.230	8.960	145	255	175

TABLE 6-3

COMPLEX STRAIN PATH NO. 2

TEST NO. 1

PT	E1*1000	E2*1000	E3*1000	S1	S2	S3
1	-.042	-.018	-.021	100	100	100
2	1.389	1.030	.906	150	150	150
3	2.548	1.994	1.849	200	200	200
4	4.349	3.942	3.803	300	300	300
5	5.533	5.579	5.489	400	400	400
6	6.705	7.525	7.456	500	500	500
7	6.833	7.841	7.766	500	500	500
8	6.910	8.026	7.945	500	500	500
9	7.535	8.083	8.009	530	490	490
10	7.856	8.074	7.994	545	485	485
11	8.066	8.024	7.943	560	480	480
12	8.580	7.998	7.912	575	475	475
13	9.080	7.883	7.822	590	465	465
14	9.348	7.788	7.706	590	450	450
15	9.509	7.725	7.647	590	440	440
16	9.621	7.683	7.606	580	430	430
17	9.595	7.660	7.578	560	420	420
18	9.537	7.649	7.561	540	410	410
19	9.538	7.599	7.521	530	400	400
20	9.522	7.565	7.489	520	390	390
21	9.456	7.558	7.466	500	380	380
22	9.435	7.514	7.427	485	365	365
23	9.302	7.443	7.356	470	350	350
24	9.320	7.381	7.291	455	335	335
25	9.138	7.372	7.276	435	325	325
26	9.108	7.326	7.247	420	315	315
27	9.073	7.313	7.204	400	305	305
28	8.998	7.361	7.196	390	315	305
29	8.919	7.487	7.172	380	335	305
30	8.886	7.676	7.054	380	355	295
31	8.872	7.666	7.031	380	355	295
32	8.697	7.891	7.107	370	375	310
33	8.525	8.064	7.152	350	395	320
34	8.262	8.334	7.223	325	415	330
35	8.237	8.395	7.236	325	415	330
36	8.407	8.291	7.180	350	395	320
37	8.606	8.130	7.095	375	370	310
38	8.822	7.921	7.096	400	345	310
39	8.997	7.717	7.094	415	320	310
40	9.200	7.439	7.155	430	295	315
41	9.505	7.051	7.197	445	270	320
42	10.086	6.425	7.303	485	245	330

TABLE B-4

COMPLEX STRAIN PATH NO. 2

TEST NO. 2

PT	E1*1000	E2*1000	E3*1000	S1	S2	S3
1	-.042	-.018	-.021	100	100	100
2	1.370	.796	.919	150	150	150
3	2.511	1.769	1.805	200	200	200
4	4.200	3.412	3.473	300	300	300
5	5.211	4.713	4.816	400	400	400
6	6.226	6.131	6.411	500	500	500
7	7.047	7.586	7.867	600	600	600
8	7.247	8.114	8.417	600	600	600
9	7.344	8.322	8.637	600	600	600
10	7.663	8.371	8.703	630	590	590
11	8.046	8.294	8.646	660	580	580
12	8.735	8.219	8.561	700	570	570
13	9.544	8.090	8.439	740	560	560
14	10.124	8.006	8.345	760	550	550
15	10.248	7.976	8.332	740	540	540
16	10.260	7.957	8.312	725	530	530
17	10.242	7.933	8.284	710	520	520
18	10.214	7.907	8.265	690	510	510
19	10.131	7.916	8.279	665	500	500
20	10.101	7.879	8.230	650	490	490
21	10.096	7.844	8.194	640	480	480
22	10.067	7.825	8.161	625	470	470
23	10.050	7.770	8.112	615	455	455
24	9.938	7.751	8.102	570	440	440
25	9.833	7.780	8.130	550	420	420
26	9.650	7.676	8.015	540	400	400
27	9.668	7.566	7.913	530	380	380
28	9.571	7.566	7.922	510	380	380
29	9.504	7.540	7.895	490	370	370
30	9.352	7.656	7.993	470	390	370
31	9.193	7.805	7.903	450	410	370
32	9.035	7.960	7.912	430	430	370
33	8.865	8.159	7.902	410	450	370
34	8.655	8.407	7.860	390	470	370
35	8.311	8.545	7.842	365	490	370
36	8.412	8.756	7.866	390	470	370
37	8.588	8.607	7.873	410	445	370
38	8.700	8.405	7.890	420	415	370
39	8.852	8.196	7.979	435	385	370
40	8.998	7.967	7.977	450	355	370
41	9.257	7.621	7.993	470	325	370
42	9.547	7.335	7.993	490	305	370
43	10.043	6.947	7.956	530	285	370

TABLE B-5

COMPLEX STRAIN PATH NO. 3

TEST NO. 1

PT	E1*1000	E2*1000	E3*1000	S1	S2	S3
1	-.042	-.018	-.021	100	100	100
2	2.169	1.552	1.619	200	200	200
3	3.697	3.174	3.299	300	300	300
4	4.833	4.684	4.864	400	400	400
5	5.917	6.389	6.624	500	500	500
6	6.981	8.178	8.467	600	600	600
7	7.926	9.712	10.081	700	700	700
8	9.007	11.616	12.023	800	800	800
9	9.487	12.405	12.833	850	850	850
10	10.063	13.390	13.852	900	900	900
11	10.570	14.269	14.768	900	900	900
12	11.088	14.334	14.823	930	890	890
13	11.620	14.299	14.814	960	880	880
14	12.063	14.255	14.767	990	870	870
15	12.775	14.216	14.722	1020	860	860
16	13.543	14.160	14.644	1055	850	850
17	14.381	14.080	14.570	1100	840	840
18	15.599	13.989	14.467	1150	830	830
19	17.293	13.867	14.370	1200	820	820
20	18.710	13.769	14.260	1245	810	810
21	20.738	13.590	14.055	1285	795	795
22	21.102	13.528	13.986	1250	765	765
23	21.282	13.453	13.924	1220	735	735
24	21.331	13.376	13.832	1190	705	705
25	21.423	13.254	13.709	1160	675	675
26	21.349	13.111	13.569	1060	625	625
27	21.517	12.894	13.343	1060	575	575
28	21.670	12.643	13.084	1010	525	525
29	22.176	12.152	12.540	970	465	465
30	23.660	11.307	11.613	925	405	405
31	24.064	10.973	11.227	885	375	375
32	24.359	10.643	10.869	840	345	345
33	24.661	10.309	10.514	790	315	315
34	24.931	9.934	10.098	740	285	285
35	25.997	9.076	9.096	710	255	255
36	31.623	5.729	5.090	680	225	225
37	32.377	5.355	4.830	595	220	235
38	32.113	5.434	5.084	550	220	245
39	31.700	5.605	5.467	510	220	255
40	31.477	5.603	5.716	470	215	265
41	31.077	5.607	6.203	430	205	275
42	30.420	5.590	6.955	350	190	285
43	29.759	5.525	7.587	300	175	285
44	28.802	5.417	8.621	250	160	285
45	27.542	5.749	9.545	210	160	275
46	26.148	5.914	10.660	170	150	265

TABLE B-6

COMPLEX STRAIN PATH NO. 3

TEST NO. 2

PT	E1*1000	E2*1000	E3*1000	S1	S2	S3
1	-.042	-.018	-.021	100	100	100
2	1.575	.954	1.012	200	200	200
3	2.872	2.368	2.453	300	300	300
4	3.958	3.963	4.015	400	400	400
5	5.247	6.097	6.138	500	500	500
6	5.612	6.909	6.890	500	500	500
7	6.541	8.316	8.327	600	600	600
8	7.880	10.484	10.510	700	700	700
9	8.686	11.629	11.678	800	800	800
10	9.869	13.310	13.408	900	900	900
11	10.546	14.364	14.436	900	900	900
12	10.737	14.641	14.738	900	900	900
13	11.127	14.817	14.908	925	900	900
14	11.514	14.855	14.942	950	890	890
15	11.970	14.846	14.950	975	880	880
16	12.335	14.834	14.925	1000	870	870
17	12.851	14.814	14.888	1025	860	860
18	13.464	14.786	14.857	1050	850	850
19	14.518	14.720	14.748	1100	840	840
20	16.249	14.634	14.666	1150	830	830
21	17.702	14.542	14.541	1200	815	815
22	19.643	14.357	14.339	1250	800	800
23	22.207	14.113	14.019	1300	775	775
24	23.142	13.969	13.884	1300	750	750
25	23.531	13.993	13.781	1275	725	725
26	23.635	13.953	13.722	1225	700	700
27	23.649	13.794	13.654	1175	675	675
28	23.717	13.726	13.582	1150	650	650
29	23.694	13.657	13.482	1125	625	625
30	23.914	13.537	13.362	1125	600	600
31	24.272	13.308	13.111	1125	575	575
32	24.773	13.086	12.855	1125	550	550
33	25.191	12.415	12.111	1100	500	500
34	25.675	12.341	11.977	1075	500	500
35	25.795	12.324	11.950	1050	500	500
36	25.853	12.232	11.849	1025	475	475
37	26.913	12.130	11.736	1000	450	450
38	27.109	11.920	11.496	975	425	425
39	27.713	11.455	10.956	950	390	390
40	31.451	9.569	8.752	925	350	350
41	32.446	9.032	8.142	975	330	330
42	32.815	8.939	7.863	925	320	320
43	33.147	8.586	7.546	925	300	300
44	38.761	5.586	4.006	925	280	280
45	40.103	5.114	3.246	925	260	260
46	40.490	5.152	3.351	925	300	300
47	40.497	5.370	3.570	925	330	330
48	40.465	5.672	3.897	925	360	360
49	40.095	6.063	4.256	900	390	390
50	39.846	6.437	4.727	750	420	420

APPENDIX C

THE SOIL MODELS -- MODIFICATIONS AND MATERIAL PARAMETERS

In order to provide some documentation of the precise forms of the soil models used to make the predictions presented herein, each of the predictors was asked to describe any changes that he made in the basic model (as described in the cited references) in order to fit the standard laboratory data given in Reference 3, and to supply a list of the values of the material parameters that resulted from the fit. This appendix contains copies of the replies submitted by the predictors in response to this request.

California
Research &
Technology, Inc.

11 February 1983
Ser: 3738

Harold E. Read
S-Cubed
P. O. Box 1620
La Jolla, CA 92038-1620

Dear Hal:

In response to your letter of February 1, 1983, the equation of state I used to calculate the behavior of the material in your study is basically the AFWL CIST model as documented by J. Amend, G. Ullrich and J. Thomas in "HAVE HOST Cylindrical In-Situ Test (CIST) Data Analysis and Material Model Report", AFWL-TR-77-81, February 1977. This EOS is also presented in "CRALE Users Manual", AFWL-TR-82-45, January 1982, which I authored. Unfortunately, distribution of the manual is limited to government personnel unless a special request is made. I am including a table and figure from the report containing the parameters used in our study. I think anyone interested can use the Amend's report and the table to reproduce my results.

I did add one modification to the basic EOS for this study. As you probably know, unloading in CIST follows a straight line. The data you provided showed a large reduction in the moduli as the material unloads so that a distinctive "heel" is present on all the load-unload paths. I modeled this behavior rather simply as follows:

a. Use the CIST EOS "as is" for loading and for unloading to pressures greater than .5 P_{max}.

b. When the material has unloaded to pressures less than .5 P_{max}, the zero pressure excess compression, μ_z, is reset to $\alpha\mu_z$ and the bulk modulus recalculated as

$$dP/d\mu = .5*P_{max}/(\mu_h - \alpha\mu_z)$$

20943 Devonshire Street • Chatsworth, California 91311 • (213) 709-3705

and the pressure is

$P = dP/d\mu * (\mu - \alpha\mu_z)$.

μ_h is the excess compression at $P = .5\ P_{max}$ and α is a new input parameter which I set to 0.3 for this study.

I hope this satisfies your request. I am looking forward to the report as I think this study could lead to some new ideas in modeling the low stress behavior of earth materials.

If there is anything else we can provide, don't hesitate to ask.

Sincerely,

Shel Schuster

SS:cd

Enclosures

cc: J. Thomas, AFWL/NTED
G. Ullrich, DNA/SPSS
J. Jones, DNA/SPAS

TABLE C-1. EQUATION OF STATE PARAMETERS FOR CIST (EOS 3)

CK	Parameter	Input	Units	Definition
1	C1	3350	ft/s	unload and initial load wave speed
2	C2	800	ft/s	2nd loading wave speed
3	C3	1400	ft/s	3rd loading wave speed
4	P1	3.45	bars	P where C changes from C1 to C2
5	P2	13.79	bars	P where C changes from C2 to C3
6	P3	238.1	bars	P where load/unload curves merge
7	BSQ	0	bars	coef. of μ^2 in high pressure fit
8	ALPHA	0.3		
9	EMU3	0.11	-----	μ where load/unload curves merge
10	EMU2	0.0138	-----	μ at P2
11	EMU1	0.258	-----	μ at P1
12	EMUX	0.0922	-----	μ at P=0 along maximum unload curve
13				
14	B1	0.01336	bars	dP/dμ corresponding to C1
15	B2	761.8	bars	dP/dμ corresponding to C2
16	B3	0.00233	bars	dP/dμ corresponding to C3
17	CTE	3.0	g/Te	coefficient of thermal expansion
18	EV	0.03	g/Te	max. vaporization energy
19	FPRL	0.375	-----	loading K/G = (1+2*PRL)/(1-PRL)
20	FPRU	0.375	-----	unloading K/G = (1+2*PRU)/(1-PRU)
21				
22				
23				
24				
25	PRL	1/3	-----	loading Poisson's ratio
26	PRU	1/3	-----	unloading Poisson's ratio
27	GMAX	1.0	bars	maximum shear modulus
28	BETAH	0	-----	rate of hardening of Y
29	BETAS	0	-----	rate of softening of Y
30	EPYLD	0	-----	hardening maximum μ/softening minimum
31	PYLD	0	bars	(FIO) min. pressure for Y=YLDVM
32				
33	YLDVM	68.95	bars	von Mises yield limit
34	YLD1	3.45	bars	cohesion of competent material
35	YLD2	1.0	-----	slope of Y-P surface for competent materia
36	COHES	3.45	bars	cohesion of 3-crack material
37	YLDCR	1.0	----	slope of Y-P surface (3-crack material)
38				
39				
40				
41				
42				
43				
44				
45				
46				
47				
48				
49	VREF	0.473	cm^3/g	1/RHOREF (ρ_0 = 1.922 gm/cc)
50				

UNIVERSITY OF CALIFORNIA, LOS ANGELES

BERKELEY · DAVIS · IRVINE · LOS ANGELES · RIVERSIDE · SAN DIEGO · SAN FRANCISCO

SANTA BARBARA · SANTA CRUZ

Rm. 3173, Engineering I
SCHOOL OF ENGINEERING AND APPLIED SCIENCE
LOS ANGELES, CALIFORNIA 90024

February 10, 1983

Mr. Harold E. Read
S-Cubed
P. O. Box 1620
LaJolla, California 92038

Dear Hal:

Thanks very much for the data and comparisons you sent me. It appears that the model predicts too stiff soil response compared with the measured results. This may be due to the fact that I had to estimate failure stresses for all the input data in order to determine the parameters. Incorrect modeling of failure will affect the predicted stress-strain behavior, also for conditions which do not involve failure.

In answer to your letter of February 1, 1983, the reference to the model is as follows:

> Lade, P.V., "Elasto-Plastic Stress-Strain Theory for Cohesionless Soil with Curved Yield Surfaces," Int. J. Solids Structures, Pergamon Press, Vol. 13, 1977, pp. 1019-1035.

The parameter values were attached as the first page to my predictions.

Sincerely yours,

Poul Lade
Professor of
Engineering & Applied Science

PL/jw

TABLE C-2.
SUMMARY OF SOIL PARAMETERS FOR RALSTON SOIL

Parameter	Value		Strain Component
Modulus, K_{ur}	800		
Exponent, n	0.85		Elastic
Poisson's Ratio, ν	0.20		
Collapse Modulus, C	0.00046		Plastic
Collapse Exponent, p	0.767		Collapse
Yield Const., n_1	450		
Yield Exponent, m	0.69		
Pl. Potent. Const., R	-7.0		
Pl. Potent. Const., S	0.40		Plastic
Pl. Potent. Const., t	0.0		Expansive
Work-hard. Const., α	3.35	$q \geq 1$	
Work-hard. Const., β	-0.064		
Work-hard. Const., P	0.25		
Work-hard. Exponent, ζ	0.73		

MEMORANDUM FOR THE RECORD

BY: H. E. Read

SUBJECT: S-CUBED Endochronic Model for Ralston Valley Soil

PURPOSE

The purpose of this memo is twofold, namely, (1) to briefly document for future reference the basic equations of the S-CUBED Endochronic model used in the Soil Models Evaluation Study to make predictions for Ralston Valley soil, and (2) to record the corresponding values of the material parameters of this model. The nomenclature used below closely parallels that adopted in previous work,* and the reader is referred there for definitions of the symbolism employed below.

Basic Equations

Elastic Moduli:

$$K = K_0\left(1 + \frac{P}{p_a}\right)^m$$

$$G = G_0\left(1 + \frac{P}{p_a}\right)^n$$

Hydrostatic:

$$d\epsilon = \frac{dP}{K} + d\Theta + d\epsilon_s$$

$$P = H\int_{-\infty}^{z_H} \phi(z_H - z')\frac{d\Theta}{dz'}\,dz'$$

where

* Read, H.E., J. A. Trangenstein and K. C. Valanis, "A New Endochronic Constitutive Model for Soils," S-CUBED, La Jolla, CA., Report No. SSS-R-81-4926 to EPRI, November 1981.

$$H = \frac{\Gamma_o\left(\frac{v_o - v}{v - v_m}\right)}{3}$$

$$\phi(z) = \sum_{i=1}^{3} R_i e^{-\beta_i z_H}$$

$$dz_H = |d\Theta|$$

Deviatoric:

$$d\underline{s} = 2G(d\underline{\varepsilon} - d\underline{\varepsilon}^{\theta})$$

$$\underline{s} = F \int_0^{z_D} \rho(z - z') \frac{d\underline{\varepsilon}^{\theta}}{dz'}$$

where

$$F = F_o\left\{1 - \exp[-q(\frac{P}{P_a} + C_1)]\right\}$$

$$\rho = \sum_{i=1}^{3} S_i e^{-\eta_i z_D}$$

$$dz_D = \|d\underline{\varepsilon}^{\theta}\|$$

Shear-Volumetric Coupling:

$$d\varepsilon_s = A_o\left[1 - \left(\frac{v_c}{v}\right)^{\gamma\sigma}\right] dz_s$$

where

$$v_c = v^* - \beta \ell n(\frac{\sigma}{a})$$

$$dz_s = \|d\underline{\varepsilon}\|$$

Values of Material Parameters for Ralston Valley Soil

K_o = 5,482 psi	C_1 = 0.812	S_1 = 591
G_o = 680 psi	A_0 = 14.64	S_2 = 84
m = 0.96	$\gamma = 2.1 \times 10^{-3}$ psi^{-1}	S_3 = 41.2
n = 1.12	α = 24.23 psi	β_1 = 525
Γ_o = 938 psi	β = 0.0465	β_2 = 125
v_o = 1.38	v* = 1.50	β_3 = 46.4
v_m = 1.28	R_1 = 140.84	n_1 = 1,892
F_o = 949 psi	R_2 = 31	n_2 = 365
q = 0.0231	R_3 = 22.4	n_3 = 90

Weidlinger Associates Consulting Engineers 333 Seventh Avenue, New York, N Y 10001

February 10, 1983

Mr. Hal E. Read
S-Cubed
P.O. Box 1620
La Jolla, California 92038

Dear Hal:

In reference to your letter of February 1, 1983, we would like to inform you that the basic model we used to fit our cap model is described in our paper "An Algorithm and a Modular Subroutine for the Cap Model", which appeared in the International Journal of Numerical Methods in Geomechanics (1979). The only extension to the functional forms indicated in Appendix A of that paper is the use of the non-linear elastic pressure-volume relation through the pressure-dependent bulk modulus

$$K = \max (K_o, -K_1 J_1) \qquad (J_1 > 0 \text{ in tension})$$

The model parameters used for this prediction are:

$K_o = 1.0$

$K_1 = 120.0$

$G = 50.0$

$A = 1.0$

$B = 0.25$

$C = 0.96$

$D = 0.5$

$R = 3.0$

$W = 0.033$

If you have any questions please contact either of us.

Sincerely,

IVAN S. SANDLER
Partner

DAVID RUBIN
Associate

ISS/DR/jh

Tel: (212) 563-5200 Telex: 620554 WEID

DEPARTMENT OF THE ARMY
WATERWAYS EXPERIMENT STATION, CORPS OF ENGINEERS
P. O. BOX 631
VICKSBURG, MISSISSIPPI 39180

February 8, 1983

REPLY TO
ATTENTION OF:

Mr. Harold E. Read
S-Cubed
P. O. Box 1620
La Jolla, California 92038

Dear Hal:

As you requested in your letter of 1 February 1983, I am sending you a copy of the detailed description of the model I used in my predictions. It is a modified version of that model described in the Proceedings of the Workshop on Limit Equilibrium, Plasticity and Generalized Stress-Strain in Geotechnical Engineering, McGill University, May 1980, pages 692-710. Also enclosed is a complete list of the numerical values of the material parameters used in making the predictions.

If you have any questions related to the enclosed material, please feel free to call me at (601) 634-2660.

Sincerely,

George Y. Baladi

George Y. Baladi
Engineer
Geomechanics Division
Structures Laboratory

PART III: AN ELASTIC-PLASTIC ISOTROPIC CONSTITUTIVE MODEL FOR SAND (MATERIAL C)

George Y. Baladi

The material studied in this section is a dry Ottawa sand and would therefore be expected to be most closely modeled by the basic cap model (Sandler, DiMaggio, and Baladi [1], Baladi [2]). Perusal of these data indicates this to be true, with the addition of work hardening to the usually ideally plastic failure envelope. The total strain increment is assumed to be the sum of the elastic and plastic strain increments; i.e.,

$$d\epsilon_{ij} = d\epsilon^{E}_{ij} + d\epsilon^{P}_{ij} \tag{1}$$

where $d\epsilon_{ij}$ = components of the total strain increment tensor; $d\epsilon^{E}_{ij}$ = components of the elastic strain increment tensor; and $d\epsilon^{P}_{ij}$ = components of the plastic strain increment tensor.

Elastic Behavior. -- The behavior of the model in the elastic range is governed by the following incremental equations:

$$dJ_1 = 3K\, d\epsilon^{E}_{kk} \tag{2}$$

$$dS_{ij} = 2G\, d\epsilon^{E}_{ij} \tag{3}$$

in which dJ_1 = the first invariant of the stress increment tensor; $d\epsilon^{E}_{kk}$ = the elastic volumetric strain increment; dS_{ij} and de_{ij} = the stress and strain deviation increment tensors, respectively; and K and G = the elastic bulk and shear moduli, respectively.

The elastic bulk modulus describes the unloading portion of the pressure-volumetric strain response of the material. The following expression is proposed for the elastic bulk modulus:

$$K = \frac{K_i}{1 - K_1}\left[1 - K_1 \exp(-K_2 J_1)\right] + K_3\left[1 + \frac{1 - K_4 \exp(-K_5 \epsilon_{kk}^P)}{1 + K_4 \exp(-K_5 \epsilon_{kk}^P)}\right] \quad (4)$$

where K_i = initial elastic bulk modulus and K_1, K_2, K_3, K_4 and K_5 = material constants.

The elastic shear modulus describes the unloading portion of the deviatoric stress-strain response of the material. The following expression is proposed for the elastic shear modulus:

$$G = \frac{G_i}{1 - G_1}\left[1 - G_1 \exp(-G_2\sqrt{J_2'})\right] + G_3\left[1 + \frac{1 - G_4 \exp(-G_5 \epsilon_{kk}^P)}{1 + G_4 \exp(-G_5 \epsilon_{kk}^P)}\right] \quad (5)$$

where G_i = initial elastic shear modulus; G_1, G_2, G_3, G_4, and G_5 = material constants; and W^{Pf} = the plastic work associated with the yield envelope.

Plastic Behavior. -- The behavior of the model in the plastic range if governed by the flow rule

$$d\epsilon_{ij}^P = d\lambda \frac{\partial f}{\partial \sigma_{ij}} \quad (6)$$

in which $d\epsilon_{ij}^P$ and σ_{ij} = the plastic strain increment and the stress tensor, respectively; f = the loading function; and $d\lambda$ = a positive scalar factor of proportionality, which is nonzero only when plastic deformation occurs and is dependent on the particular form of the loading function f.

The loading function f is assumed to be isotropic and to consist of two parts: an elliptically shaped strain-hardening yield surface described by

$$F(J_1, \sqrt{J_2'}, \kappa) = (J_1 + C)^2 + 6J_2' - [X(\kappa) + C]^2 = 0 \quad (7)$$

and a Prager-Drucker type yield envelope defined by

$$f(J_1, \sqrt{J_2}, \alpha) = \frac{\sqrt{J_2}}{J_1 + C} - \alpha = 0 \tag{8}$$

where $\bar{J}_2$ = the second invariant of the stress deviation tensor; C is a material constant representing the location of the center of the strain-hardening yield surface F and coincides with the intersection of the yield envelope f and the J_1 axis; κ is a hardening parameter which is generally a function of the history of plastic volumetric strain; $X(\kappa)$ represents the intersection of the strain-hardening surface with the J_1 axis; and α is a work-hardening and -softening parameter which allows the yield envelope f to expand and contract isotropically (Figure 1).

The hardening parameter κ in this model was chosen to be

$$\kappa = \varepsilon_{kk}^{PH} = A[1 - \exp(-DX)] - A_1\left[1 + \frac{1 - D_1 \exp(-D_2X)}{1 + D_1 \exp(-D_2X)}\right] - A_2X^2 \exp(-D_3X)$$

where A, A_1, A_2, D, D_1, D_2 and D_3 = material constants and ε_{kk}^{PH} is the plastic volumetric strain associated with the strain-hardening yield surface F. The parameter A defines the maximum plastic volumetric compaction that the material can experience under hydrostatic loading. Note that the strain-hardening surface F is chosen so that the plastic strain increment vector associated with it is always parallel to the yield envelope f.

The parameter α in Eq. 8 is assumed to be a function of plastic work W^{Pf} associated with the yield envelope f through the following expression:

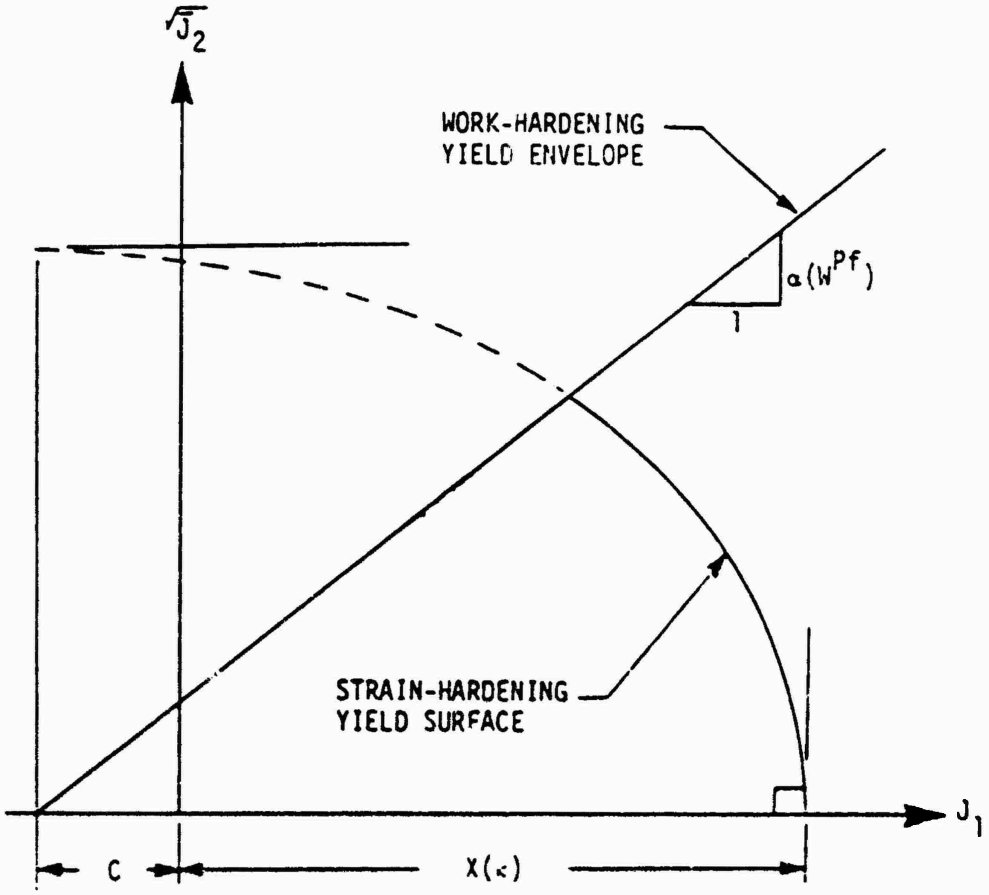

Figure C-1. Proposed yield surfaces for strain-hardening and -softening model.

$$\alpha = \left\{C_1[1 - \exp(-C_2\, W^{Pf})] + C_3[1 - \exp(-C_4\, W^{Pf})] + C_5\right\}(1 - m)$$

$$+ \left\{C_6[1 - \exp(C_2\, W^{Pf})] + C_7[1 - \exp(-C_4 W^{Pf})] + C_8\right\} m \quad (10)$$

where C_1, C_2, C_3, C_4, C_5, C_6, C_7 and C_8 = material constants, and m = stress ratio given by

$$m = \frac{\sigma_{int.} - \sigma_{min.}}{\sigma_{max} - \sigma_{min}}$$

where σ_{int}, σ_{min} and σ_{max} are the intermediate, the minimum and the maximum principal strains. The proportionality factor $d\lambda$ (Eq. 5) can be shown to be (Baladi and Rohani [3])

$$d\lambda = \frac{3K \frac{\partial F}{\partial J_1}(d\epsilon_{kk} - d\epsilon_{kk}^{Pf}) + \frac{G}{\sqrt{J_2}\partial\sqrt{J_2}} \frac{\partial F}{} S_{ij}(de_{ij} - de_{ij}^{Pf})}{9K\left(\frac{\partial F}{\partial J_1}\right)^2 + G\left(\frac{\partial F}{\partial\sqrt{J_2}}\right)^2 - 3\frac{\partial F}{\partial J_1}\frac{\partial F}{\partial \epsilon_{kk}^{PH}}} \quad (15)$$

for the strain-hardening surface. In the case of the yield envelope f (Eq. 8), due to the hardening parameter α (Eq. 10), it is more convenient to express $d\lambda$ in terms of plastic work. Thus

$$d\lambda = \frac{dW^{Pf}}{\frac{\partial F}{\partial \sigma_{ij}}\sigma_{ij}} \quad (16)$$

for the yield envelope f, where $d\epsilon_{kk}^{Pf}$ and de_{ij}^{Pf} are, respectively, the volumetric and deviatoric components of plastic strain increment tensor associated with f. The total strain increment tensor given by Eq. 1 can, therefore, be written as

$$d\epsilon_{ij} = d\epsilon_{ij}^{E} + d\epsilon_{ij}^{PH} + d\epsilon_{ij}^{Pf} \quad (17)$$

where $d\epsilon_{ij}$, $d\epsilon^{E}_{ij}$, $d\epsilon^{PH}_{ij}$, and $d\epsilon^{Pf}_{ij}$ = the total strain increment, the elastic strain, the plastic strain associated with the hardening function, and plastic strain associated with the yield condition, respectively.

Appendix. -- References

1. Sandler, I.S., DiMaggio, F. L., and Baladi, G. Y., "A Generalized Cap Model for Geological Materials," J. of Geotechn. Engrg. Div., ASCE, Vol. 102, No. GT 7, July 1976.

2. Baladi, G. Y., "The Latest Development in the Nonlinear-Elastic-Nonideally Plastic Work Hardening Cap Model," Proc. of the Symp. on the Role of Plasticity in Soil Mech., Cambridge, England, September 1973.

3. Baladi, G. Y., and Rohani, B., "Liquefaction Potential of Dams and Foundation; Development of an Elastic-Plastic Constitutive Relationship for Saturated Sand," Research Report S-76-?, Report 3, 1977, U.S. Army Engineer Waterways Experiment Station, CE, Vicksburg, Miss.

Table C-3

Numerical Values of Material Constants

Material Constants			
Name	Notation	Units	Numerical Values
Hardening failure envelope parameter	C	psi	74
	C_1	---	0.1034
	C_2	psi^{-1}	4
	C_3	---	0.1
	C_4	psi^{-1}	50
	C_5	---	0.035
	C_6	---	0.0751
	C_7	---	0.0629
	C_8	---	0.022
Hardening surface parameter	A	---	0.035
	A_1	---	0.003
	A_2	psi^{-2}	0.00000005
	D	psi^{-1}	0.001
	D_1	---	10.0
	D_2	psi^{-1}	0.003
	D_3	psi^{-1}	0.004
Bulk modulus function	K_i	psi	3,750.00
	K_1	---	0.6
	K_2	psi^{-1}	0.0015
	K_3	psi	62,500.00
	K_4	---	100.00
	K_5	---	400.00
Shear modulus function	G_i	psi	1,000.00
	G_1	psi	0.6
	G_2	psi^{-1}	0.00625
	G_3	psi	45,000.00
	G_4	---	100.00
	G_5	---	400.00

APPENDIX D

NUMERICAL DESCPIPTIONS OF THE COMPLEX STRAIN PATHS

This appendix contains three tables which provide numerical descriptions of the complex strain paths considered in the present study. These tables were supplied to the predictors to define the paths along which they were to exercise their models.

TABLE D-1

COMPLEX STRAIN PATH NO. 1

Pt. No.	Principal Strains*		
	$\epsilon_1 \times 10^3$	$\epsilon_2 \times 10^3$	$\epsilon_3 \times 10^3$
1	0	0	0
2	9	0	0
3	7	0	0
4	8.8	-1.8	0
5	3.4	3.6	0

*Measured from an initial hydrostatic compression state of 300 psi.

TABLE D-2

COMPLEX STRAIN PATH NO. 2

Pt. No.	Principal Strains*		
	$\varepsilon_1 \times 10^3$	$\varepsilon_2 \times 10^3$	$\varepsilon_3 \times 10^3$
1	0	0	0
2	0.52	-0.018	-0.018
3	0.73	-0.026	-0.026
4	1.00	-0.052	-0.052
5	1.35	-0.078	-0.078
6	1.72	-0.13	-0.13
7	1.98	-0.18	-0.18
8	2.24	-0.23	-0.23
9	2.39	-0.29	-0.29
10	2.52	-0.34	-0.34
11	2.60	-0.39	-0.39
12	2.55	-0.45	-0.45
13	2.42	-0.52	-0.52
14	2.26	-0.57	-0.57
15	2.03	-0.65	-0.65
16	1.25	0.13	-0.65
17	2.16	-0.78	-0.65

*Measured from an initial hydrostatic compression state of 550 psi.

TABLE D-3

COMPLEX STRAIN PATH NO. 3

Pt. No.	Principal Strains*		
	$\epsilon_1 \times 10^3$	$\epsilon_2 \times 10^3$	$\epsilon_3 \times 10^3$
1	0	0	0
2	2.2	-0.11	-0.11
3	4.4	-0.22	-0.22
4	6.7	-0.33	-0.33
5	8.0	-0.44	-0.44
6	9.1	-0.56	-0.56
7	9.8	-0.67	-0.67
8	10.3	-0.78	-0.78
9	10.7	-0.89	-0.89
10	11.1	-1.11	-1.11
11	20.0	-10.0	-10.0
12	17.1	-7.22	-10.0

*Measured from an initial hydrostatic compression state of 900 psi.

DISTRIBUTION LIST

DEPARTMENT OF DEFENSE

Assistant to the Secretary of Defense
Atomic Energy
ATTN: Executive Assistant

Defense Advanced Rsch Proj Agency
ATTN: Library

Defense Intelligence Agency
ATTN: DB-4C
ATTN: DB-4N

Defense Nuclear Agency
2 cy ATTN: SPSS, M. Shore
4 cy ATTN: STTI-CA

Defense Technical Information Center
12 cy ATTN: DD

Field Command, DNA, Det 1
Lawrence Livermore National Lab
ATTN: FC-1

Field Command, DNA
ATTN: FCPR
ATTN: FCTT
ATTN: FCTXE
ATTN: FCTT, W. Summa
ATTN: FCTK, C. Keller

Interservice Nuclear Weapons School
ATTN: TTV

Joint Strat Tgt Planning Staff
ATTN: JPST
ATTN: JPTM
ATTN: JLKC
ATTN: JLKS
ATTN: JLK, DNA Rep

Under Secretary of Defense for Rsch & Engrg
ATTN: Strat & Space Sys (OS)
ATTN: Strat & Theater Nuc For, B. Stephan

DEPARTMENT OF THE ARMY

BMD Advanced Technology Center
ATTN: ATC-T
ATTN: ICRDABH-X

Department of the Army
ATTN: DAEN-MPE-T
ATTN: DAEN-RDL

Harry Diamond Laboratories
ATTN: DELHD-NW-P, 20240
ATTN: DELHD-TA-L, 81100, Tech Lib

US Army Ballistic Research Labs
ATTN: DRDAR-BLT, J. Keefer
ATTN: DRDAR-BLA-S, Tech Lib

US Army Concepts Analysis Agency
ATTN: CSSA-ADL, Tech Lib

US Army Engineer Ctr & Ft Belvoir
ATTN: DT-LRC

DEPARTMENT OF THE ARMY (Continued)

US Army Engineer Div Huntsville
ATTN: HNDED-SR

US Army Engineer Div Ohio River
ATTN: ORDAS-L, Tech Lib

US Army Engr Waterways Exper Station
ATTN: J. Strange
ATTN: J. Zelasko
ATTN: WESSE
ATTN: Library
ATTN: WESSA, W. Flathau
2 cy ATTN: WESSD, J. Jackson

US Army Material & Mechanics Rsch Ctr
ATTN: Tech Library

US Army Material Command
ATTN: DRXAM-TL, Tech Lib

US Army Nuclear & Chemical Agency
ATTN: Library

USA Missile Command
ATTN: Documents Section

DEPARTMENT OF THE NAVY

Naval Civil Engineering Laboratory
ATTN: Code L51, J. Crawford

Naval Electronic Systems Command
ATTN: PME 117-21

Naval Facilities Engineering Command
ATTN: Code 04B

Naval Material Command
ATTN: MAT 08T-22

Naval Postgraduate School
ATTN: Code 1424, Library
ATTN: G. Lindsay

Naval Research Laboratory
ATTN: Code 2627, Tech Lib

Naval Surface Weapons Center
ATTN: Code F31

Naval Surface Weapons Center
ATTN: Tech Lib & Info Svcs Br

Naval War College
ATTN: Code E-11, Tech Service

Naval Weapons Evaluation Facility
ATTN: Code 10, Tech Lib

Naval Underwater Systems Center
ATTN: Code EM, J. Kalinowski

Office of the Deputy Chief of Naval Ops
ATTN: NOP 03EG
ATTN: NOP 981

DEPARTMENT OF [illegible] AVY (Continued)

Office of Naval Research
ATTN: Code 474, N. Perrone

Strategic Systems Project Office
ATTN: NSP-43, Tech Lib

DEPARTMENT OF THE AIR FORCE

Air Force
ATTN: INT

Air Force Geophysics Laboratory
ATTN: LWH, H. Ossing

Air Force Institute of Technology
ATTN: Library

Air Force Office of Scientific Rsch
ATTN: J. Allen
ATTN: W. Best

Air Force Systems Command
ATTN: DLW

Air Force Weapons Laboratory
ATTN: NTES, J. Thomas
ATTN: NTE, M. Plamondon
ATTN: NTES-C, R. Henny
ATTN: SUL

Air University Library
ATTN: AUL-LSE

Ballistic Missile Office/DAA
ATTN: EN
ATTN: ENSN, A. Schenker
ATTN: ENSN, E. Furbee
ATTN: PP

Deputy Chief of Staff
Logistics & Engineering
ATTN: LEEE

Deputy Chief of Staff
Research, Development & Acq
ATTN: AF/RDQI

Foreign Technology Division
ATTN: NIIS, Library

Rome Air Development Center
ATTN: TSLD

Strategic Air Command
ATTN: NRI/STINFO Library
ATTN: INAO
ATTN: XPFS
ATTN: XPQ

DEPARTMENT OF ENERGY

Department of Energy
Albuquerque Operations Office
ATTN: R. Jones
ATTN: CTID

Department of Energy
Nevada Operations Office
ATTN: Doc Con for Tech Lib

OTHER GOVERNMENT AGENCIES

Central Intelligence Agency
ATTN: OSWR/NED

Department of the Interior
Bureau of Mines
ATTN: Tech Lib

NATO

NATO School, SHAPE
ATTN: US Documents Officer

DEPARTMENT OF ENERGY CONTRACTORS

University of California
Lawrence Livermore National Lab
ATTN: Tech Info Dept Lib
ATTN: D. Glenn

Los Alamos National Laboratory
ATTN: Reports Library
ATTN: J. Hopkins

Oak Ridge National Laboratory
ATTN: Civil Def Res Proj
ATTN: Central Rsch Library

Sandia National Laboratories
ATTN: Org 7112, A. Chabai
ATTN: Tech Lib 3141
ATTN: Org 7111, L. Hill

Sandia National Laboratories
ATTN: Library & Sec Class Div

DEPARTMENT OF DEFENSE CONTRACTORS

Aerospace Corp
ATTN: Library Acq M1/199

Agbabian Associates
ATTN: M. Agbabian

Applied Research Associates, Inc
ATTN: D. Piepenburg

Applied Research Associates, Inc
ATTN: R. Frank

Applied Research Associates, Inc
ATTN: S. Blouin

Applied Research Associates, Inc
ATTN: N. Higgins
ATTN: H. Auld
ATTN: J. Bratton
ATTN: J. Drake

Applied Theory, Inc
2 cy ATTN: J. Trulio

AVCO Systems Division
ATTN: Library A830

BDM Corp
ATTN: Corporate Lib
ATTN: T. Neighbors

BDM Corp
ATTN: F. Leech

DEPARTMENT OF DEFENSE CONTRACTORS (Continued)

Boeing Co
ATTN: Aerospace Library

Boeing Co
ATTN: MS-85-20, D. Choate

California Institute of Technology
ATTN: T. Ahrens

California Research & Technology, Inc
ATTN: Library
ATTN: K. Kreyenhagen
ATTN: S. Schuster
ATTN: M. Rosenblatt

California Research & Technology, Inc
ATTN: D. Orphal
ATTN: F. Sauer

Calspan Corp
ATTN: Library

University of Denver
ATTN: Sec Officer for J. Wisotski

EG&G Washington Analytical Services Center, Inc
ATTN: Library

Electro-Mech Systems, Inc
ATTN: R. Shunk

GARD
ATTN: G. Neidhardt

Horizons Technology, Inc
ATTN: R. Kruger

IIT Research Institute
ATTN: M. Johnson
ATTN: R. Welch
ATTN: Documents Library

Institute for Defense Analyses
ATTN: Classified Library

Kaman AviDyne
ATTN: N. Hobbs
ATTN: Library

Kaman Sciences Corp
ATTN: Library

Kaman Tempo
ATTN: DASIAC

Kaman Tempo
ATTN: DASIAC

Lockheed Missiles & Space Co, Inc
ATTN: J. Weisner

Lockheed Missiles & Space Co, Inc
ATTN: Tech Info Center
ATTN: T. Geers

Martin Marietta Denver Aerospace
ATTN: D-6074, G. Freyer

DEPARTMENT OF DEFENSE CONTRACTORS (Continued)

Maxwell Laboratories, Inc
ATTN: J. Murphy

McDonnell Douglas Corp
ATTN: R. Halprin

Merritt CASES, Inc
ATTN: J. Merritt
ATTN: Library

University of New Mexico
ATTN: N. Baum

Pacific-Sierra Research Corp
ATTN: H. Brode, Chairman SAGE

Patel Enterprises, Inc
ATTN: M. Patel

Physics International Co
ATTN: E. Moore
ATTN: L. Behrmann
ATTN: Tech Library

R&D Associates
ATTN: W. Wright
ATTN: J. Lewis
ATTN: Tech Info Center
ATTN: D. Simons
ATTN: C. Lee
ATTN: P. Haas

Rand Corp
ATTN: B. Bennett

Rand Corp
ATTN: P. Davis

S-CUBED
ATTN: D. Grine
ATTN: Library
ATTN: T. Riney
ATTN: H. Read
ATTN: J. Prevost
ATTN: J. Trulio
ATTN: K. Ko
ATTN: I. Sandler
ATTN: G. Baladi
ATTN: S. Schuster
ATTN: P. Lade

Science Applications Intl Corp
ATTN: W. Layson

Science Applications, Inc
ATTN: Tech Library

Science Applications, Inc
ATTN: D. Maxwell

Southwest Research Institute
ATTN: A. Wenzel
ATTN: W. Baker

SRI International
ATTN: D. Keough
ATTN: G. Abrahamson
ATTN: Y. Gupta

DEPARTMENT OF DEFENSE CONTRACTORS (Continued)

Structural Mechanics Associates, Inc
ATTN: R. Kennedy

Teledyne Brown Engineering
ATTN: F. Leopard
ATTN: D. Ormond

Terra Tek, Inc
ATTN: S. Green
ATTN: Library
ATTN: A. Abou-Sayed
ATTN: J. Schatz

Tetra Tech, Inc
ATTN: L. Hwang

TRW Electronics & Defense Sector
ATTN: E. Wong
ATTN: P. Dai

DEPARTMENT OF DEFENSE CONTRACTORS (Continued)

TRW Electronics & Defense Sector
ATTN: P. Bhuta
ATTN: Tech Info Center
2 cy ATTN: N. Lipner

Universal Analytics, Inc
ATTN: E. Field

Weidlinger Assoc, Consulting Engrg
ATTN: T. Deevy

Weidlinger Assoc, Consulting Engrg
ATTN: M. Baron

Weidlinger Assoc, Consulting Engrg
ATTN: J. Isenberg

SUPPLEMENTARY

INFORMATION

AD-A156 853

ERRATA SHEET

for

DNA-TR-82-116 dated 30 April 1983

STUDY OF THE CAPABILITIES OF SIX ADVANCED SOIL MODELS TO PREDICT RESPONSES TO COMPLEX STRAIN PATHS TYPICAL OF EXPLOSIVELY-INDUCED GROUND MOTION.

Please exchange the enclosed DD Form 1473 and Distribution List pages for those in your document.

UNCLASSIFIED
SECURITY CLASSIFICATION OF THIS PAGE

REPORT DOCUMENTATION PAGE

Form Approved
OMB No. 0704-0188
Exp. Date: Jun 30, 1986

1a. REPORT SECURITY CLASSIFICATION UNCLASSIFIED	1b. RESTRICTIVE MARKINGS
2a. SECURITY CLASSIFICATION AUTHORITY	3. DISTRIBUTION/AVAILABILITY OF REPORT Approved for public release; distribution is unlimited.
2b. DECLASSIFICATION/DOWNGRADING SCHEDULE	
4. PERFORMING ORGANIZATION REPORT NUMBER(S) SSS-R-83-6081	5. MONITORING ORGANIZATION REPORT NUMBER(S) DNA-TR-82-116
6a. NAME OF PERFORMING ORGANIZATION S-CUBED, A Division of Maxwell Laboratories, Inc 6b. OFFICE SYMBOL (If applicable)	7a. NAME OF MONITORING ORGANIZATION Director Defense Nuclear Agency
6c. ADDRESS (City, State, and ZIP Code) P.O. Box 1620 La Jolla, CA 92038-1620	7b. ADDRESS (City, State, and ZIP Code) Washington, DC 20305-1000
8a. NAME OF FUNDING/SPONSORING ORGANIZATION 8b. OFFICE SYMBOL (If applicable)	9. PROCUREMENT INSTRUMENT IDENTIFICATION NUMBER DNA 001-82-C-0236
8c. ADDRESS (City, State, and ZIP Code)	10. SOURCE OF FUNDING NUMBERS PROGRAM ELEMENT NO. 62715H; PROJECT NO. H11CAXS; TASK NO. X; WORK UNIT ACCESSION NO. DH006217

11. TITLE (Include Security Classification)
STUDY OF THE CAPABILITIES OF SIX ADVANCED SOIL MODELS TO PREDICT RESPONSES TO COMPLEX STRAIN PATHS TYPICAL OF EXPLOSIVELY-INDUCED GROUND MOTION

12. PERSONAL AUTHOR(S) H.E. Read, H. Y. Ko, G.Y. Baladi, P.V. Lade, J.H. Prevost, I.S. Sandler, S.H. Schuster, J.G. Trulio

13a. TYPE OF REPORT	13b. TIME COVERED	14. DATE OF REPORT (Year, Month, Day)	15. PAGE COUNT
Technical	FROM 820430 TO 821231	830430	116

16. SUPPLEMENTARY NOTATION
This work was sponsored by the Defense Nuclear Agency under RDT&E RMSS Code B344082466 H11CAXSX00012 H2590D.

17. COSATI CODES		
FIELD	GROUP	SUB-GROUP
8	7	
8	11	

18. SUBJECT TERMS (Continue on reverse if necessary and identify by block number)
Complex Strain Paths; Measured Stress Histories

19. ABSTRACT (Continue on reverse if necessary and identify by block number)

The capabilities of six advanced soil models to predict the response of remolded Ralston Valley soil to complex strain paths were investigated in a joint, cooperative effort among several organizations. The complex strain paths were typical of those experienced by soil elements during nearby near-surface explosive ground motion events. The investigation involved both analysis and extensive laboratory testing. Standard laboratory tests were conducted to provide the usual type of data for fitting the models, while non-standard laboratory tests were done to drive the soil around prescribed fully three-dimensional complex strain paths and simultaneously measure the corresponding stress histories. To avoid possible unknown differences in testing equipment, all laboratory tests were done with a true triaxial device. The models were fit to the data from the standard laboratory tests, and then driven around the prescribed complex strain paths to predict the corresponding stress histories. Comparison between the predicted and measured stress histories formed the basis for evaluating the models. However, because of uncertainties that occurred in the data for the complex strain paths, a meaningful evaluation of the models

20 DISTRIBUTION/AVAILABILITY OF ABSTRACT ☐ UNCLASSIFIED/UNLIMITED ☒ SAME AS RPT. ☐ DTIC USERS	21. ABSTRACT SECURITY CLASSIFICATION UNCLASSIFIED
22a NAME OF RESPONSIBLE INDIVIDUAL Betty L. Fox	22b TELEPHONE (Include Area Code) (202) 325-7024 22c OFFICE SYMBOL DNA/STTI

DD FORM 1473, 84 MAR — 83 APR edition may be used until exhausted. All other editions are obsolete.

SECURITY CLASSIFICATION OF THIS PAGE
UNCLASSIFIED

12. PERSONAL AUTHOR(S) (Continued)

1. H. E. Read
P.O. Box 1620
La Jolla, CA 92038-0620

2. H. Y. Ko
Civil Engineering Department
University of Colorado
Boulder, CO 90309

3. G. Y. Baladi
U. S. Army Engineers Waterways
Experiment Station
Vicsburg, Mississippi 39180

4. P. V. Lade
Mechanics and Structures Dept.
3173 Engineering I
University of California at
Los Angeles
Los Angeles, CA 90024

5. J. H. Provost
Department of Civil Engineering
Princeton University
Princeton, New Jersey 08540

6. I. S. Sandler
Weidlinger Associates
333 Seventh Avenue
New York, NY 10001

7. S. H. Schuster
California Research & Technology
20943 Devonshire Street
Chatsworth, CA 91311

8. J. G. Trulio
Applied Theory, Inc.
930 South La Brea Avenue
Suite 2
Los Angeles, CA 90036

13. ABSTRACT (Continued)

could not be conducted. Recommendations are given for improving the testing procedures so that data of the required quality can be obtained in the future.